Evaluation of Green Infrastructure for Stormwater Quality Management

A Dissertation

Presented to

the faculty of the School of Engineering and Applied Science

University of Virginia

in partial fulfillment
of the requirements for the degree

Doctor of Philosophy

by

Charles R. Burgis

May 2020

APPROVAL SHEET

This Dissertation
is submitted in partial fulfillment of the requirements
for the degree of
Doctor of Philosophy

Author Signature: ____________________

This Dissertation has been read and approved by the examining committee:

Advisor: Dr. James A. Smith

Committee Member: Dr. Lisa Colosi Peterson

Committee Member: Dr. Teresa B. Culver

Committee Member: Dr. Jon L. Goodall

Committee Member: Dr. Stephen A. Macko

Committee Member: ____________________

Accepted for the School of Engineering and Applied Science:

Craig H. Benson, School of Engineering and Applied Science

May 2020

Abstract

Non-point source pollution, such as stormwater runoff, has become a leading threat to the quality of water resources and aquatic ecosystems near highly developed watersheds. Sudden discharges of stormwater from paved surfaces results in flooding, erosion, sewer overflows, and pollution into receiving waters. Improved stormwater management is needed to protect global water resources. Green infrastructure (GI) stormwater management practices mimic natural landscape hydrology by slowing, spreading, and infiltrating stormwater runoff before discharging it to receiving waters. GI is increasingly designed into urban landscapes to protect waterways from detrimental effects of urban stormwater, but it is still a young and developing technology with many performance knowledge gaps. This dissertation aims to explore the performance of a variety of modern GI practices over an annual range of weather conditions and storm events along Lorton Road in Northern Virginia. There are three primary objectives: (1) compare overall performance of four different GI designs, (2) determine the transport and attenuation of deicing salt in infiltration-based GI, and (3) track denitrification within GI using dual stable nitrate isotope analysis.

There are many different GI designs with sometimes greatly varying levels of stormwater management performance. Additionally, GI performance can be dependent on watershed, storm event, local climate, and maintenance characteristics. Studies have documented the performance of individual GI designs, but few have compared multiple GI designs side by side in the same location and climate. The evaluation of the performance of different operational GI designs receiving similar stormwater runoff conditions is needed to minimize climate and watershed variance and help guide watershed managers in GI selection. This study compares the performance of four different GI designs (bioretention, grass channel (GC), compost amended grass channel (CAGC), and bioswale) receiving the same weather conditions along Lorton Road in Northern Virginia. Stormwater runoff volumes and water quality parameter concentrations were measured at inlets and outlets of each GI during 27 storm events in all seasons over 14 months. The four different GI designs had a wide range of performances with respect to traditional stormwater quality criteria, some acting as pollutant sinks and others as pollutant sources. The bioretention and GC had significantly higher total surface load reduction averages of all water quality parameters than the CAGC and bioswale.

Winter deicing salt application has led to water quality impairment as stormwater carries salt ions (Cl^- and Na^+) through watersheds. GI is not yet designed to remove salt, but may have potential to mitigate its loading to surface waters. Two infiltration-based GI practices (bioretention and bioswale) were monitored year-round over 28 precipitation events to investigate the transport of salt through modern stormwater infrastructure. Both the bioretention and bioswale significantly reduced effluent surface loads of Cl^- and Na^+ (76% to 82%), displaying ability to temporarily retain and infiltrate salts and delay their release to surface waters. Changes in bioretention soil chemistry revealed a small percentage of Na^+ was stored long-term by ion exchange, but no long-term Cl^- storage was observed. Limited soil storage along with groundwater observations suggest the majority of salt removed from stormwater by the bioretention infiltrates into groundwater. Infiltration GI can seasonally buffer surface waters from salt, but are also an avenue for groundwater salt loading.

Strategies to mitigate watershed nitrogen export are critical in managing water resources. GI has shown ability to remove nitrogen from stormwater, but the removal mechanism is often unclear. Denitrification removes nitrate from water permanently, making it the most desirable removal mechanism. The year-round field performance of the bioretention was monitored to investigate the transport of nitrogen and the occurrence and contribution of denitrification. Stormwater runoff volumes, nitrogen concentrations, and nitrate isotope ratios ($\delta^{15}N\text{-}NO_3^-$ and $\delta^{18}O\text{-}NO_3^-$) were measured at the inlet and outlet of the bioretention during 24 storm events over 14 months. Nitrate concentration reductions displayed seasonal trends, with higher reductions happening in warmer months and lower reductions or increases occurring in winter. Cumulative bioretention nitrate and total nitrogen load reductions were 73% and 70%, respectively, but only two out of 24 monitored events displayed denitrification isotope trends, indicating other nitrogen removal mechanisms (i.e. infiltration and plant uptake) are primarily responsible for nitrogen surface effluent reductions. Only approximately 1.4% of the total reduced nitrate surface effluent load over the monitoring period was attributable to denitrification. Conditions leading to monitored denitrification suggest future GI designs should consider increasing hydraulic retention time (HRT) to encourage the important ecosystem service denitrification provides.

Table of Contents

Abstract ... *i*

List of Figures ... *v*

List of Tables ... *viii*

Acknowledgements ... *ix*

Related Publications and Presentations ... *x*

Chapter 1: Introduction ... *1*

1.1 Introduction ... **1**

1.2 Types of Transportation Green Infrastructure in this Study ... **2**

1.2.1 Swales ... 3

1.2.2 Bioretention ... 4

1.3 Research Objectives ... **5**

1.4 References ... **5**

Chapter 2: Evaluation of Green Stormwater Infrastructure Options for Transportation Water Quality Improvement ... *8*

2.1 Introduction ... **9**

2.2 Materials and Methods ... **10**

2.2.1 Study Site ... 10

2.2.2 Stormwater Field Monitoring ... 14

2.2.3 Stormwater Analysis ... 16

2.2.4 Statistical Analysis ... 17

2.3 Results ... **17**

2.3.1 Stormwater monitoring weather conditions ... 17

2.3.2 Stormwater runoff reduction ... 18

2.3.3 Stormwater quality ... 18

2.4 Discussion ... **24**

2.4.1 GI Stormwater Quality Concentration Performance ... 25

2.4.2 GI Stormwater Quality Surface Load Reduction ... 26

2.4.3 Fate of Reduced Stormwater Quality Parameters ... 27

2.4.4 Applying Results to Future GI Strategies ... 28

2.4.5 Suggestions for Future Research ... 29

2.5 Conclusions ... **29**

2.6 References ... **30**

Chapter 3: Green Stormwater Infrastructure Redirects Deicing Salt from Surface Water to Groundwater ... *34*

3.1 Introduction ... **35**

3.2 Materials and Methods ... **37**

3.2.1 Study Site ... 37

3.2.2 Stormwater Field Monitoring ... 38

3.2.3 Stormwater Analysis ... 40

3.2.4 Soil Monitoring and Analysis 40
3.2.5 Groundwater Monitoring and Analysis 41

3.3 Results 41
3.3.1 Stormwater Field Observations 41
3.3.2 Soil Observations 48
3.3.3 Groundwater Observations 49

3.4 Discussion 51
3.4.1 GI Salt Performance 51
3.4.2 Uptake by Vegetation 52
3.4.3 Bioretention Soil Changes Over Time 53
3.4.4 Infiltration into Groundwater 54

3.5 Conclusions 55

3.6 References 56

Chapter 4: Tracking Denitrification in Green Stormwater Infrastructure with Nitrate Stable Isotopes 61

4.1 Introduction 62

4.2 Materials and Methods 64
4.2.1 Study Site 64
4.2.2 Stormwater Field Monitoring 65
4.2.3 Sample Water Quality Analysis 67
4.2.4 Isotopic Analysis 67
4.2.5 Identification and Quantification of Denitrification 68
4.2.6 Statistical Analysis 68

4.3 Results 68
4.3.1 Stormwater monitoring conditions 68
4.3.2 Stormwater Quality 69
4.3.3 Overall Bioretention Performance 71
4.3.4 Stable Isotopes 72

4.4 Discussion 77
4.4.1 Bioretention Surface Water Nitrogen Removal 77
4.4.2 Denitrification Identification 78
4.4.3 Sources of Nitrate 79
4.4.4 Fate of Nitrogen in Bioretention 81
4.4.5 Encouraging Denitrification in Future GI Designs 82

4.5 Conclusions 82

4.6 References 83

Chapter 5: Conclusions and Future Study 88

Appendix A 91

Appendix B 99

Appendix C 111

List of Figures

Figure 2.1. Lorton Road stormwater research site and positioning of four GI types. Map from Hayes et al. (2020). 11
Figure 2.2. Bioretention north of Lorton Road. Solid blue lines indicate surface stormwater flow direction, while dotted blue lines show underground drains. Orange stars indicate stormwater monitoring locations and red circles show groundwater monitoring wells. 12
Figure 2.3. Compost-amended grass channel north of Lorton Road (top) and grass channel and bioswale south of Lorton Road (bottom). Solid blue lines indicate stormwater surface flow direction, while dotted black lines show the bioswale underdrain. Orange stars indicate stormwater monitoring locations and the orange rectangle shows the position of the sheet flow collector........ 13
Figure 2.4. GI EMC inlet and outlet concentrations from mutually monitored events. From top to bottom: nitrate as N (9 events), TDN (9 events), Phosphate as P (7 events), TP (2 events), DOC (9 events), and TSS (6 events). concentrations in EMC inlet and outlet samples. Outlet concentrations for the bioretention are from the underdrain outlet. Boxplots depict median values (thick black line), mean values (diamond), 25th to 75th percentiles (boxes), 1.5 times the interquartile range (whiskers), and outlier values (points). 21
Figure 2.5. GI surface water inlet and outlet water quality parameter total loads from mutually monitored events. From left to right: nitrate as N (9 events), TDN (9 events), phosphate as P (7 events), TP (2 events), DOC (9 events), and TSS (6 events). Outlet loads for the bioretention are a sum of the underdrain outlet and bypass channel. The vertical total load axis is log-scaled..... 23
Figure 2.6. GI stormwater management performance over the 12 month mutual monitoring period. From left to right: total stormwater runoff reductions, average concentration reductions (in vs. out), and total load reductions. Outlet concentrations for the bioretention are the underdrain outlet, while outlet loads are a sum of the underdrain outlet and bypass channel...... 24
Figure 2.7. GI stormwater quality parameter effluent loads per unit CDA over the 12 month mutual monitoring period. Bioretention outlet loads are a sum of the underdrain outlet and bypass channel. 24

Figure 3.1. Stormwater runoff inlet event mean concentrations (EMCs) of Cl^- and Na^+ (top) and Ca^{2+}, Mg^{2+}, and K^+ (middle), as well as sodium adsorption ratio (SAR; bottom) of the bioretention and bioswale by season. Monitoring data ranges between March 2018 and June 2019 (7 winter, 8 spring, 6 summer, 7 fall events for the bioretention and 7 winter, 2 spring, 4 summer, 2 fall events for the bioswale). Boxplots depict median values (thick black line), mean values (diamond), 25th to 75th percentiles (colored boxes), 1.5 times the interquartile range (whiskers), and outlier values (points)........ 43
Figure 3.2. Bioretention inlet and outlet Cl^- EMCs (top) and loads (bottom) for 28 monitored rain and snowmelt events. White and green bars show loads or concentrations going in and out of the bioretention, respectively, and correspond to the left y-axis. Grey and blue bars show rain and snow, respectively, and correspond to the right inverted y-axis. Bypass concentrations were not considered for outlet concentrations, but do factor into out loads. No outlet flow-weighted sample was collected on 2/20/19 (*), but a grab sample was taken. 44
Figure 3.3. Bioswale inlet and outlet Cl^- EMCs (top) and loads (bottom) for 15 monitored rain and snowmelt events. White and green bars show loads or concentrations going in and out of the

bioretention, respectively, and correspond to the left y-axis. Grey and blue bars show rain and snow, respectively, and correspond to the right inverted y-axis. 46
Figure 3.4. Bioretention soil extractible Cl^- and Na^+ concentrations (A) and base saturation of Na^+, K^+, Mg^{2+}, and Ca^{2+} (B) between October 2016 and July 2019. Error bars indicate +/- 1 standard error. 48
Figure 3.5. Groundwater concentrations of Cl^- and Na^+ (left) and Ca^{2+}, Mg^{2+}, K^+ (right) from two shallow wells next to the bioretention. Nine samples were collected from Well 1 and Well 2 between December 12, 2018 and October 11, 2019. Boxplots depict median values (thick black line), mean values (diamond), 25th to 75th percentiles (colored boxes), 1.5 times the interquartile range (whiskers), and outlier values (points). The dotted grey line indicates U.S. EPA Cl^- chronic freshwater quality criteria of 230 mg/L. 50
Figure 3.6. Molar Na^+ vs. Cl^- concentrations from bioretention, bioswale, and groundwater samples. Dotted grey lines indicate 1:1 molar ratio and colored lines are linear regressions. 51

Figure 4.1. Bioretention weather conditions and water quality results from the 24 monitored events. From top to bottom: rain/snow event depths, average daily temperature for each event, and nitrate, TDN, and DOC concentrations in EMC inlet and outlet samples. Average daily temperature data is from the nearby Ronald Reagan Airport Weather Station. 71
Figure 4.2. Bioretention stormwater management performance over the 14 month monitoring period. From left to right: total stormwater runoff reduction, average concentration reductions (in vs. out), total load reductions, and the percentage of nitrate that made up the TDN load at each monitoring location. 72
Figure 4.3. Dual $\delta^{15}N\text{-}NO_3^-$ and $\delta^{18}O\text{-}NO_3^-$ plots of bioretention stormwater from the inlet (blue), outlet (red), and outlet tail grab samples (green), as well as a rain sample from the 3/21/2019 event (orange). Boxes represent typical $\delta^{15}N\text{-}NO_3^-$ and $\delta^{18}O\text{-} NO_3^-$ ranges from different nitrate sources from Kendall et al. (2007) [35]. 74
Figure 4.4. Dual $\delta^{15}N\text{-}NO_3^-$ and $\delta^{18}O\text{-}NO_3^-$ plots of bioretention stormwater inlet and outlet EMC samples broken up by storm event. Blue arrows show the directional shift in isotope signatures from inlet to outlet samples. Background color gradient indicates nitrate concentration reduction between the inlet and outlet. 75
Figure 4.5. Dual $\delta^{15}N\text{-}NO_3^-$ and $\delta^{18}O\text{-}NO_3^-$ plots of five bioretention stormwater inlet and outlet EMCs with corresponding outlet tail grab samples broken up by storm event. Blue arrows show the directional shift in isotope signatures from inlet to outlet to outlet tail grab samples. Background color gradient indicates nitrate concentration reduction between the inlet and outlet. 76
Figure 4.6. Relation between the fraction of nitrate concentration remaining in water and the enrichment of $\delta^{15}N\text{-}NO_3^-$ in systems with different enrichment factors (ε). These curves are used to estimate the percentage of nitrate concentration reduction that denitrification is responsible for. The blue circle and red triangle show the two events with denitrification isotope trends with their calculated denitrification percentages in parenthesis. 77

Figure B1. Bioretention basin on January 16th, 2019 (left) and October 11th, 2019 (right). Both pictures facing east. 100
Figure B2. Bioswale on January 16th, 2019 (left) and October 11th, 2019 (right). Both pictures facing east. 100

Figure B3. Bioretention inlet and outlet Na^+, K^+, Mg^{2+}, and Ca^{2+} EMCs for 28 monitored rain and snowmelt events. White and green bars show loads or concentrations going in and out of the bioretention (respectively) and correspond to the left y-axis. Grey and blue bars show rain and snow (respectively) and correspond to the right inverted y-axis. Bypass concentrations were not considered for the outlet concentrations. No outlet flow-weighted sample was collected on 2/20/19, but a grab sample was taken. 105
Figure B4. Bioretention inlet and outlet Na^+, K^+, Mg^{2+}, and Ca^{2+} loads for 28 monitored rain and snowmelt events. White and green bars show loads or concentrations going in and out of the bioretention (respectively) and correspond to the left y-axis. Grey and blue bars show rain and snow (respectively) and correspond to the right inverted y-axis. No outlet flow-weighted sample was collected on 2/20/19 (*). 106
Figure B5. Bioswale inlet and outlet Na^+, K^+, Mg^{2+}, and Ca^{2+} EMCs for 15 monitored rain and snowmelt events. White and green bars show loads or concentrations going in and out of the bioretention (respectively) and correspond to the left y-axis. Grey and blue bars show rain and snow (respectively) and correspond to the right inverted y-axis. 107
Figure B6. Bioswale inlet and outlet Na^+, K^+, Mg^{2+}, and Ca^{2+} loads for 15 monitored rain and snowmelt events. White and green bars show loads or concentrations going in and out of the bioretention (respectively) and correspond to the left y-axis. Grey and blue bars show rain and snow (respectively) and correspond to the right inverted y-axis. 108
Figure B7. Groundwater Cl^- (top) and Na^+ (bottom) concentrations in two wells near the bioretention between August 2018 and October 2019. Well 1 was installed in August 2018 and Well 2 in October 2018. 109
Figure B8. Groundwater elevations of Well 1 and 2 (left y-axis) and rain intensity (right y-axis) between August 2018 and October 2019. Levels are depths of groundwater relative to mean sea level. Rain intensity from March 2019 is missing. 110

Figure C1. Relationship between nitrate concentration reduction between the bioretention inlet and underdrain outlet and average daily temperature during each monitored storm. The green line shows a linear regression with corresponding equation, R^2 and p values at the top of the figure. 113
Figure C2. Relationship between TN concentration reduction between the bioretention inlet and underdrain outlet and average daily temperature during each monitored storm. The blue line shows a linear regression with corresponding equation, R^2 and p values at the top of the figure. 114
Figure C3. Relationship between DOC concentration reduction between the bioretention inlet and underdrain outlet and average daily temperature during each monitored storm. The blue line shows a linear regression with corresponding equation, R^2 and p values at the top of the figure. 115
Figure C4. Relationship between bioretention nitrate concentration reduction between inlet and outlet and changes in $\delta^{15}N\text{-}NO_3^-$ (top) and $\delta^{18}O\text{-}NO_3^-$ (bottom) from inlet to outlet during each monitored storm. Colored lines show linear regressions with corresponding equations, R^2 and p values listed. 118
Figure C5. Relationship between sample $\delta^{15}N\text{-}NO_3^-$ and $\delta^{18}O\text{-}NO_3^-$ for the bioretention inlet (top) and outlet (bottom) during each monitored storm. Colored lines show linear regressions with corresponding equations, R^2 and p values listed. 119

Figure C6. Relationship between the fraction of nitrate concentration remaining in water and the enrichment of $\delta^{15}N\text{-}NO_3^-$ in systems with different enrichment factors (ε). These curves are used to estimate the percentage of nitrate concentration reduction that denitrification is responsible for (as shown). The blue circle and red triangle show the two events with denitrification isotope trends with their calculated denitrification percentages in parenthesis. 120

List of Tables

Table 2.1. Lorton Road GI design parameters. 14

Table 3.1. Average concentrations, standard error (SE), and *p-values* of concentrations, and total loads of Cl^-, Na^+, K^+, Mg^{2+}, and Ca^{2+} in and out of the bioretention and bioswale. Average concentration reductions and total load reductions are calculated as percent change in vs. out. *p-values* approximately less than or equal to 0.05 are in bold. 47

Table 4.1. Engineering specifications of the Lorton Road bioretention study site. 65

Table A1. Vegetation planting palette for Lorton Road GI. 91
Table A2. Storm sample representation percentages (**Equation A5**) and number of samples in each flow-weighted composite sample at each of the five monitoring locations for each storm. * indicates a grab sample. 94
Table A3. Weather conditions from monitored precipitation events. * indicates missing data... 95
Table A4. Monitored and calculated stormwater runoff volumes at all monitoring locations and calculated runoff reductions for each GI during each monitored event...................................... 96
Table A5. Calculated loads of nitrate, TDN, DOC, phosphate, TP, and TSS travelling through each monitoring location per storm event as well as load reductions for each GI. 96

Table B1. Storm sample representation percentages (**Appendix A Equation A5**) and number of samples in each flow-weighted composite sample at each of the five monitoring locations for each storm. * indicates a grab sample.. 101
Table B2. Weather conditions from monitored precipitation events. * indicates missing data. 102
Table B3. Stormwater runoff volumes at each monitoring location per precipitation event and runoff reductions (per event and cumulative)... 103
Table B4. Stormwater EMCs of Cl^-, $Ca2^+$, Mg^{2+}, and K^+ for each monitored event in the bioretention (top) and bioswale (bottom). 104

Table C1. Weather conditions from monitored precipitation events. * indicates missing data. 111
Table C2. Concentrations of nitrate, TN, and DOC in all stormwater samples as well as concentration reductions and the nitrate percentage of TN concentration. * indicates missing data.. 112
Table C3. Stormwater runoff volumes at the three monitoring locations and calculated bioretention runoff reductions for each monitored event. 116
Table C4. Calculated loads of nitrate, TN, and DOC through each monitoring location over each storm as well as load reductions and the nitrate percentage of TN load. * indicates missing data. 117

Acknowledgements

The following research is the result of the teamwork of many students and faculty at UVA and beyond. I am truly thankful for the help of so many people that made this work possible.

First, I thank my advisor, Dr. James Smith for giving me the opportunity to work on this project for the past five years. Your calm guidance and expertise has been very appreciated. Working with and learning from you has been an incredible experience.

None of this work would be possible without the contributions of my co-researchers, Dr. Derek Henderson, Gail Hayes, and Wuhuan Zhang. Derek's work paved the way for this project and I'm very thankful to have the opportunity to build off of what he started. Gail and Wuhuan, this work wouldn't be possible (or nearly as enjoyable) without your indispensable help. It's been such a pleasure to work with you all.

Thanks also to the Virginia Transportation Research Council (VTRC), and especially Dr. Michael Fitch and Lewis Lloyd for your support. VTRC's support of this project has meant so much to our research team and I've greatly appreciated your perspectives and guidance.

My dissertation committee members, Dr. Lisa Colosi Peterson, Dr. Teresa Culver, Dr. Jon Goodall, and Dr. Stephen Macko, have helped guide this research and have all been fantastic mentors. I'm very grateful that each of you has been a part of my research journey. Thank you all so much for taking the time to make our research better.

Several undergraduate students have also helped us along the way. Thanks to Cecil Johnson and Brett Conklin for dependable field research support. And thanks to Leah Scully and Tyler Privott for your work on phosphorus retention.

Thanks also to all the greater members of the Smith Water Quality Research Group I've had the pleasure to know over the past five years. It's been great discussing research progress/struggles with you all. Best of luck and looking forward to hearing about all your future research endeavors!

Finally, thanks to my family, friends, and girlfriend for their unwavering support throughout this experience. I'm so privileged to have you all in my life.

Related Publications and Presentations

The following publications are planned for the research presented in this dissertation:

1. **Chapter 1**: Henderson, D.; Hayes, G.; Burgis, C.; Smith, J. A. Low Impact Development Technologies for Highway Stormwater Runoff. In *Encyclopedia of Water: Science, Technology, and Society*; Wiley, 2019; pp 1–18. https://doi.org/10.1002/9781119300762.wsts0009.

2. **Chapter 2**: Hayes, G. M., Burgis, C., Zhang, W., Henderson, D., Smith, J.A. (2020) "Runoff reduction by four green stormwater infrastructure systems in a shared environment." *J. Sust. Water in the Built Env.* (*under review*).

3. **Chapter 2**: Burgis, C.R., Hayes, G., Henderson, Zhang, W., D.A., Smith, J.A. (2020) "Evaluation of Green Stormwater Infrastructure Options for Transportation Water Quality Improvement." (*in preparation*)

4. **Chapter 3**: Burgis, C.R., Hayes, G., Henderson, D.A., Zhang, W., Smith, J.A. (2020) "Green Stormwater Infrastructure Redirects Deicing Salt from Surface Water to Groundwater." *Sci. Total Environ.* (*under review*)

5. **Chapter 4**: Burgis, C.R., Hayes, G., Zhang, W., Henderson, D.A., Macko, S.A., Smith, J.A. (2020) "Tracking Denitrification in Green Stormwater Infrastructure with Dual Nitrate Stable Isotopes." (*manuscript in preparation*)

This dissertation has resulted in the following presentations:

1. Burgis, C.R., Hayes, G., Zhang, W., Smith, J.A. "Tracking Denitrification in Green Stormwater Infrastructure with Nitrogen and Oxygen Stable Isotopes." ASCE International Low Impact Development Conference. July 19-22, 2020, Bethesda, MD (*accepted podium presentation*)

2. Burgis, C.R., Hayes, G., Henderson, D.A., Zhang, W., Smith, J.A. "Green Stormwater Infrastructure Buffers Surface Water from Deicing Salt Loading." ASCE International Low Impact Development Conference. July 19-22, 2020, Bethesda, MD (*accepted podium presentation*)

3. Burgis, C. R., Hayes, G., Zhang, W., Smith, J.A., "Tracking Denitrification in Green Stormwater Infrastructure." Lectern presentation at the University of Virginia Global Water Initiative Graduate Research Symposium. Charlottesville, VA, November 2019.

4. Zhang, W., Burgis, C., Hayes, G. M., Henderson, D., Smith, J.A., "Water Quality Performance of Green Stormwater Infrastructure along Lorton Road." Session 11. Poster presentation at the American Water Resources Association's Annual Water Resources Conference. Salt Lake City, Utah, November 2019.

5. Hayes, G. M., Burgis, C., Zhang, W., Henderson, D., Smith, J.A., "Comparing flow reductions of four green infrastructure systems in a roadside environment and early results from groundwater monitoring receiving infiltrated runoff." Session 12. Lectern presentation at the American Water Resources Association's Annual Water Resources Conference. Salt Lake City, Utah, November 2019.

6. Hayes, G. M., Burgis, C., Henderson, D., Smith, J.A., "Low-Impact Development for Roadside Stormwater Management: Performance of Several Stormwater Control Techniques in a Shared Watershed." P19-20488. Lectern presentation at Transportation Research Board Annual Meeting. Washington, DC, January 2019.

7. Burgis, C.R., Hayes, G., Henderson, D.A., Smith, J.A. "Assessment of Green Stormwater Infrastructure Practices on Lorton Road, Fairfax County, VA." ASCE International Low Impact Development Conference. August 12-15, 2018, Nashville, TN (*podium presentation*)

8. Burgis, C.R., Hayes, G., Henderson, D.A., Smith, J.A., Fitch, M. "Assessment of Green Stormwater Infrastructure Performance on Lorton Road." VDOT Virginia Transportation Research Center Environmental Research Advisory Council. June 8th, 2018, Richmond, VA

9. Burgis, C.R. "How Does Green Stormwater Infrastructure Handle Road Salt?" Poster presentation at the University of Virginia Engineering Research Symposium. March 22nd, 2018, Charlottesville, VA

10. Burgis, C.R., Hayes, G., Henderson, D.A., Smith, J.A., Fitch, M. "Assessment of the Low Impact Development Strategies Used for the Lorton Road Widening Project." VDOT Virginia Transportation Research Center Environmental Research Advisory Council. June 12th, 2017, Richmond, VA

Chapter 1: Introduction

Work from this chapter was published as an encyclopedia chapter:

Henderson, D.; Hayes, G.; Burgis, C.; Smith, J. A. Low Impact Development Technologies for Highway Stormwater Runoff. In *Encyclopedia of Water: Science, Technology, and Society*; Wiley, 2019; pp 1–18. https://doi.org/10.1002/9781119300762.wsts0009.

1.1 Introduction

Urbanization has led to more impervious surfaces covering natural landscapes. During storm events, these surfaces accumulate stormwater and convey it to storm sewers, changing the natural hydrologic cycle. Sudden discharges of stormwater from impervious surfaces can result in flooding, higher runoff volumes and peak flow rates, erosion, and pollution into receiving waters[1–4]. Additionally, in urban areas with combined stormwater-wastewater sewers, high stormwater flows can lead to combined sewer overflows. Urban stormwater runoff has been shown to be detrimental to ecosystem health. In recent decades, non-point source pollution has become the leading threat to aquatic ecosystem habitats in the US and other highly developed countries[5,6].

One setting where stormwater is a concern is linear transportation systems, particularly highways, where large impervious roads create significant stormwater runoff [7,8]. Stormwater carries pollutants from tires, brakes, engine wear, fuel, lubricating fluids of vehicles, road materials, and road maintenance into the environment [9,10]. Managing stormwater runoff from highways has become a primary goal of many departments of transportation as it is a major factor affecting water quality degradation. Common contaminants in highway stormwater runoff include sediment, nutrients, salt, dissolved organic carbon, oil and grease, and metals such as copper, lead and zinc [7,11–14]. Studies have suggested that even though highways may only compose 5-8% of an urban catchment area, highway drainage area can contribute as much as

50% of TSS, 16% of total hydrocarbons, and 35% - 75% of the total metal input budgets to receiving waters[15]. Conventional stormwater infrastructure immediately conveys stormwater to storm sewers and receiving waters, without treatment. Particularly in highway settings, stormwater is removed as quickly as possible from roads to minimize road flooding related vehicle safety issues.

In the 1990s, green infrastructure (GI), also known as low impact development (LID), emerged as an alternative to conventional stormwater management. GI mimics natural landscape hydrologic conditions by slowing, spreading, and infiltrating urban stormwater runoff before discharging it to receiving waters. This is done using a variety of landscape features that encourage retention, detention, settling, filtration, and biological interaction of stormwater runoff. The U.S. Environmental Protection Agency describes GI as site design strategy with the goal of maintaining or replicating the pre-development hydrologic regime through the use of design techniques to create a functionally equivalent hydrologic landscape. Hydrologic functions of storage, infiltration, and groundwater recharge, as well as the volume and frequency of discharges are maintained through the use of integrated and distributed micro-scale (decentralized, non-point source) stormwater retention and detention areas, reduction of impervious surfaces, and the lengthening of flow paths and runoff time[2,16–18]. Many GI strategies have been shown to be effective at protecting waterways from the detrimental effects of urban stormwater, while also potentially providing economic, social, and public health benefits to urban communities[17–22].

1.2 Types of Transportation Green Infrastructure in this Study

Common GI designs are outlined below. This information is intended as a general guideline as terminology, usage, and performance vary by region. Similarly, the stormwater regulations that often guide the design of GI vary with location and are changing over time. Ideally, GI is designed to fit site specific characteristics (e.g. climate, soil quality, watershed area, expected pollutants, regulations).

1.2.1 Swales

Grass channels, also known as vegetated swales, grassy swales, and grass lined channels, are vegetated, open-channel management practice designed specifically to treat and attenuate runoff for a specified water quality volume. In addition to water quality improvement, grass channels provide concentrated flow stormwater conveyance. Pollutant removal is primarily achieved by sedimentation and filtration of particulate matter. High density vegetative cover provides resistance to flow, decreasing flow velocity and thereby improving sedimentation efficiency. Grass channels are particularly well suited for highways and rural road implementation due to their linear nature[23]. Grass channels may employ check dams for increased water retention and compost amended soils for improved soil structure and stormwater infiltration rate[24].

In a study of Grass channels in Texas, a removal efficiency of 35% for total nitrogen and 37% for total phosphorus was observed[13]. Davis et al. (2012) found that vegetated swales including check dams, significantly reduced runoff volume during rain events totaling less than 3 cm of rainfall[25]. Larger rain events resulted in virtually no runoff reduction, acting instead as a means of stormwater conveyance. A study by Stagge et al. (2012) reported event mean concentration (EMC) removal efficiency of 65-71% of total suspended solids and 30-60% of zinc[26].

Bioswales, also commonly referred to as dry swales, are swales with an underlying engineered soil media for enhanced runoff volume reduction due to an improved infiltration rate and retention volume provided by the void space of the soil media. This arrangement can also lead to improved water quality as the infiltrated stormwater is filtered by the soil matrix. Underlying native soils and/or construction fill may not provide sufficient infiltration rates to adequately drain the engineered soil media, so an underdrain system consisting of perforated pipe within a gravel sump is often used to ensure adequate drainage (particularly for sites with C or D category soils). The underdrain generally discharges directly to a storm sewer system or to receiving waters. The engineered soil media may contain compost amendment. Bioswales have been found to provide total runoff reduction between 78% - 98% and concentration reductions of 73% - 88% for TSS, 61% - 77% for TN, and 61% - 79% for TP[27,28].

1.2.2 Bioretention

Bioretention is a GI practice which detains stormwater runoff in a shallow, vegetated depression and then rapidly infiltrates it into an underlying layer of engineered soil media[29]. Bioretention filters are designed to allow for a limited ponding above the topsoil layer. Infiltration through the engineered soil media provides an environment for pollutant removal due to filtration, plant uptake, and biological activity. In addition to effective reduction of EMC of suspended solids, metals, and sometimes nutrients, bioretention filters achieve moderate to high levels of runoff reduction, which further decrease pollutant load transport to receiving waters[30]. As with other GI, Bioretention engineered soil media may incorporate compost.

Bioretention performance has been reported to have significant variability, but Virginia Department of Environmental Quality stormwater design specifications consider bioretention capable of 40% runoff reduction, 64% total nitrogen load reduction, and 55% total phosphorus load reduction for a level one design and 80% runoff volume reduction, 90% total nitrogen load reduction, and 90% target total phosphorus load reduction for a level two design[30–34]. Although nutrient reductions by bioretention have been documented, Hurley et al. (2017) reported significant nutrient leaching from compost used in bioretention (or other GI) soil[24,34].

1.3 Research Objectives

This dissertation aims to explore the performance of a variety of modern GI practices over an annual range of weather conditions and storm events along Lorton Road in Northern Virginia. There are three primary objectives of this research: (1) compare overall performance of four different GI designs (Chapter 2), (2) determine the transport and attenuation of deicing salt in infiltration-based GI (Chapter 3), and (3) track denitrification within GI using dual stable nitrate isotope analysis (Chapter 4). The remainder of the dissertation documents these three objectives. Knowledge gained from this research will immediately aid stormwater managers in the selection of GI practices and improve future GI designs, helping to manage water resources, revitalize urban aquatic ecosystems, and protect public health.

1.4 References

(1) Dhakal, K. P.; Chevalier, L. R. Urban Stormwater Governance: The Need for a Paradigm Shift. *Environ. Manage.* **2016**, *57* (5), 1112–1124. https://doi.org/10.1007/s00267-016-0667-5.

(2) Ahiablame, L. M.; Engel, B. A.; Chaubey, I. Effectiveness of Low Impact Development Practices in Two Urbanized Watersheds: Retrofitting with Rain Barrel/Cistern and Porous Pavement. *J. Environ. Manage.* **2013**, *119*, 151–161. https://doi.org/10.1016/j.jenvman.2013.01.019.

(3) United States Environmental Protection Agency (USEPA). NPDES Stormwater Program https://www.epa.gov/npdes/npdes-stormwater-program (accessed Feb 8, 2018).

(4) Wardynski, B. J.; Winston, R. J.; Line, D. E.; Hunt, W. F. Metrics for Assessing Thermal Performance of Stormwater Control Measures. *Ecol. Eng.* **2014**, *71*, 551–562. https://doi.org/10.1016/J.ECOLENG.2014.07.068.

(5) Walsh, C. J.; Roy, A. H.; Feminella, J. W.; Cottingham, P. D.; Groffman, P. M.; Morgan Ii, R. P. The Urban Stream Syndrome: Current Knowledge and the Search for a Cure. *Benthol. Soc* **2005**, *24* (3), 706–723.

(6) Spromberg, J. A.; Baldwin, D. H.; Damm, S. E.; Mcintyre, J. K.; Huff, M.; Sloan, C. A.; Anulacion, B. F.; Davis, J. W.; Scholz, N. L. EDITOR'S CHOICE: Coho Salmon Spawner Mortality in Western US Urban Watersheds: Bioinfiltration Prevents Lethal Storm Water Impacts. *J. Appl. Ecol.* **2016**, *53* (2), 398–407. https://doi.org/10.1111/1365-2664.12534.

(7) Rotaru, C.; Woodard, T. L.; Choi, S.; Nevin, K. P. Spatial Heterogeneity of Bacterial Communities in Sediments from an Infiltration Basin Receiving Highway Runoff. *Microb. Ecol.* **2012**, *64* (2), 461–473. https://doi.org/10.1007/s00248-012-0026-x.
(8) Kim, L.-H.; Kayhanian, M.; Zoh, K.-D.; Stenstrom, M. K. Modeling of Highway Stormwater Runoff. *Sci. Total Environ.* **2005**, *348* (1–3), 1–18. https://doi.org/10.1016/J.SCITOTENV.2004.12.063.
(9) OREGON STATE UNIVERSITY, GEOSYNTEC CONSULTANTS, UNIVERSITY OF FLORIDA, THE LOW IMPACT DEVELOPMENT CENTER, I. Evaluation of Best Management Practices for Highway Runoff Control. *Transp. Res. Board* **2006**.
(10) United States Environmental Protection Agency (US EPA). Stormwater Discharges from Transportation Sources https://www.epa.gov/npdes/stormwater-discharges-transportation-sources (accessed Feb 8, 2018).
(11) Barrett, M. E.; Irish, L. B.; Malina, J. F.; Charbeneau, R. J. Characterization of Highway Runoff in Austin, Texas, Area. *J. Environ. Eng.* **1998**, *124* (2), 131–137. https://doi.org/10.1061/(ASCE)0733-9372(1998)124:2(131).
(12) Li, M.-H.; Barrett, M. E.; Rammohan, P.; Olivera, F.; Landphair, H. C. Documenting Stormwater Quality on Texas Highways and Adjacent Vegetated Roadsides. *J. Environ. Eng.* **2008**, *134* (1), 48–59. https://doi.org/10.1061/(ASCE)0733-9372(2008)134:1(48).
(13) Walsh, P. M.; Barrett, M. E.; Joseph, P. E.; Malina, F.; Randall, P. E.; Charbeneau, J. *USE OF VEGETATIVE CONTROLS FOR TREATMENT OF HIGHWAY RUNOFF*; 1997.
(14) Yu, S. L.; Barnes, S. L.; Gerde, V. W. Testing of Best Management Practices for Controlling Highway Runoff. *FHWA/VA-93-R16* **1993**.
(15) Ellis, J. B.; Revitt, D. M.; Shutes, R. B. E.; Langley, J. M. The Performance of Vegetated Biofilters for Highway Runoff Control. *Sci. Total Environ.* **1994**, *146/147*, 543–550.
(16) US EPA. What is Green Infrastructure? https://www.epa.gov/green-infrastructure/what-green-infrastructure (accessed Mar 20, 2020).
(17) Coffman, L. *Low-Impact Development Design Strategies An Integrated Design Approach*; Prince George's County, Maryland, 2000.
(18) Vogel, J. R.; Moore, T. L.; Coffman, R. R.; Rodie, S. N.; Hutchinson, S. L.; McDonough, K. R.; McLemore, A. J.; McMaine, J. T. Critical Review of Technical Questions Facing Low Impact Development and Green Infrastructure: A Perspective from the Great Plains. *Water Environ. Res.* **2015**, *87* (9), 849–862. https://doi.org/10.2175/106143015X14362865226392.
(19) Morse, N. R.; Mcphillips, L. E.; Shapleigh, J. P.; Walter, M. T.; Wrigley, J. A. The Role of Denitrification in Stormwater Detention Basin Treatment of Nitrogen. *Environ. Sci. Technol. 2017,* **2017**, *51*, 7928−7935. https://doi.org/10.1021/acs.est.7b01813.
(20) Kramer, M. G. *Enhancing Sustainable Communities with Green Infrastructure (EPA 100-R-14-006)*; 2014.
(21) McIntyre, J. K.; Davis, J. W.; Hinman, C.; Macneale, K. H.; Anulacion, B. F.; Scholz, N. L.; Stark, J. D. Soil Bioretention Protects Juvenile Salmon and Their Prey from the Toxic Impacts of Urban Stormwater Runoff. *Chemosphere* **2015**, *132*, 213–219. https://doi.org/10.1016/j.chemosphere.2014.12.052.
(22) McIntyre, J. K.; Davis, J. W.; Incardona, J. P.; Stark, J. D.; Anulacion, B. F.; Scholz, N. L. Zebrafish and Clean Water Technology: Assessing Soil Bioretention as a Protective Treatment for Toxic Urban Runoff. *Sci. Total Environ.* **2014**, *500*, 173–180. https://doi.org/10.1016/j.scitotenv.2014.08.066.

(23) Virginia Department of Environmental Quality. *VIRGINIA DEQ STORMWATER DESIGN SPECIFICATION No. 3 GRASS CHANNELS*; 2013.
(24) Hurley, S.; Shrestha, P.; Cording, A. Nutrient Leaching from Compost: Implications for Bioretention and Other Green Stormwater Infrastructure. *J. Sustain. Water Built Environ.* **2017**, *3* (3), 04017006. https://doi.org/10.1061/JSWBAY.0000821.
(25) Davis, A. P.; Stagge, J. H.; Jamil, E.; Kim, H. Hydraulic Performance of Grass Swales for Managing Highway Runoff. *Water Res.* **2012**, *46* (20), 6775–6786. https://doi.org/10.1016/J.WATRES.2011.10.017.
(26) Stagge, J. H.; Davis, A. P.; Jamil, E.; Kim, H. Performance of Grass Swales for Improving Water Quality from Highway Runoff. *Water Res.* **2012**, *46* (20), 6731–6742. https://doi.org/10.1016/J.WATRES.2012.02.037.
(27) Xiao, Q.; McPherson, E. G. Performance of Engineered Soil and Trees in a Parking Lot Bioswale. *Urban Water J.* **2011**, *8* (4), 241–253. https://doi.org/10.1080/1573062X.2011.596213.
(28) Jiang, C.; Li, J.; Li, H.; Li, Y.; Chen, L. Field Performance of Bioretention Systems for Runoff Quantity Regulation and Pollutant Removal. *Water, Air, Soil Pollut. 2017 22812* **2017**, *228* (12), 1–13. https://doi.org/10.1007/S11270-017-3636-6.
(29) Li, M.-H.; Swapp, M.; Kim, M. H.; Chu, K.-H.; Sung, C. Y. Comparing Bioretention Designs With and Without an Internal Water Storage Layer for Treating Highway Runoff. *Water Environ. Res.* **2014**, *86* (5), 387–397. https://doi.org/10.2175/106143013X13789303501920.
(30) Virginia Department of Environmental Quality. *VIRGINIA DEQ STORMWATER DESIGN SPECIFICATION No. 9 BIORETENTION*; 2013.
(31) Line, D. E.; Hunt, W. F. Performance of a Bioretention Area and a Level Spreader-Grass Filter Strip at Two Highway Sites in North Carolina. *J. Irrig. Drain. Eng.* **2009**, *135* (2), 217–224. https://doi.org/10.1061/(ASCE)0733-9437(2009)135:2(217).
(32) Brown, R. A.; Hunt, W. F. Underdrain Configuration to Enhance Bioretention Exfiltration to Reduce Pollutant Loads. *J. Environ. Eng.* **2011**, *137* (11), 1082–1091. https://doi.org/10.1061/(ASCE)EE.1943-7870.0000437.
(33) Li, L.; Davis, A. P. Urban Stormwater Runoff Nitrogen Composition and Fate in Bioretention Systems. *Environ. Sci. Technol.* **2014**, *48* (6), 3403–3410. https://doi.org/10.1021/es4055302.
(34) Shrestha, P.; Hurley, S. E.; Wemple, B. C. Effects of Different Soil Media, Vegetation, and Hydrologic Treatments on Nutrient and Sediment Removal in Roadside Bioretention Systems. *Ecol. Eng.* **2018**, *112*, 116–131. https://doi.org/10.1016/J.ECOLENG.2017.12.004.

Chapter 2: Evaluation of Green Stormwater Infrastructure Options for Transportation Water Quality Improvement

This study will result in two publications. The first manuscript is focused on stormwater runoff volume reduction and is under review by the Journal of Sustainable Water in the Built Environment. The second focuses on stormwater quality performance and is in preparation.

(1) Hayes, G. M., Burgis, C., Zhang, W., Henderson, D., Smith, J.A. (2020) "Runoff reduction by four green stormwater infrastructure systems in a shared environment." *J. Sust. Water in the Built Env.* (*under review*).

(2) Burgis, C.R., Hayes, G., Henderson, Zhang, W., D.A., Smith, J.A. (2020) "Evaluation of Green Stormwater Infrastructure Options for Transportation Water Quality Improvement." (*in preparation*)

2.1 Introduction

Non-point source pollution, like stormwater runoff, has become a leading threat to the quality of water resources and aquatic ecosystems near highly developed watersheds[1,2]. Sudden discharges of stormwater from paved surfaces results in flooding, erosion, sewer overflows, and pollution into receiving waters [1,3–6]. Improved stormwater management is needed to protect global water resources. As efforts have increased to limit the impact of land use development on water quality impairment, stormwater regulations have arisen, generally based on total maximum daily load (TMDL) studies. In the Chesapeake Bay Watershed, stormwater from transportation surfaces is regulated under the Chesapeake Bay TMDL, based on nitrogen, phosphorus, and total suspended solids (TSS) load reductions[7].

Green infrastructure (GI) is a promising stormwater management technique with potential to ameliorate many of these problems[2,8–11]. GI (e.g. bioretention, swales, green roofs) is designed to return an area to pre-development hydrology by slowing, spreading, and infiltrating stormwater runoff before discharging it to receiving waters. GI mimics natural landscape features, employing physical (e.g. settling and filtration) and biological (e.g. plant uptake and microbial cycling) processes to remove pollutants from stormwater. GI is increasingly designed into urban landscapes to protect waterways from detrimental effects of urban stormwater, while also potentially providing economic, social, and public health benefits to urban communities [9,10,12–15]. However, GI is also a relatively new and still developing technology with many performance knowledge gaps.

There are many different GI designs with sometimes greatly varying levels of stormwater management performance[16–24]. Additionally, GI performance can be dependent on watershed, storm event, local climate, and maintenance characteristics[20,25]. Studies have documented the performance of individual GI designs, but few have compared multiple GI designs side by side in the same location and climate. The evaluation of the performance of different operational GI designs receiving similar stormwater runoff conditions is needed to minimize climate and watershed variance and help guide watershed managers in GI selection.

This study compares the performance of four different GI designs (Bioretention, Grass channel, compost amended grass channel, and bioswale) receiving the same weather conditions along Lorton Road in Northern Virginia. GI performance was assessed based on stormwater quality improvements, including nitrogen, phosphorus, TSS, and DOC. Stormwater runoff volumes and water quality parameter concentrations were measured at inlets and outlets of each GI during 27 storm events in all seasons over 14 months. We use this information to evaluate the GI designs based on water quality concentration and load reduction criteria and determine the relationship between GI design and stormwater management performance. We also suggest ways to improve future GI designs and highlight areas in need of further study.

2.2 Materials and Methods

2.2.1 Study Site

Four GI practices, a bioretention basin (hereafter bioretention), a grass channel (GC), a compost-amended grass channel (CAGC), and a bioswale, were monitored along Lorton Road, in Fairfax County, Virginia. The bioretention is north of Lorton Road, the CAGC (also north of the road) is 0.4 km east of the bioretention, while the GC and bioswale are 0.8 km east of the Bioretention, on the south side of the road (**Figure 2.1**). All GI practices were designed for 1 year, 24 hour frequency storms and their construction was completed in spring 2017. Maintenance was performed bi-annually (once in spring and once in fall) to remove trash, mow roadside grass slopes, clear decaying vegetation, and maintain mulch levels (where applicable). Lorton Road is a four-lane divided road with an average daily traffic volume of 100,000 vehicles/day[26] and is part of the Giles Run watershed, within the Chesapeake Bay watershed.

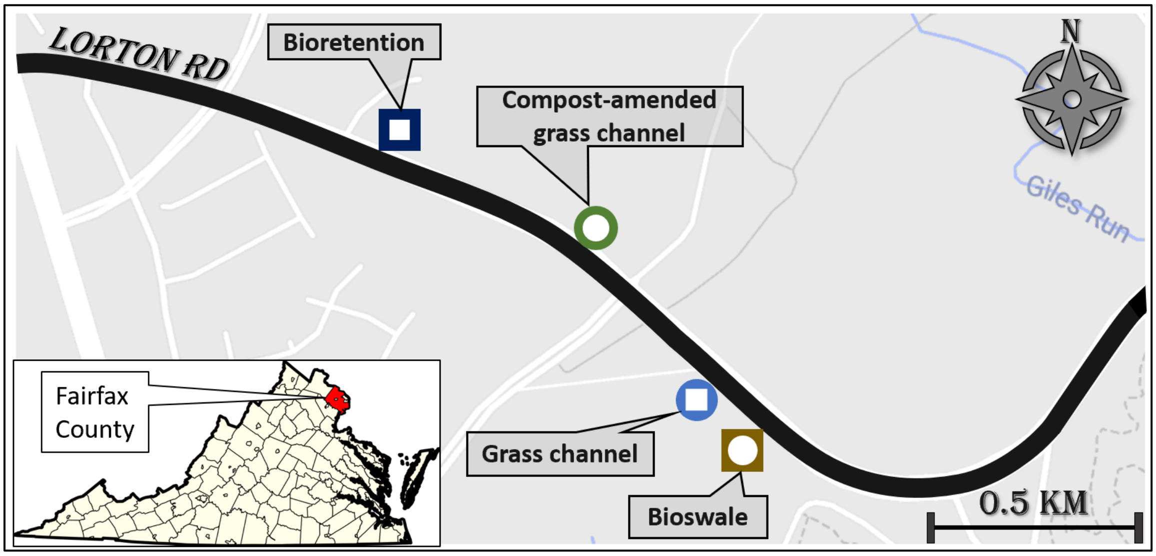

Figure 2.1. Lorton Road stormwater research site and positioning of four GI types. Map from Hayes et al. (2020).

The bioretention (**Figure 2.2**) has a 47,753 m^2 contributing drainage area (CDA), 35% of which is impervious road surface. Concentrated stormwater from Lorton Road is conveyed to the bioretention via curb and gutters. Stormwater first flows into a forebay before traveling into a basin with engineered soil media (ESM) on top of underlying gravel. An underdrain at the top of the gravel layer drains the basin. For larger than designed precipitation events, a channel in the forebay allows overflow stormwater to bypass the basin. Engineering specifications of the bioretention are further detailed in **Table 2.1**. Both the basin and the forebay utilize a variety of sedges, wildflowers, trees, and shrubs (**Appendix A Table A1**).

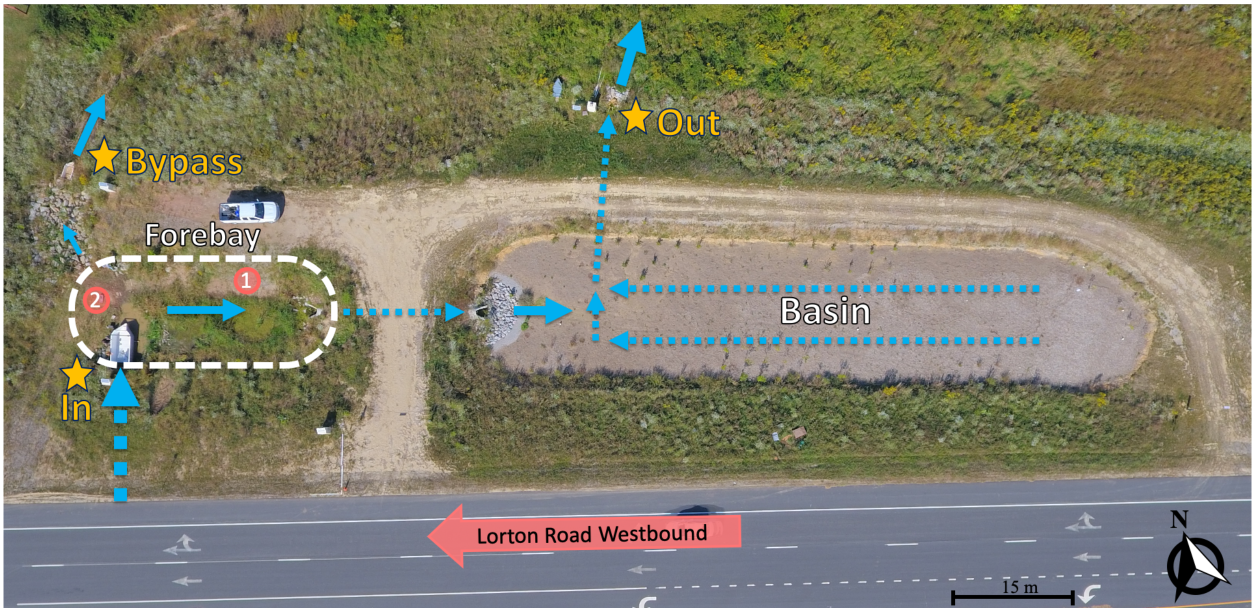

Figure 2.2. Bioretention north of Lorton Road. Solid blue lines indicate surface stormwater flow direction, while dotted blue lines show underground drains. Orange stars indicate stormwater monitoring locations and red circles show groundwater monitoring wells.

The grass channel (GC) (**Figure 2.3**) has a CDA of 2,266 m^2 (39% impervious). Stormwater enters the GC as sheet flow from Lorton Road (and a sidewalk) and is infiltrated though the existing native soil of the site along the 85-m-long, 1:20 linear sloped swale. Three wooden check dams intercept stormwater along the swale, encouraging infiltration. The GC utilizes a variety of grasses and wildflowers (**Appendix A Table A1**). Engineering specifications of the GC are further detailed in **Table 2.1**.

The compost-amended grass channel (CAGC) (**Figure 2.3**) has a CDA of 6,070 m^2 (18% impervious). Stormwater enters the CAGC as sheet flow from Lorton Road and is infiltrated though the existing native soil of the site along the 232-m-long, 1:60 linear sloped swale. Six wooden check dams intercept stormwater along the swale, encouraging infiltration. The CAGC utilizes a variety of grasses, wildflowers, trees, and shrubs (**Appendix A Table A1**). Engineering specifications of the CAGC are further detailed in **Table 2.1**.

The bioswale (**Figure 2.3**) has a CDA of 1,943 m^2 (40% impervious). Stormwater enters the bioswale as sheet flow from Lorton Road (and a sidewalk) and is infiltrated though ESM (the same soil used in the bioretention) and underlying gravel along the 65-m-long, 1:27 linear sloped swale. Six wooden check dams intercept stormwater along the swale, encouraging infiltration. An underdrain at the top of the gravel layer drains the soil and gravel. The bioswale utilizes a variety of grasses, sedges, wildflowers, trees, and shrubs (**Appendix A Table A1**). Engineering specifications of the bioswale are further detailed in **Table 2.1**.

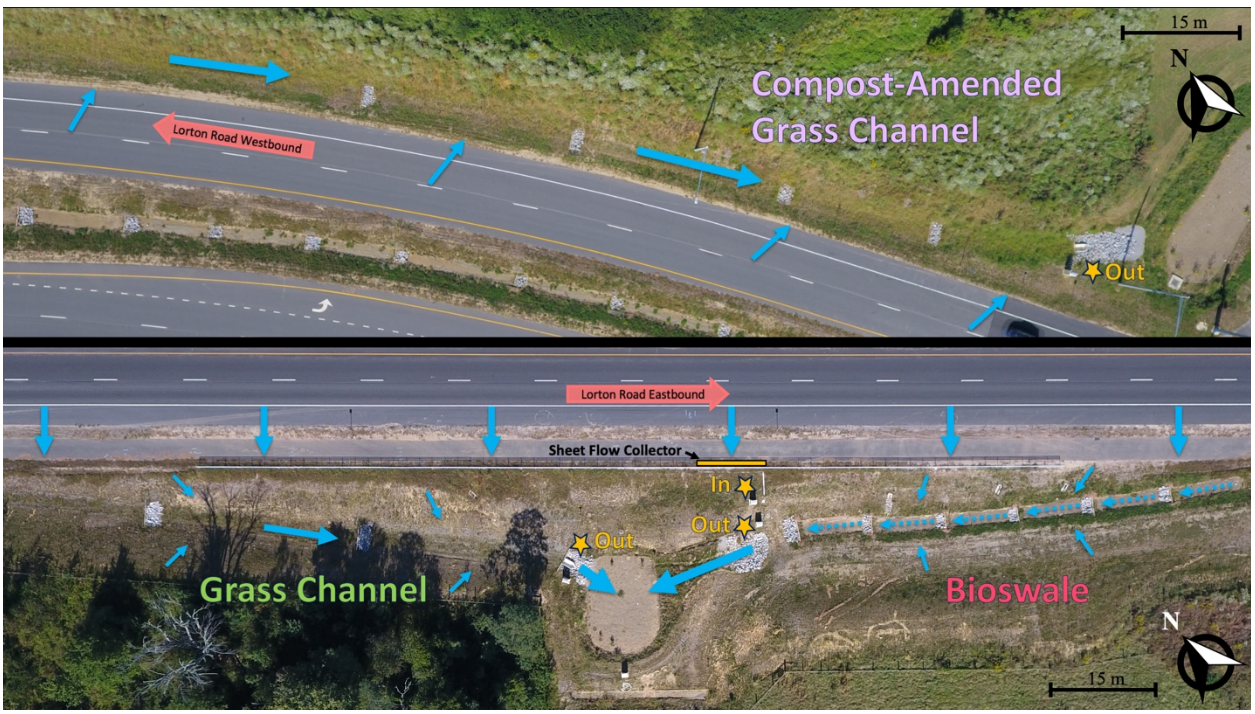

Figure 2.3. Compost-amended grass channel north of Lorton Road (top) and grass channel and bioswale south of Lorton Road (bottom). Solid blue lines indicate stormwater surface flow direction, while dotted black lines show the bioswale underdrain. Orange stars indicate stormwater monitoring locations and the orange rectangle shows the position of the sheet flow collector.

Table 2.1. Lorton Road GI design parameters.

Design Parameter	Units	Bioretention	Grass Channel	Compost-Amended Grass Channel	Bioswale
CDA	m2	47,753	2,266	6,070	1,943
Impervious CDA	%	35	39	18	40
GI footprint	m2	1,012	121	364	81
CDA:footprint	ratio	47.2	18.7	16.7	24.0
Engineered storage volume	m3	447	2.2	8	55
Ponding depth	cm	15.2	N/A	N/A	N/A
CDA land use		roadway, residential, grass, woods	roadway, sidewalk, grass	roadway, grass	roadway, sidewalk, grass
Stormwater inflow		curb and gutter sewer	sheetflow	sheetflow	sheetflow
Stormwater outflow		10 cm diameter basin underdrain + bypass channel	swale channel	swale channel	10 cm diameter underdrain
Mulch depth	cm	5	N/A	N/A	N/A
Engineered soil depth	cm	76	N/A	N/A	46
Underlying gravel depth	cm	40	N/A	N/A	40
Engineered soil makeup		sand, topsoil, compost (5%)	native soil	compost amended native soil (5 cm layer tilled to 30.5 cm depth)	sand, topsoil, compost (5%)
Engineered soil particle distrubution		91.2% sand, 5.6% silt, 3.2% clay	N/A	N/A	91.2% sand, 5.6% silt, 3.2% clay
Vegetation type (see Table A1 for species)		trees, shrubs, sedges, wildflowers	grasses, wildflowers	trees, shrubs, grasses, wildflowers	trees, shrubs, grasses, sedges wildflowers
Length	m	N/A	85	232	65
Base-width	m	N/A	1.5	1.5	1.5
Linear slope	rise/run	N/A	1:20	1:60	1:27
Side slopes	rise/run	N/A	4:1	5:1	5:1
# wooden check dams		N/A	3	6	6
Check dam height	cm	N/A	30.5	15	30.5

2.2.2 Stormwater Field Monitoring

We monitored 26 rain and snow events at the bioretention between April 2018 and June 2019, 16 events at the GC between June 2018 and June 2019, 16 events at the CAGC between June 2018 and June 2019, and 15 events at the bioswale between May 2018 and June 2019 (detailed weather conditions in **Appendix A Table A3**). Monitoring was attempted for all four GI each event, but not all monitoring locations produced successful samples every event (hence the different number of storms monitored). A tipping bucket rain gauge next to the bioretention recorded 10-minute precipitation data with a 0.025 cm measurement resolution. Only rain events with more than 0.25 cm of precipitation and at least 12 hours of no precipitation preceding each event were monitored. This rule did not apply for snow/snow melt events. If the rain gauge malfunctioned, publicly available weather data from the nearest weather station were used.

At each GI monitoring location, stormwater runoff flow rate and water quality parameter concentrations were determined to calculate the mass of pollutants traveling in and out of the bioretention and bioswale. Runoff flow rates were measured using custom sized flumes at each monitoring location to intercept stormwater flow from the road, pipe, or channel. Ultrasonic sensors measured the height of water in each flume and stormwater flow rates were calculated by solar powered Hach AS950 autosamplers based on an empirically derived equation (**Appendix A Equation A1**) relating water height in each flume to flow rate. Flow rate data over time were used to calculate volume of water passing through each monitoring location per storm.

The bioretention had three monitoring points (inlet culvert, basin outlet underdrain, and bypass channel; **Figure 2.2**). All three monitoring points were used to calculate runoff and salt load reductions (reduction = inlet – outlet – bypass). Together, the three swales have four monitoring locations: a shared roadside sheet flow collector to estimate extrapolated inlet flow, and the three individual outlets of each swale (**Figure 2.3**). The GC and CAGC outlet monitoring locations measure outflow as channelized surface effluent, while the bioswale outlet monitoring location measures effluent exiting the underdrain. To monitor sheet flow entering into the swales, a 9.1 m sheet flow collection gutter was used to channel sheet flow (adjacent to the swales CDAs) from Lorton Road into a flume. An impervious roadside area extrapolation was used to calculate the volume of water expected from the impervious roadside CDA of the three swales based on the volume of water measured from the 9.1-meter sheet flow collector CDA (**Appendix A Equation A2**). To account for the pervious CDA of each swale not included in road sheet flow (a relatively small fraction of the total inflow runoff), the Soil Conservation Service (SCS) curve number method was used (**Appendix A Equations A3 and A4**). For seven high intensity storm events (5/19/2018, 6/2/2018, 8/31/2018, 12/15/2018, 1/25/2019, 2/24/2019, and 3/21/2019), flow rate data from the bioswale outlet were corrected for flume flooding by setting the maximum flow rate to the empirically observed max flow rate of the bioretention outlet pipe (same diameter as bioswale outlet)[27].

Autosamplers collected flow-weighted composite stormwater samples throughout each storm event at preprogrammed volume increments. For each storm, subsamples at each monitoring location spanned as much stormwater volume as possible to makeup representative flow-weighted composite samples (number and spread of sub-samples in **Appendix A Equation A5 & Table A2**). Samples were taken within the flumes, stored in 9.5 L glass jars on ice within each autosampler, and collected within 24 hours of each storm event for lab analysis. Autosamplers operated with purge/withdrawal cycles for each sample. All flumes, sample lines, and bottles were cleaned between storms and field blanks were taken to ensure equipment was clean. Concentrations in flow-weighted composite samples were used as event mean concentrations (EMCs) for each monitoring location. Pollutant loads through each monitoring station were determined by multiplying EMC values by total stormwater volume over a monitoring period.

2.2.3 Stormwater Analysis

Concentrations of nitrate, nitrite, ammonium, and phosphate in all water samples were determined using ion chromatography (IC). Samples were filtered (0.45 µm PTFE) and analyzed by IC (Dionex ICS-5000). IC runs included blanks which were all below relevant detection limits. When sample ion concentrations were higher than the upper range of calibration, samples were diluted and re-run within calibration range. Total dissolved nitrogen (TDN) and dissolved organic carbon (DOC) were analyzed by a Shimadzu TOC-L with a coupled TNM-L analyzer. Stormwater samples were acidified with 2% HCL and filtered (0.45 μm PTFE) before TOC-L/TDN analysis. Total suspended solids (TSS) was measured by filtration (Whatman 1.5 μm glass microfiber) and gravimetric determination, based on USEPA method 160.2. Total Phosphorus was analyzed using Hach low range (0.05 – 1.5 mg/L as P) Phosphorus TNTplus kits (ascorbic acid digestion followed by spectrophotometric determination, based on EPA 365.1).

2.2.4 Statistical Analysis

Statistical analysis was preformed using the software R (version 3.6.1). P values were calculated by paired t-tests with 95% confidence intervals ($\alpha = 0.05$).

2.3 Results

2.3.1 Stormwater monitoring weather conditions

27 precipitation events (24 rain and 3 snow) were monitored between April 16th, 2018 and June 18th, 2019. Storm events ranged from 0.7 to 10.5 cm. All 27 events totaled 124.7 cm with a mean event size of 4.6 cm. Total precipitation over the same time period at nearby Ronald Reagan Airport Weather Station was 198.0 cm. Monitored events accounted for 63% of the total rain from the weather station. Weather conditions for each of the 27 monitored events (e.g. event size, intensity, duration, temperature) are displayed in **Appendix A Table A3.**

10 of the 27 monitored precipitation events included successful stormwater monitoring from all monitoring locations for all four GI. These 10 events occurred between June 2nd, 2018 and June 18th, 2019. Storm events ranged from 1.4 to 7.3 cm. All 10 events totaled 36.1 cm with a mean event size of 3.6 cm. Total precipitation over the same time period at nearby Ronald Reagan Airport Weather Station was 170.2 cm. Mutually monitored events accounted for 21% of the total rain from the weather station over the same time period.

2.3.2 Stormwater runoff reduction

For the mutually monitored 10 storm events, cumulative runoff reductions over the monitoring period was 65%, 75%, 40%, and 36% for the bioretention, GC, CAGC, and bioswale, respectively (**Appendix A Table A4**). For the bioretention, 89% of total surface effluent exited through the underdrain outlet and 11% exited through the bypass channel. More detailed GI runoff reduction comparisons and trends are discussed in Hayes et al. (2020)[27]. Hayes et al. compared the runoff reductions of the same four GI over 29 precipitation events, finding that while the four GI practices have somewhat large differences in cumulative runoff reductions, there was not a statistically significant difference in their average runoff reduction.

2.3.3 Stormwater quality

Stormwater EMC samples from all four GI were found to have detectable levels of nitrate, TDN, phosphate, TP, DOC, and TSS but no detectable nitrite or ammonium was measured in any stormwater samples. EMCs of detectable water quality parameters from GI inlets and outlets are displayed in **Figure 2.4**. Outlet concentrations and concentration reductions for the bioretention are reported as inlet vs. underdrain outlet, due to the bypass channel outlet only accounting for a small fraction of the total flow of stormwater.

Mean nitrate inlet concentrations from nine mutually monitored storms were 0.52, 0.07, 0.07, and 0.07 mg/L as N, while mean outlet nitrate concentrations were 0.41, 0.03, 0.03, and 0.11 mg/L as N for the bioretention, GC, CAGC, and bioswale, respectively (**Figure 2.4**). Relative nitrate concentrations between the inlets and outlets (concentration reductions) were 20%, 63%, 55%, and -53%, for the bioretention, GC, CAGC, and bioswale, respectively.

Mean TDN inlet concentrations from nine mutually monitored storms were 0.86, 0.43, 0.43, and 0.43 mg/L as N, while mean outlet TDN concentrations were 0.60, 0.46, 0.73, and 0.55

mg/L as N for the bioretention, GC, CAGC, and bioswale, respectively (**Figure 2.4**). Concentration reductions of TDN between the inlets and outlets were 30%, -6%, -69%, and -28%, for the bioretention, GC, CAGC, and bioswale, respectively. Mean nitrate inlet EMCs made up 60%, 17%, 17%, and 17% of inlet TDN EMC, while mean nitrate outlet EMCs made up 68%, 6%, 4%, and 20% of outlet TDN EMC for the bioretention, GC, CAGC, and bioswale, respectively.

Mean phosphate inlet concentrations from seven mutually monitored storms were 0.06, 0.07, 0.07, and 0.07 mg/L as P, while mean outlet phosphate concentrations were 0.06, 0.09, 0.22, and 0.11 mg/L as P for the bioretention, GC, CAGC, and bioswale, respectively (**Figure 2.4**). Phosphate concentration reductions between the inlets and outlets were 6%, -31%, -224%, and -65%, for the bioretention, GC, CAGC, and bioswale, respectively.

Mean TP inlet concentrations from two mutually monitored storms were 0.07, 0.12, 0.12, and 0.12 mg/L as P, while mean outlet TP concentrations were 0.04, 0.12, 0.40, and 0.16 mg/L as P for the bioretention, GC, CAGC, and bioswale, respectively (**Figure 2.4**). TP concentration reductions between the inlets and outlets were 48%, -3%, -234%, and -34%, for the bioretention, GC, CAGC, and bioswale, respectively. Mean phosphate inlet EMCs made up 123%, 100%, 100%, and 100% of inlet TP EMC, while mean phosphate outlet EMCs made up 218%, 80%, 72%, and 77% of outlet TDN EMC for the bioretention, GC, CAGC, and bioswale, respectively.

Mean DOC inlet concentrations from nine mutually monitored storms were 5.6, 5.5, 5.5, and 5.5 mg/L, while mean outlet DOC concentrations were 6.0, 9.3, 15.3, and 9.1 mg/L for the bioretention, GC, CAGC, and bioswale, respectively (**Figure 2.4**). DOC concentration reductions between the inlets and outlets were -6%, -69%, -178%, and -67%, for the bioretention, GC, CAGC, and bioswale, respectively.

Mean TSS inlet concentrations from six mutually monitored storms were 59, 135, 135, and 135 mg/L, while mean outlet TSS concentrations were 9, 25, 60, and 22 mg/L for the bioretention, GC, CAGC, and bioswale, respectively (**Figure 2.4**). TSS concentration reductions between the inlets and outlets were 85%, 82%, 56%, and 84%, for the bioretention, GC, CAGC, and bioswale, respectively.

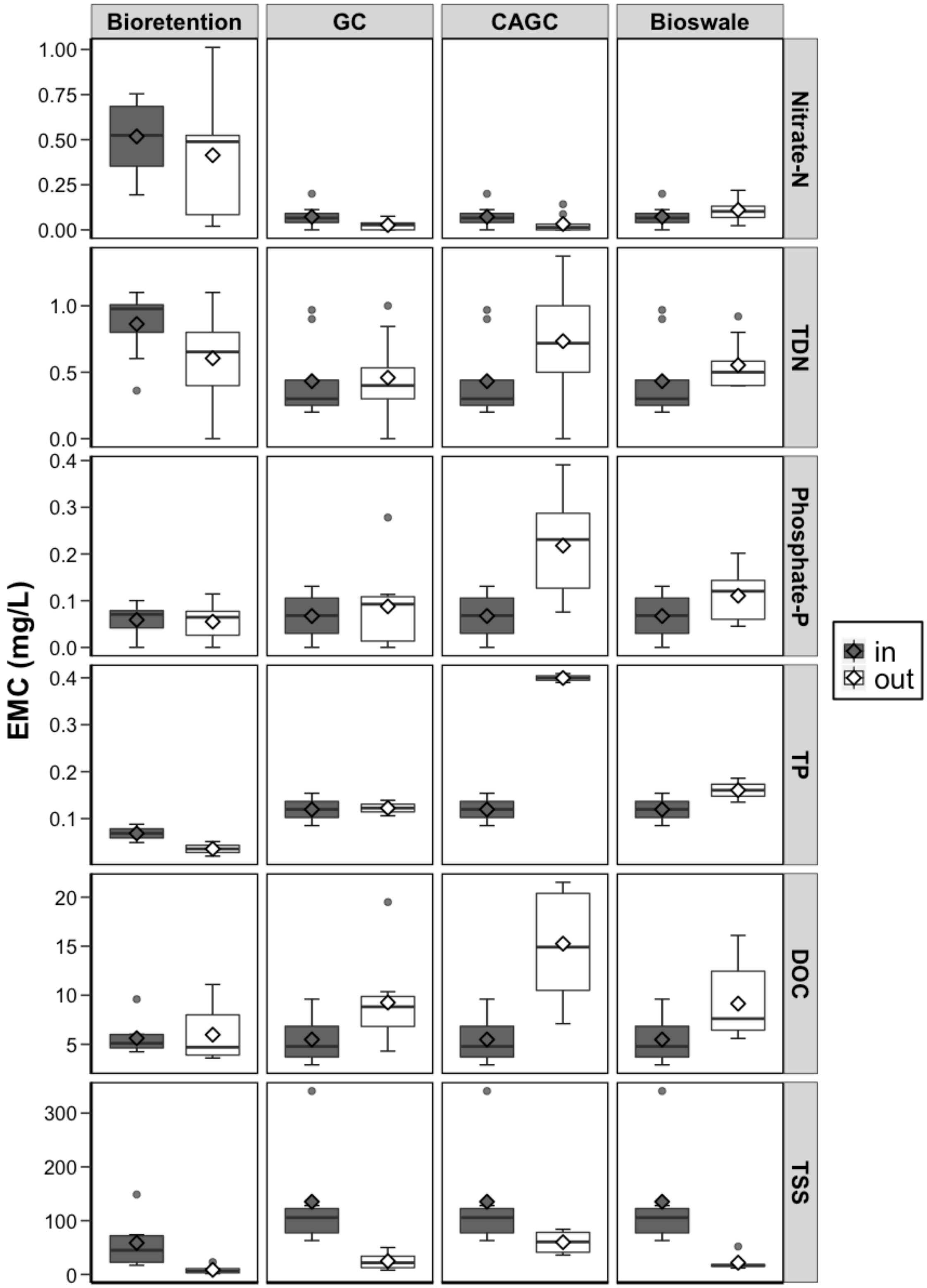

Figure 2.4. GI EMC inlet and outlet concentrations from mutually monitored events. From top to bottom: nitrate as N (9 events), TDN (9 events), Phosphate as P (7 events), TP (2 events), DOC (9 events), and TSS (6 events). concentrations in EMC inlet and outlet samples. Outlet concentrations for the bioretention

are from the underdrain outlet. Boxplots depict median values (thick black line), mean values (diamond), 25th to 75th percentiles (boxes), 1.5 times the interquartile range (whiskers), and outlier values (points).

Factoring stormwater water quality parameter concentrations and runoff volumes together resulted in total surface water influent and effluent loads for each GI over mutually monitored storms (**Figure 2.5**). The bioretention has much larger influent loads than the swales for all water quality parameters, largely due to its much larger CDA. Bioretention outlet loads are the sum of underdrain outlet loads and bypass channel loads. 3.4%, 7.5%, 13.5%, 18.7%, 12.6%, and 31.8% of nitrate, TDN, phosphate, TP, DOC, and TSS bioretention surface effluent loads were bypassed, respectively, while remaining surface effluent loads exited the bioretention through the underdrain outlet. Nitrate total effluent surface load reductions were 20%, 63%, 55%, and -53% for the bioretention, GC, CAGC, and bioswale, respectively. TDN total effluent surface load reductions were 30%, -6%, -69%, and -28% for the bioretention, GC, CAGC, and bioswale, respectively. Phosphate total effluent surface load reductions were 6%, -31%, -224%, and -65% for the bioretention, GC, CAGC, and bioswale, respectively. TP total effluent surface load reductions were 48%, -3%, -234%, and -34% for the bioretention, GC, CAGC, and bioswale, respectively. DOC total effluent surface load reductions were -6%, -69%, -178%, and -67% for the bioretention, GC, CAGC, and bioswale, respectively. DOC total effluent surface load reductions were 85%, 82%, 56%, and 84% for the bioretention, GC, CAGC, and bioswale, respectively. Water quality parameter loads per event are displayed in **Appendix A Table A5**.

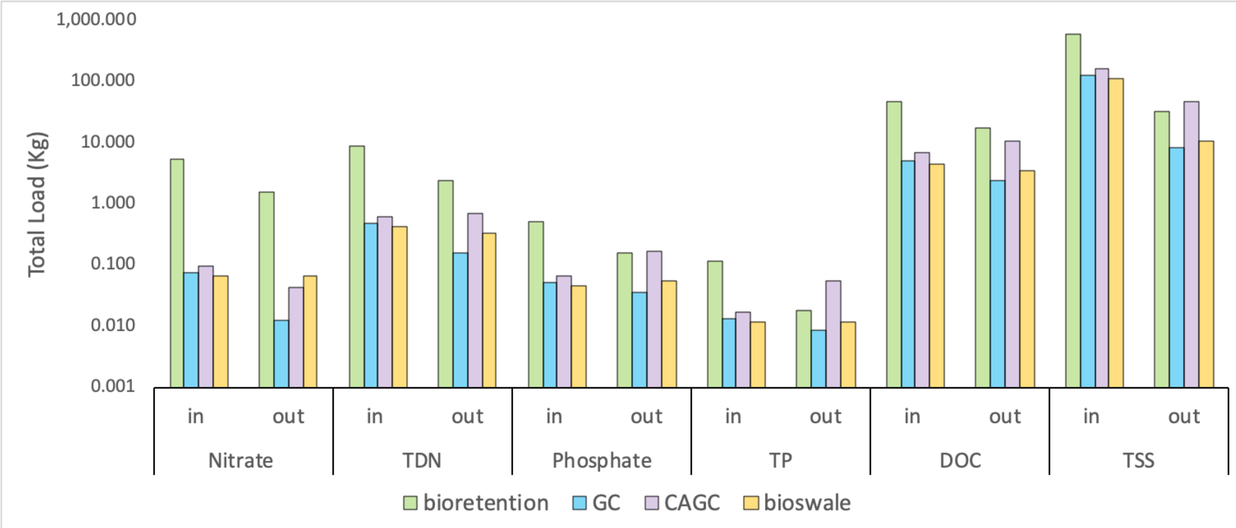

Figure 2.5. GI surface water inlet and outlet water quality parameter total loads from mutually monitored events. From left to right: nitrate as N (9 events), TDN (9 events), phosphate as P (7 events), TP (2 events), DOC (9 events), and TSS (6 events). Outlet loads for the bioretention are a sum of the underdrain outlet and bypass channel. The vertical total load axis is log-scaled.

A summary of the overall performance of the four GI types with respect to total stormwater runoff and average concentrations and total loads of nitrate, TDN, phosphate, TP, DOC, and TSS is presented in **Figure 2.6**. There was considerable variability in stormwater management performance criteria between the four GI and across different water quality parameters. The bioretention and GC had positive load reductions for all water quality parameters, while the bioswale had one load export (phosphate) and the CAGC had four load exports (TDN, phosphate, TP, and DOC. The bioretention had the most consistent load reduction performance for all water quality parameters of the four GI, and of the three swales, the GC was the most consistent. The load reduction average of all six water quality parameters was 76 ± 5 standard error, 61 ± 10, -55 ± 48, and 20 ± 16 for the bioretention, GC, CAGC, and bioswale, respectively. The bioretention's average load reduction of all water quality parameters was significantly higher than that of the CAGC (p = 0.042) and bioswale (p = 0.008), but not the GC. The GC's average load reduction of all water quality parameters was also significantly higher than that of the CAGC ($p = 0.030$) and bioswale ($p = 0.013$). The CAGC and the bioswale did not have significant differences in average load reduction.

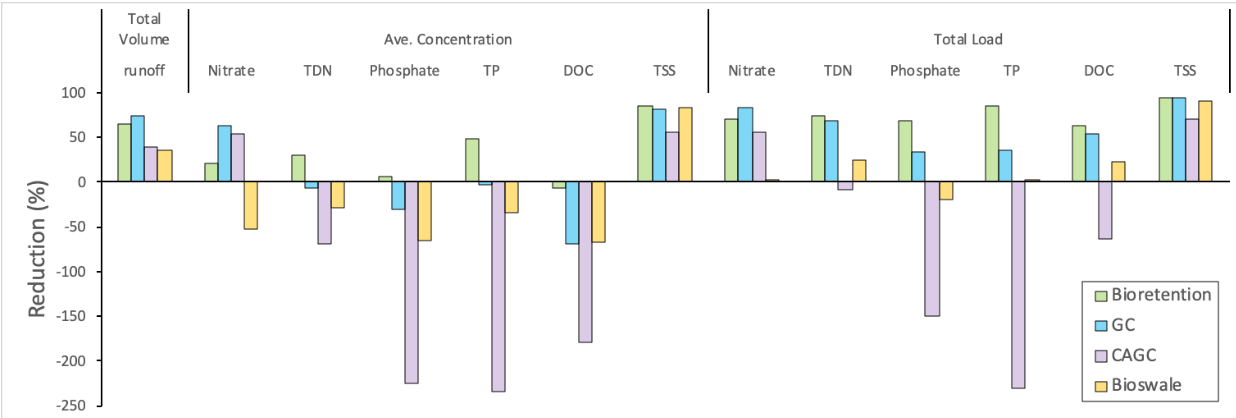

Figure 2.6. GI stormwater management performance over the 12 month mutual monitoring period. From left to right: total stormwater runoff reductions, average concentration reductions (in vs. out), and total load reductions. Outlet concentrations for the bioretention are the underdrain outlet, while outlet loads are a sum of the underdrain outlet and bypass channel.

Total GI effluent loads per unit CDA were lowest for the bioretention for each water quality parameter except nitrate, which was lowest for the GC (**Figure 2.7**). The sum of the six water quality parameter total effluent loads per unit CDA were 1104 Kg/Km^2, 4801 Kg/Km^2, 9434 Kg/Km^2, and 7566 Kg/Km^2 for the bioretention, GC, CAGC, and bioswale, respectively.

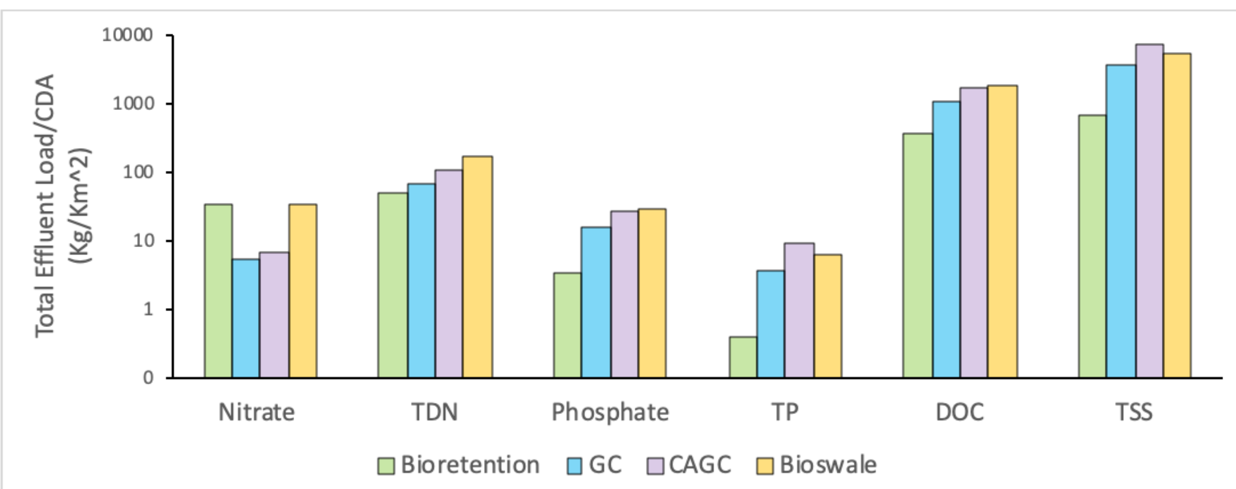

Figure 2.7. GI stormwater quality parameter effluent loads per unit CDA over the 12 month mutual monitoring period. Bioretention outlet loads are a sum of the underdrain outlet and bypass channel.

2.4 Discussion

2.4.1 GI Stormwater Quality Concentration Performance

The two stormwater runoff influent monitoring locations (one for the concentrated inflow of the bioretention and one for road sheet flow into the swales) revealed differences in stormwater quality entering the bioretention vs. the three swales. Nitrogen (nitrate and TDN) was significantly higher, phosphorus (phosphate and TP) and DOC were similar, and TSS was lower in bioretention inlet water relative to the sheet flow inlet of the swales (**Figure 2.4**). These differences reflect the differences in land use of the CDAs of the bioretention and swales. In addition to road and grass surfaces, the bioretention's CDA includes residential property and woods, while the swales CDAs do not. Addition of fertilizers to residential properties is suggested as the reason for the increased nitrogen concentrations in the bioretention CDA (**Chapter 4**). These differences in influent nitrogen and TSS introduce more complexity when comparing concentration and load reductions of the bioretention and the swales and are important to consider[28]. In general, measured concentrations in stormwater runoff entering into the GI (especially the lower nitrogen concentrations of the swales) were more in line with typical rural highway runoff concentrations than urban highways[29,30].

Stormwater effluent EMC concentrations and concentration reductions between influent and effluent indicate that all four monitored GI had limited ability to reduce nutrient concentrations, with all GI at least periodically showing negative concentration reductions for nitrate, TDN, phosphate, and TP (**Figures 2.4 and 2.6**). The CAGC in particular had much higher TDN, phosphate, and TP concentrations in effluent samples than influent, indicative of it leaching its nutrient rich compost amended soils into stormwater. The bioswale also had average negative concentration reductions for all nutrients, perhaps also due to leaching nitrogen and phosphorus from its ESM (which contains 5% compost). The bioretention uses the same ESM, but had all (modestly) positive nutrient concentration reductions. This significant difference between the bioretention and the bioswale (similar GI designs) is surprising, but may be explained by their difference in stormwater retention time (the bioretention retains stormwater for significantly longer than the bioswale, allowing more time for biological nutrient removal mechanisms) and also the higher nitrogen concentrations going into the bioretention. TSS outlet EMCs, however, indicate that all four GI have significant ability to reduce TSS concentrations in stormwater. This is expected for the GI that employ filtering mechanisms (bioretention and bioswale) but the equally high TSS concentration reduction of the GC is surprising [31,32].

2.4.2 GI Stormwater Quality Surface Load Reduction

The bioretention had the highest average total surface load reduction but not statistically higher than that of the GC. Both the bioretention and GC did have statistically higher average total load reductions than the CAGC and bioswale. In terms of engineering, the bioretention is probably the most complex GI design and the GC is the least complex. So increasing levels of engineering complexity in GI are not necessarily leading to increased reduction of water quality parameter surface loads. The CAGC is actually a net source of TDN, phosphate, TP, and DOC, while the bioswale is a net source of phosphate (**Figure 2.6**). The CAGC has both low concentration reduction of TDN, phosphate, TP, and DOC and also low overall runoff reduction, leading to its especially low load reduction numbers for those parameters. Most stormwater regulations are based on load reductions and the bioretention and GC were statistically the best based solely on their percentage reduction of incoming loads.

When normalizing outlet loads for CDA size, again the bioretention had the best performance for each individual water quality parameter total effluent load per CDA except nitrate (**Figure 2.7**). The bioretention has a much larger CDA than any of the swales and is treating much higher stormwater pollutant loads across the board (**Figure 2.5**). Because of differences in both CDA and influent concentrations, there is uncertainty in swale performance if scaled up. However, the swales would likely not ever be have a designed CDA of the size of the bioretention, due to their intended purpose as roadside sheet flow conveyers. Generally the swales are designed to convey stormwater, while the bioretention is designed to retain stormwater longer.

2.4.3 Fate of Reduced Stormwater Quality Parameters

Several of the GI displayed significant stormwater surface effluent load reductions of water quality parameters, but that does not necessarily mean that the GI are permanently removing those loads. A primary load reduction mechanism of GI is stormwater volume reduction, largely by infiltration. If reduced loads of contaminants are merely infiltrated, GI is protecting surface waters but potentially risking groundwater quality. In general, contaminants will reside for a much longer time in slow moving groundwater than in faster moving surface waters[33]. Once in groundwater some contaminants may be reduced (e.g. nitrate by denitrification), but other more conservative contaminants may build up for over time and potentially impact drinking water or eventually return to surface water[33–36].

Concentration reductions of stormwater contaminants within GI indicate removal mechanisms more than just volume reduction. In the case of nitrogen and phosphorus, uptake by vegetation is a suggested removal mechanism accounting for concentration reductions in GI (**Figure 2.6**). Vegetation, however is only a short term sink for nutrients and maintenance efforts are necessary to prevent decaying vegetation from seasonally exporting stored nitrogen[37–39]. As discussed in Chapter 3, denitrification is also a possible nitrogen removal mechanism, but it's occurrence in the bioretention was found to be low. Because longer hydraulic retention times (HRTs) are required for denitrification and little denitrification was identified in the bioretention

(GI with highest HRT), denitrification is very likely not a significant removal mechanism in the only ephemerally stormwater saturated swales. Additionally, physical filtration of contaminants by soil is the likely removal mechanism responsible for TSS and some TP reductions as phosphorus is known to bind to particles[40,41].

2.4.4 Applying Results to Future GI Strategies

Results indicate that of the four monitored GI the bioretention and GC are preferred choices for roadside stormwater management based on surface water quality improvement. These two GI work well together for the needs for the transportation environment, with the GC well suited for linear roadside space with smaller sheet flow CDAs and the bioretention for larger concentrated flow CDAs. The two may also work well in tandem.

The bioretention displayed ability to receive and treat high loads of stormwater contaminants. Its loading ratio (47) is higher than typical bioretention but that did not appear to limit it's performance[16]. It's CDA (47,753 m^2) is significantly larger than the maximum CDA recommended for bioretention by the Virginia Department of Environmental Quality (20,234 m^2), but it's initial performance suggests that that recommendation may be too small[16]. The Lorton Road bioretention does employ a forebay and a bypass channel to regulate high flows and sediment loads. The additional future maintenance of that forebay (dredging) may by considerable.

For the swales, the more complex CAGC and bioswale underperformed relative to the simple GC. Because our water quality criteria primarily emphasized nutrient reduction (four out of the six water quality parameters), the CAGC and bioswale were disadvantaged by their nutrient leaching soils. As has been noted by others, soil compost amendment has advantages and disadvantages in stormwater management, and it appears that the CAGC in particular used too much compost amendment to observe any benefits relative to the GC. The bioswale served more as a method of stormwater conveyance than treatment. It is possible that the success of the GC in this study is site specific, due to GC's reliance on native soil conditions. The Lorton Road GC performed better during larger storm events than monitored GCs in Davis et al. (2012)[42,43].

2.4.5 Suggestions for Future Research

This study shows the initial stormwater quality performance of four operational roadside GI practices. These GI were approximately one year old at the beginning of monitoring. Future research should look into long-term temporal changes in GI performance. Because GI is a relatively new stormwater management strategy, there is little data on the longevity of GI, which may have considerable differences in performance over time. Monitoring the comparative need/effect of maintenance on the GI is also in need of further study as each GI has different maintenance needs which change as the GI age. GI that require more maintenance (e.g. bioretention and bioswale) may also be less cost effective over time than low maintenance designs (e.g. GC).

Additionaly, the identification of GI contaminant removal mechanisms should continue to be explored. The black box approach to GI performance monitoring is missing the complete picture of contaminant fate and transport in the environment and needs to be supplemented with more experiments that dig deeper into GI function (e.g. **Chapters 3 and 4**). If GI is protecting stormwater but risking groundwater, it is important for stormwater managers to recognize that tradeoff. A better understanding of removal mechanisms is necessary in order to optimize GI design and stormwater management.

2.5 Conclusions

This study compared the stormwater quality performance of four distinct GI practices over 12 months as they received the same storm event conditions. The different GI designs had a wide range of performances, some acting as pollutant sinks and others as pollutant sources. The total load reduction average of all six water quality parameters was 76 ± 5, 61 ± 10, -55 ± 48, and 20 ± 16 for the bioretention, GC, CAGC, and bioswale, respectively, with the bioretention and GC statistically significantly higher than the CAGC and bioswale. Of the four GI studied, bioretention and GC are the best choices for nutrient, DOC, and TSS water quality performance and work well together for the needs of the transportation environment. Results indicate that more complex GI designs don't necessarily have better performance than simple GI and that small differences in design (e.g. compost amendment) can significantly alter GI performance. Future research is needed in long-term GI performance and maintenance monitoring, as well as identification of removal mechanisms. When designed well, GI is an effective stormwater management practice, but when designed poorly it may have unintended consequences. These monitoring results along with others will help future GI designs achieve their full potential.

Supplementary Data: Appendix A

2.6 References

(1) Walsh, C. J.; Roy, A. H.; Feminella, J. W.; Cottingham, P. D.; Groffman, P. M.; Morgan Ii, R. P. The Urban Stream Syndrome: Current Knowledge and the Search for a Cure. *Benthol. Soc* **2005**, *24* (3), 706–723.

(2) Spromberg, J. A.; Baldwin, D. H.; Damm, S. E.; Mcintyre, J. K.; Huff, M.; Sloan, C. A.; Anulacion, B. F.; Davis, J. W.; Scholz, N. L. EDITOR'S CHOICE: Coho Salmon Spawner Mortality in Western US Urban Watersheds: Bioinfiltration Prevents Lethal Storm Water Impacts. *J. Appl. Ecol.* **2016**. https://doi.org/10.1111/1365-2664.12534.

(3) Spromberg, J. A.; Baldwin, D. H.; Damm, S. E.; Mcintyre, J. K.; Huff, M.; Sloan, C. A.; Anulacion, B. F.; Davis, J. W.; Scholz, N. L. EDITOR'S CHOICE: Coho Salmon Spawner Mortality in Western US Urban Watersheds: Bioinfiltration Prevents Lethal Storm Water Impacts. *J. Appl. Ecol.* **2016**, *53* (2), 398–407. https://doi.org/10.1111/1365-2664.12534.

(4) Dhakal, K. P.; Chevalier, L. R. Urban Stormwater Governance: The Need for a Paradigm Shift. *Environ. Manage.* **2016**, *57* (5), 1112–1124. https://doi.org/10.1007/s00267-016-

0667-5.
(5) Ahiablame, L. M.; Engel, B. A.; Chaubey, I. Effectiveness of Low Impact Development Practices in Two Urbanized Watersheds: Retrofitting with Rain Barrel/Cistern and Porous Pavement. *J. Environ. Manage.* **2013**, *119*, 151–161. https://doi.org/10.1016/j.jenvman.2013.01.019.
(6) Wardynski, B. J.; Winston, R. J.; Line, D. E.; Hunt, W. F. Metrics for Assessing Thermal Performance of Stormwater Control Measures. *Ecol. Eng.* **2014**, *71*, 551–562. https://doi.org/10.1016/J.ECOLENG.2014.07.068.
(7) US EPA. *Chesapeake Bay TMDL*; 2010.
(8) McIntyre, J. K.; Davis, J. W.; Hinman, C.; Macneale, K. H.; Anulacion, B. F.; Scholz, N. L.; Stark, J. D. Soil Bioretention Protects Juvenile Salmon and Their Prey from the Toxic Impacts of Urban Stormwater Runoff. *Chemosphere* **2015**, *132*, 213–219. https://doi.org/10.1016/j.chemosphere.2014.12.052.
(9) Vogel, J. R.; Moore, T. L.; Coffman, R. R.; Rodie, S. N.; Hutchinson, S. L.; McDonough, K. R.; McLemore, A. J.; McMaine, J. T. Critical Review of Technical Questions Facing Low Impact Development and Green Infrastructure: A Perspective from the Great Plains. *Water Environ. Res.* **2015**, *87* (9), 849–862. https://doi.org/10.2175/106143015X14362865226392.
(10) Coffman, L. *Low-Impact Development Design Strategies An Integrated Design Approach*; Prince George's County, Maryland, 2000.
(11) McIntyre, J. K.; Davis, J. W.; Incardona, J. P.; Stark, J. D.; Anulacion, B. F.; Scholz, N. L. Zebrafish and Clean Water Technology: Assessing Soil Bioretention as a Protective Treatment for Toxic Urban Runoff. *Sci. Total Environ.* **2014**, *500*, 173–180. https://doi.org/10.1016/j.scitotenv.2014.08.066.
(12) Henderson, D.; Hayes, G.; Burgis, C.; Smith, J. A. Low Impact Development Technologies for Highway Stormwater Runoff. In *Encyclopedia of Water: Science, Technology, and Society*; Wiley, 2019; pp 1–18. https://doi.org/10.1002/9781119300762.wsts0009.
(13) Pennino, M. J.; McDonald, R. I.; Jaffe, P. R. Watershed-Scale Impacts of Stormwater Green Infrastructure on Hydrology, Nutrient Fluxes, and Combined Sewer Overflows in the Mid-Atlantic Region. *Sci. Total Environ.* **2016**, *565*, 1044–1053. https://doi.org/10.1016/j.scitotenv.2016.05.101.
(14) McIntyre, J. K.; Davis, J. W.; Hinman, C.; Macneale, K. H.; Anulacion, B. F.; Scholz, N. L.; Stark, J. D. Soil Bioretention Protects Juvenile Salmon and Their Prey from the Toxic Impacts of Urban Stormwater Runoff. *Chemosphere* **2015**. https://doi.org/10.1016/j.chemosphere.2014.12.052.
(15) Kramer, M. G. *Enhancing Sustainable Communities with Green Infrastructure (EPA 100-R-14-006)*; 2014.
(16) Virginia Department of Environmental Quality. *VIRGINIA DEQ STORMWATER DESIGN SPECIFICATION No. 9 BIORETENTION*; 2013.
(17) Li, M.-H.; Swapp, M.; Kim, M. H.; Chu, K.-H.; Sung, C. Y. Comparing Bioretention Designs With and Without an Internal Water Storage Layer for Treating Highway Runoff. https://doi.org/10.2175/106143013X13789303501920.
(18) Virginia Department of Environmental Quality. *VIRGINIA DEQ STORMWATER DESIGN SPECIFICATION No. 3 GRASS CHANNELS*; 2013.
(19) Virginia Department of Environmental Quality. *VIRGINIA DCR STORMWATER DESIGN*

SPECIFICATION No. 10 DRY SWALES; 2013.
(20) Henderson, D.; Smith, J. A.; Fitch, G. M. Impact of Vegetation Management on Vegetated Roadsides and Their Performance as a Low-Impact Development Practice for Linear Transportation Infrastructure. *Transp. Res. Rec. J. Transp. Res. Board* **2016**, *2588*, 172–180. https://doi.org/10.3141/2588-19.
(21) Li, M.-H.; Barrett, M. E.; Rammohan, P.; Olivera, F.; Landphair, H. C. Documenting Stormwater Quality on Texas Highways and Adjacent Vegetated Roadsides. *J. Environ. Eng.* **2008**, *134* (1), 48–59. https://doi.org/10.1061/(ASCE)0733-9372(2008)134:1(48).
(22) Askarizadeh, A.; Rippy, M. A.; Fletcher, T. D.; Feldman, D. L.; Peng, J.; Bowler, P.; Mehring, A. S.; Winfrey, B. K.; Vrugt, J. A.; Aghakouchak, A.; et al. From Rain Tanks to Catchments: Use of Low-Impact Development To Address Hydrologic Symptoms of the Urban Stream Syndrome. *Environ. Sci. Technol.* **2015**. https://doi.org/10.1021/acs.est.5b01635.
(23) Leroy, M. charlotte; Portet-Koltalo, F.; Legras, M.; Lederf, F.; Moncond'huy, V.; Polaert, I.; Marcotte, S. Performance of Vegetated Swales for Improving Road Runoff Quality in a Moderate Traffic Urban Area. *Sci. Total Environ.* **2016**. https://doi.org/10.1016/j.scitotenv.2016.05.027.
(24) Li, H. Green Infrastructure for Highway Stormwater Management: Field Investigation for Future Design, Maintenance, and Management Needs. *J. Infrastruct. Syst.* **2015**, *21* (4), 05015001. https://doi.org/10.1061/(ASCE)IS.1943-555X.0000248.
(25) Ahiablame, L. M.; Engel, B. A.; Chaubey, I. Effectiveness of Low Impact Development Practices: Literature Review and Suggestions for Future Research. *Water, Air, Soil Pollut.* **2012**, *223* (7), 4253–4273. https://doi.org/10.1007/s11270-012-1189-2.
(26) VDOT. *AVERAGE DAILY TRAFFIC VOLUMES with VEHICLE CLASSIFICATION DATA on INTERSTATE, ARTERIAL and PRIMARY ROUTES*; 2018.
(27) Hayes, G. M.; Burgis, C.; Zhang, W.; Henderson, D.; Smith, J. A. Runoff Reduction by Four Green Stormwater Infrastructure Systems in a Shared Environment. *J. Sustain. Water Built Environ. (under Rev.*
(28) Bäckström, M. Grassed Swales for Stormwater Pollution Control during Rain and Snowmelt. *Water Sci. Technol.* **2003**, *48* (9), 123–132. https://doi.org/10.2166/wst.2003.0508.
(29) Kayhanian, M.; Suverkropp, C.; Ruby, A.; Tsay, K. Characterization and Prediction of Highway Runoff Constituent Event Mean Concentration. *J. Environ. Manage.* **2007**. https://doi.org/10.1016/j.jenvman.2006.09.024.
(30) Driscoll, E. D.; Shelley, P. E.; Strecker, E. W. *POLLUTANT LOADINGS AND IMPACTS FROM HIGHWAY STORMWATER RUNOFF. VOLUME III: ANALYTICAL INVESTIGATION AND RESEARCH REPORT*; 1990.
(31) Leroy, M. charlotte; Portet-Koltalo, F.; Legras, M.; Lederf, F.; Moncond'huy, V.; Polaert, I.; Marcotte, S. Performance of Vegetated Swales for Improving Road Runoff Quality in a Moderate Traffic Urban Area. *Sci. Total Environ.* **2016**, *566–567*, 113–121. https://doi.org/10.1016/j.scitotenv.2016.05.027.
(32) Trowsdale, S. A.; Simcock, R. Urban Stormwater Treatment Using Bioretention. *J. Hydrol.* **2011**, *397* (3), 167–174. https://doi.org/10.1016/j.jhydrol.2010.11.023.
(33) Ledford, S. H.; Lautz, L. K.; Stella, J. C. Hydrogeologic Processes Impacting Storage, Fate, and Transport of Chloride from Road Salt in Urban Riparian Aquifers. *Environ. Sci. Technol.* **2016**, *50* (10), 4979–4988. https://doi.org/10.1021/acs.est.6b00402.

(34) Rivett, M. O.; Buss, S. R.; Morgan, P.; Smith, J. W. N.; Bemment, C. D. Nitrate Attenuation in Groundwater: A Review of Biogeochemical Controlling Processes. *Water Res.* **2008**, *42* (16), 4215–4232. https://doi.org/10.1016/J.WATRES.2008.07.020.
(35) Seitzinger, S.; Harrison, J. A.; Böhlke, J. K.; Bouwman, A. F.; Lowrance, R.; Peterson, B.; Tobias, C.; Van Drecht, G. Denitrification across Landscapes and Waterscapes: A Synthesis. *Ecol. Appl.* **2006**, *16* (6), 2064–2090. https://doi.org/10.1890/1051-0761(2006)016[2064:dalawa]2.0.co;2.
(36) Perera, N.; Gharabaghi, B.; Howard, K. Groundwater Chloride Response in the Highland Creek Watershed Due to Road Salt Application: A Re-Assessment after 20 Years. *J. Hydrol.* **2013**, *479*, 159–168. https://doi.org/10.1016/J.JHYDROL.2012.11.057.
(37) Morse, N. R.; Mcphillips, L. E.; Shapleigh, J. P.; Walter, M. T.; Wrigley, J. A. The Role of Denitrification in Stormwater Detention Basin Treatment of Nitrogen. *Environ. Sci. Technol. 2017,* **2017**, *51*, 7928−7935. https://doi.org/10.1021/acs.est.7b01813.
(38) Payne, E. G. I.; Fletcher, T. D.; Cook, P. L. M.; Deletic, A.; Hatt, B. E. Processes and Drivers of Nitrogen Removal in Stormwater Biofiltration. *Crit. Rev. Environ. Sci. Technol.* **2014**, *44* (7), 796–846. https://doi.org/10.1080/10643389.2012.741310.
(39) Payne, E. G. I.; Pham, T.; Deletic, A.; Hatt, B. E.; Cook, P. L. M.; Fletcher, T. D. Which Species? A Decision-Support Tool to Guide Plant Selection in Stormwater Biofilters. *Adv. Water Resour.* **2018**, *113*, 86–99. https://doi.org/10.1016/j.advwatres.2017.12.022.
(40) River, M.; Richardson, C. J. Particle Size Distribution Predicts Particulate Phosphorus Removal. *Ambio* **2018**, *47* (S1), 124–133. https://doi.org/10.1007/s13280-017-0981-z.
(41) Hsieh, C.; Davis, A. P.; Needelman, B. A. Bioretention Column Studies of Phosphorus Removal from Urban Stormwater Runoff. *Water Environ. Res.* **2007**, *79* (2), 177–184. https://doi.org/10.2175/106143006X111745.
(42) Davis, A. P.; Stagge, J. H.; Jamil, E.; Kim, H. Hydraulic Performance of Grass Swales for Managing Highway Runoff. *Water Res.* **2012**, *46* (20), 6775–6786. https://doi.org/10.1016/J.WATRES.2011.10.017.
(43) Stagge, J. H.; Davis, A. P.; Jamil, E.; Kim, H. Performance of Grass Swales for Improving Water Quality from Highway Runoff. *Water Res.* **2012**, *46* (20), 6731–6742. https://doi.org/10.1016/J.WATRES.2012.02.037.

Chapter 3: Green Stormwater Infrastructure Redirects Deicing Salt from Surface Water to Groundwater

This chapter resulted in one publication currently under review by the journal Science of the Total Environment.

Burgis, C.R., Hayes, G., Henderson, D.A., Zhang, W., Smith, J.A. (2020) "Green Stormwater Infrastructure Redirects Deicing Salt from Surface Water to Groundwater." *Sci. Total Environ.* (*under review*)

3.1 Introduction

Urbanization has made non-point source pollution a leading threat to aquatic ecosystems in developed landscapes. Sudden discharges of stormwater from impervious surfaces results in flooding, erosion, sewer overflows, and pollution into receiving waters [1–5]. Green infrastructure (GI) stormwater management techniques mimic natural landscape hydrology by slowing, spreading, and infiltrating stormwater runoff before discharging it to receiving waters. GI is increasingly designed into urban landscapes as a way to protect waterways from detrimental effects of urban stormwater, while also potentially providing economic, social, and public health benefits to urban communities [6–14].

The use of deicing salts on impervious surfaces in cold climates has become a significant source of associated salt ions to watersheds [15–23]. In 2018, an estimated 25 million metric tons of salt was used in the U.S. for highway deicing [24]. Sodium chloride (NaCl) is the most common deicing agent used in North America and Na^+ and Cl^- ions easily travel with stormwater runoff from impervious surfaces to soil, plants, and receiving waters, impairing water quality and stressing plants and animals [25–29]. Cl^- is a relatively conservative constituent with respect to aqueous-phase transport and has U.S. EPA acute and chronic freshwater aquatic life ambient water quality criteria of 860 mg/L and 230 mg/L [30]. Na^+ has a U.S. EPA recommended drinking water level of 20 mg/L for low-sodium diets [31].

Numerous studies have documented the transport of deicing salt by stormwater runoff into receiving waters. Perera et al. (2013) reported that as much as 40% of Cl^- applied to roadways as road salt in a Toronto area watershed infiltrated into a shallow aquifer, leading to a steady increase in aquifer Cl^- concentrations over 30 years of monitoring [16]. Robinson et al. (2017) demonstrated that roadside soil can store significant Cl^- and Na^+ and gradually release them over several months [32]. Snodgrass et al. (2017) reported that stormwater management ponds were not effectively buffering receiving waters from deicing salt and were leading to Cl^- groundwater plumes throughout the year [33]. Denich et al. (2013) investigated synthetic stormwater NaCl transport through small bioretention mesocosms, finding temporary retention, but no long-term removal of salt [34].

Although there are no current national stormwater regulations for Cl^-, Na^+, or other deicing salt ions in the U.S., efforts are increasing to limit the spread of salt through municipal-scale Total Maximum Daily Load (TMDL) studies and salt management plans [35,36]. GI is not yet designed to treat salt and there are very limited data on Cl^- and Na^+ transport, especially in field-operational stormwater infrastructure. However, infiltration GI practices (e.g. bioretention and bioswale) may have potential to store Cl^- and Na^+ in soil, plants, and underlying groundwater. Na^+ can attach to soil particles through ion exchange, but negatively charged Cl^- is more conservative. Cl^- may impair GI vegetation, infiltrate into underlying groundwater, and runoff into surface waters [37]. However, some salt tolerant vegetation have shown potential to uptake Cl^- [38,39]. The evaluation of GI as a salt mitigation strategy and as a pathway for salt transport is needed to help determine its potential for cold-climate winter watershed management.

In this study, we monitored the year-round field performance of two common infiltration-based GI practices (bioretention and bioswale) along a suburban highway in Northern Virginia to investigate the transport of deicing salt through modern stormwater infrastructure. We monitored stormwater runoff volumes and concentrations of deicing salt-associated ions entering and exiting each GI practice over 15 months to determine mass (load) and concentration reductions of salt ions. We monitored changes in soil chemistry and groundwater quality over this period to map potential reservoirs of salt transport. Using this information, we discuss the potential of infiltration GI practices as a means of mitigating salt transport and outline areas in need of further study.

3.2 Materials and Methods

3.2.1 Study Site

Two GI practices, a bioretention basin (hereafter bioretention) and a bioswale, were monitored along Lorton Road, in Fairfax County, Virginia. The bioretention is north of Lorton Road while the bioswale is 0.8 km east, on the south side of the road. Both GI practices were designed for 1 year, 24 hr frequency storms and their construction was completed in spring 2017. Maintenance was performed bi-annually (once in spring and once in fall) on both the bioretention and bioswale to remove trash, mow roadside grass slopes, and clear decaying vegetation. Lorton Road is part of the Giles Run watershed, within the Chesapeake Bay watershed. Virginia Department of Transportation generally applies 15.8 to 43.4 metric tons of salt/km^2 of paved road (per application)[40]. Lorton Road is a four-lane divided road with an average daily traffic volume of 100,000 vehicles/day[41].

The bioretention (**Figure 2.2**) has a 47,753 m^2 contributing drainage area (CDA), 35% of which is impervious road surface. Concentrated stormwater from Lorton Road is conveyed to the bioretention via curb and gutters. Stormwater first flows into a forebay before traveling into a basin with 76 cm of engineered soil media (ESM) on top of 40 cm of underlying gravel. A 10 cm diameter underdrain at the top of the gravel layer drains the basin. For larger than designed precipitation events, a channel in the forebay allows overflow stormwater to bypass the basin. The ESM is a highly permeable mix of sand, topsoil, and compost (91.2% sand, 5.6% silt, 3.2% clay). Including the forebay and basin, the bioretention has a footprint of 1,012 m^2 (CDA:footprint ratio = 47) and a storage volume of 447 m^3 [42]. Both the basin and the forebay have a variety of sedges, wildflowers, trees, and shrubs (**Appendix A Table A1 and Appendix B Figure B1**).

The bioswale (**Figure 2.3**) has a CDA of 1,943 m^2 (40% impervious). Stormwater enters the bioswale as sheet flow from Lorton Road (and a sidewalk) and is infiltrated though ESM (the same soil used in the bioretention) along the 65-m-long, 1:7 linear sloped swale. Six wooden check dams intercept stormwater along the swale, encouraging infiltration. The ESM is 46 cm deep with 40 cm of gravel below. A 10.2 cm diameter underdrain at the top of the gravel layer drains the soil and gravel. The bioswale has an 81 m^2 footprint (CDA:footprint ratio = 24), an engineered storage volume of 54 m^3, and a variety of grasses, sedges, wildflowers, trees, and shrubs over the soil media and side slopes (**Appendix A Table A1 and Appendix B Figure B2**) [42].

3.2.2 Stormwater Field Monitoring

We monitored 28 rain and snow events at the bioretention between March 2018 and June 2019 and 15 events at the bioswale between May 2018 and June 2019 (detailed weather conditions in **Appendix B Table B2**). Monitoring was attempted for both GI each storm, but some monitoring attempts were unsuccessful (hence the different number of storms monitored). A tipping bucket rain gauge next to the bioretention recorded 10-minute precipitation data with a 0.025 cm measurement resolution. Only rain events with more than 0.25 cm of precipitation and at least 12 hours of no precipitation preceding each event were monitored. This rule did not apply for snow/snow melt events. If the rain gauge malfunctioned, publicly available weather data from the nearest weather station were used.

At each GI monitoring location, stormwater runoff flow rate and ion concentrations were determined to calculate the mass of deicing salt associated ions traveling in and out of the bioretention and bioswale. Runoff flow rates were measured using custom sized flumes at each monitoring location to intercept stormwater flow from the road, pipe, or channel. Ultrasonic sensors measured the height of water in each flume and stormwater flow rates were calculated by solar powered Hach AS950 autosamplers based on an empirically derived equation (**Appendix A Equation A1**) relating water height in each flume to flow rate. Flow rate data over time were used to calculate volume of water passing through each monitoring location per storm. The bioretention had three monitoring points (inlet culvert, basin outlet underdrain, and bypass channel; **Figure 2.2**). All three monitoring points were used to calculate runoff and salt load reductions (reduction = inlet – outlet – bypass). The bioswale has two monitoring points (an inlet sheet flow collector and an outlet underdrain; **Figure 2.3**). To monitor sheet flow entering into the bioswale, a 9.1 m sheet flow collection gutter was used to channel sheet flow (adjacent to the bioswale CDA) from Lorton Road into a flume. An impervious roadside area extrapolation was used to calculate the volume of water expected from the impervious roadside CDA of the bioswale based on the volume of water measured from the 9.1-meter sheet flow collector CDA (**Appendix A Equation A2**). To account for the pervious CDA of the bioswale not included in road sheet flow (a relatively small fraction of the total inflow runoff), the Soil Conservation Service (SCS) curve number method was used (**Appendix A Equations A3 and A4**). For seven high intensity storm events (5/19/2018, 6/2/2018, 8/31/2018, 12/15/2018, 1/25/2019, 2/24/2019, and 3/21/2019), flow rate data from the bioswale outlet were corrected for flume flooding by setting the maximum flow rate to the empirically observed max flow rate of the bioretention outlet pipe (same diameter as bioswale outlet)[43].

Autosamplers collected flow-weighted composite stormwater samples throughout each storm event at preprogrammed volume increments. For each storm, subsamples at each monitoring location spanned as much stormwater volume as possible to makeup representative flow-weighted composite samples (number and spread of sub-samples in **Appendix A Equation A5 & Appendix B Table B1**). Samples were taken within the flumes, stored in 9.5 L glass jars on ice within each autosampler, and collected within 24 hours of each storm event for lab analysis. Autosamplers operated with purge/withdrawal cycles for each sample. All flumes, sample lines, and bottles were cleaned between storms and field blanks were taken to ensure equipment was clean. Concentrations in flow-weighted composite samples were used as event mean concentrations (EMCs) for each monitoring location. Ion loads through each monitoring station were determined by multiplying EMC values by total stormwater volume over a monitoring period.

3.2.3 Stormwater Analysis

Concentrations of deicing salt associated ions in all water samples were determined using ion chromatography (IC). Samples were filtered (0.45 μm PTFE) and analyzed by IC (Dionex ICS-5000) for Cl^-, Na^+, K^+, Mg^{2+}, and Ca^{2+}. IC runs included blanks which were all below relevant detection limits. When sample ion concentrations were higher than the upper range of calibration, samples were diluted and re-run within calibration range. Sodium adsorption ratio (SAR) was calculated for stormwater inlet samples (**Appendix B Equation B1)**[44]**.**

3.2.4 Soil Monitoring and Analysis

Soil samples were taken of the ESM within the bioretention basin at four points in time (October 2016, July 2018, April 2019, and July 2019). Samples were taken from three different distances along the bioretention basin (near the basin inlet, center of the basin, and far from the basin inlet; **Figure 2.2**) and at three different depths (0-15, 15-30, and 30-45 cm). Soil samples were analyzed for extractible Cl^-, Na^+, K^+, Mg^{2+}, and Ca^{2+}. Extractible Cl^- was measured by adding 25 mL of 0.01 M $CaNO_3$ to 10 g of dry soil. This mixture was shaken for 15 minutes, filtered (0.45 µm PTFE) and analyzed for Cl^- by IC [32]. Major extractible cations were measured by Waypoint Analytical (Richmond, VA) using an ammonium acetate extraction. Four grams of dry soil (sieved through 2 mm) were added to 20 mL of ammonium acetate (1 M, pH 7), shaken for 10 minutes, filtered (Whatman #1), and analyzed by ICP-OES (Perkin Elmer Optima 8300) for Na^+, K^+, Mg^{2+}, and Ca^{2+}. Effective cation exchange capacity (CEC) was calculated based on the sum of extractible Na^+, K^+, Mg^{2+}, Ca^{2+}, and H^+. Average bulk density of the bioretention soil was calculated by averaging six soil samples (same three distances along the bioretention as above, at 0-15 cm and 30-45 cm) taken with a soil core sampling auger, dried, and weighed.

3.2.5 Groundwater Monitoring and Analysis

Two groundwater monitoring wells were installed near the forebay of the bioretention (**Figure 2.2**). Well 1 (closer to the basin) was installed in August 2018 and Well 2 (further from the basin) in October 2018. Monitoring wells were installed by manually augering 10.2 cm diameter boreholes 3.4 m below grade. Polyvinyl chloride casing (5.1 cm inner diameter) was used with a 1.5 m screen length. The void between the screen and the borehole was packed with sand to 0.6 m above the screened interval. Bentonite was used to seal the void above the sand-packed screened interval. Groundwater levels were monitored with an electric water level meter and groundwater samples were taken with polyethylene bailers. Wells were purged three well volumes before sampling. Samples were collected approximately monthly in 0.5 L HDPE bottles, filtered (0.45 µm PTFE) and analyzed by IC for Cl^-, Na^+, K^+, Mg^{2+}, and Ca^{2+}.

3.3 Results

3.3.1 Stormwater Field Observations

Concentrations of stormwater Cl^- and Na^+ entering the bioretention and bioswale showed strong seasonal variation, while concentrations of K^+, Mg^+, and Ca^{2+} were more consistent throughout the year (**Figure 3.1**). Mean wintertime Cl^- and Na^+ road runoff concentrations (Cl^-=1745 mg/L, Na^+=1015 mg/L for the bioretention and Cl^-=1929 mg/L, Na^+=1161 mg/L for the bioswale) were about two orders of magnitude greater than inlet Ca^{2+} concentrations and three orders of magnitude greater than K^+ and Mg^+ concentrations for both GI types. Mean SAR was about one and a half orders of magnitude higher in winter than summer for both GI. Seasons are defined by four groups of three months (meteorological seasons).

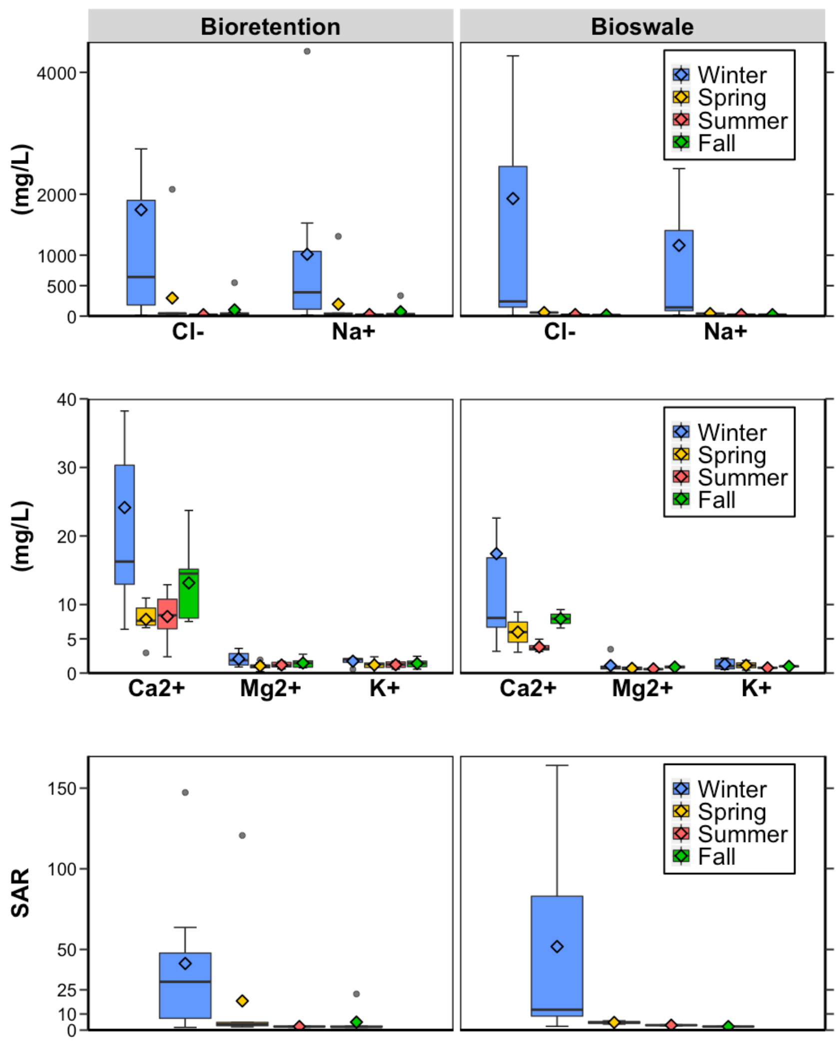

Figure 3.1. Stormwater runoff inlet event mean concentrations (EMCs) of Cl^- and Na^+ (top) and Ca^{2+}, Mg^{2+}, and K^+ (middle), as well as sodium adsorption ratio (SAR; bottom) of the bioretention and bioswale by season. Monitoring data ranges between March 2018 and June 2019 (7 winter, 8 spring, 6 summer, 7 fall events for the bioretention and 7 winter, 2 spring, 4 summer, 2 fall events for the bioswale). Boxplots depict median values (thick black line), mean values (diamond), 25^{th} to 75^{th} percentiles (colored boxes), 1.5 times the interquartile range (whiskers), and outlier values (points).

Cl^- concentrations entering and exiting the bioretention varied significantly by storm event, with the highest concentrations and loads in and out of the bioretention occurring in close proximity to snow events (**Figure 3.2**). 24 out of the 28 monitored events were rain, while 4 were snow (or a mix of rain and snow). Rain events ranged from 0.7 to 10.5 cm and snow events ranged from (2.3 to 6.1 cm as liquid). Together, all monitored precipitation events totaled 130.8 cm with a mean event size of 4.7 cm (**Appendix Table B2**). The total precipitation from March 2018 through June 2019 at nearby Ronald Reagan Airport Weather Station was 206.8 cm. Monitored bioretention events accounted for 63% of the total rain from the weather station.

Cl^- EMCs entering the bioretention ranged from 4 mg/L (8/31/2019) to 7,395 mg/L (1/16/2019), while Cl^- EMCs exiting the bioretention ranged between 17 mg/L (8/21/2019) and 3,748 mg/L (1/16/2019). Mean bioretention inlet Cl^- EMC (552 mg/L ± 277 standard error) was higher than mean outlet Cl^- EMC (329 mg/L ± 139). All four monitored snow events had higher inlet Cl^- concentrations than outlet, but higher outlet Cl^- concentrations than inlet for the next (and usually several) monitored event (**Figure 3.2**).

Winter, spring, summer, and fall account for 79%, 13%, 2%, and 6% of total Cl^- loads into the bioretention and 67%, 21%, 3%, and 10%, respectively, of the total loads out. The single highest Cl^- load in (the multi-day snowmelt event 1/16/2019) accounts for 60% of the total Cl^- load in and 25% of the total load out. The bioretention cumulative Cl^- surface water effluent load reduction was 80% over the monitoring period. The vast majority of Cl^- surface effluent loads traveled through the basin underdrain outlet (96.2%), with the remaining surface effluent exiting through the bypass (3.8%). The bioretention had an overall runoff reduction of 61%, but 82% for the highest single salt load event (**Appendix B Table B3**). The bioretention inlet sampler failed for the 1/19/2019 storm, so the bioswale inlet sample was used for both inlets. The outlet sampler failed on 2/20/2019, but a grab sample was taken. The 2/20/2019 storm was included in concentration averaging but excluded from cumulative loads.

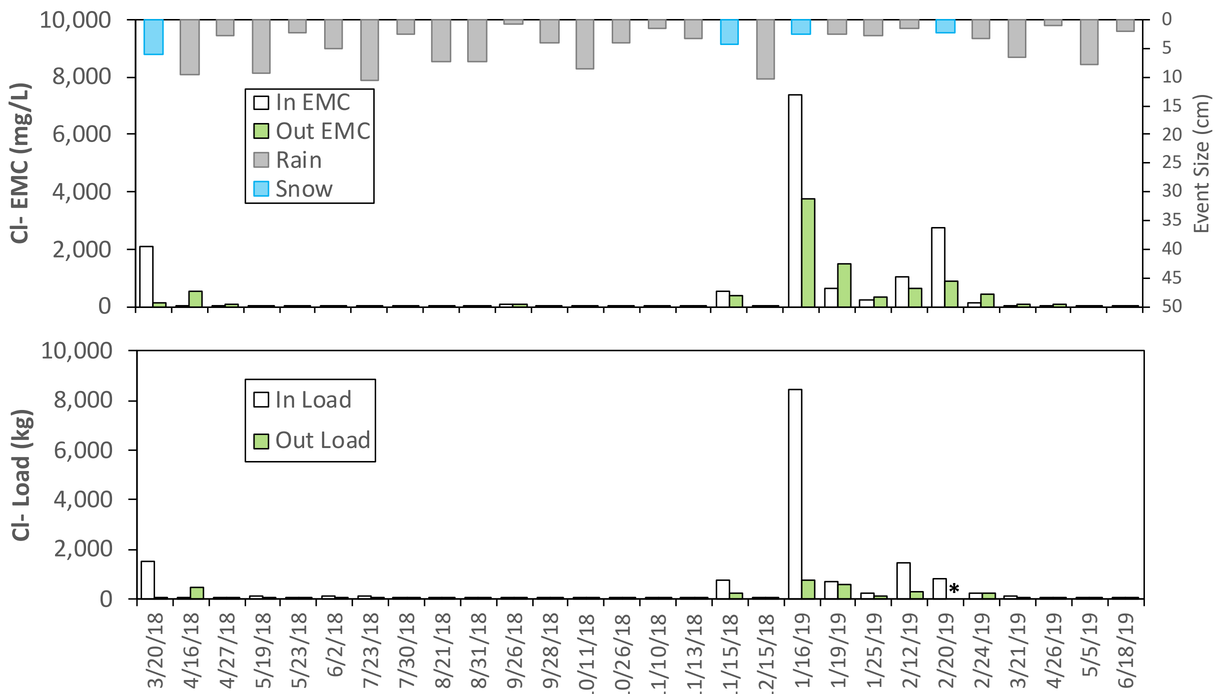

Figure 3.2. Bioretention inlet and outlet Cl^- EMCs (top) and loads (bottom) for 28 monitored rain and snowmelt events. White and green bars show loads or concentrations going in and out of the bioretention, respectively, and correspond to the left y-axis. Grey and blue bars show rain and snow, respectively, and correspond to the right inverted y-axis. Bypass concentrations were not considered for outlet concentrations, but do factor into out loads. No outlet flow-weighted sample was collected on 2/20/19 (*), but a grab sample was taken.

Na^+ concentrations and loads entering and exiting the bioretention follow a similar pattern to Cl^- over the monitoring period (**Appendix B Figures B3 & B4**). Inlet bioretention Na^+ EMCs ranged from 15 mg/L (8/31/2019) to 4,346 mg/L (1/16/2019), while outlet Na^+ EMCs were between 31 mg/L (12/15/2018) and 1,788 mg/L (1/16/2019). Mean bioretention inlet Na^+ EMC (334 mg/L ± 162) was higher than mean outlet Na^+ EMC (178 mg/L ± 65). Just like Cl^-, snow events had higher inlet Na^+ concentrations than outlet, but higher outlet Na^+ concentrations than inlet for subsequent events. Winter, spring, summer, and fall events account for 76%, 15%, 3%, and 7% of the total Na^+ load into the bioretention and 62%, 22%, 8%, and 8% of the total load out, respectively. The single highest Na^+ load in (1/16/2019) accounts for 57% of the total Na^+ load in and 22% of the total load out over the entire monitoring period. The bioretention cumulative Na^+ surface water load reduction was 82% over the monitoring period.

Cl^- concentrations entering and exiting the bioswale were similar to those of the bioretention during and after snow events, though loads were much lower for the bioswale due to its smaller CDA (**Figure 3.3**). 13 of the 15 monitored events for the bioswale were rain, while 2 were snow (or a mix of rain and snow). Rain event depths ranged from 1.39 to 10.4 cm and snow event depths were 2.4 and 2.3 cm. Together, all precipitation events totaled 63.0 cm with a mean event size of 4.2 cm. The total precipitation from May 2018 through June 2019 at nearby Ronald Reagan Airport Weather Station was 192.7 cm. Monitored bioswale events accounted for 33% of the total rain from the weather station.

Cl^- EMCs into the bioswale ranged from 7 mg/L (12/15/2018) to 8,050 mg/L (1/16/2019), while Cl^- EMCs out of the bioswale were between 9 mg/L (8/31/2019) and 7,112 mg/L (1/16/2019). Mean bioswale inlet Cl^- EMC (918 mg/L ± 562) was higher than mean outlet Cl^- EMC (878 mg/L ± 457). The two snow events had higher inlet Cl^- concentrations than outlet, but higher outlet Cl^- concentrations than inlet the next three events (**Figure 3.3**).

Winter, spring, summer, and fall account for 98%, 1.5%, 0.4%, and 0.1% of total Cl^- loads into the bioswale and 93.8%, 4.8%, 1.1%, and 0.2%, respectively, of the total loads out. The single highest Cl^- load in (the multi-day snowmelt event 1/16/2019) accounts for 85% of the total Cl^- load in and 27% of the total load out. The bioswale cumulative Cl^- surface water load reduction was 76% over the monitoring period. Overall runoff reduction for the bioswale was 37%, but 92% for the highest single salt load event (**Appendix B Table B3**).

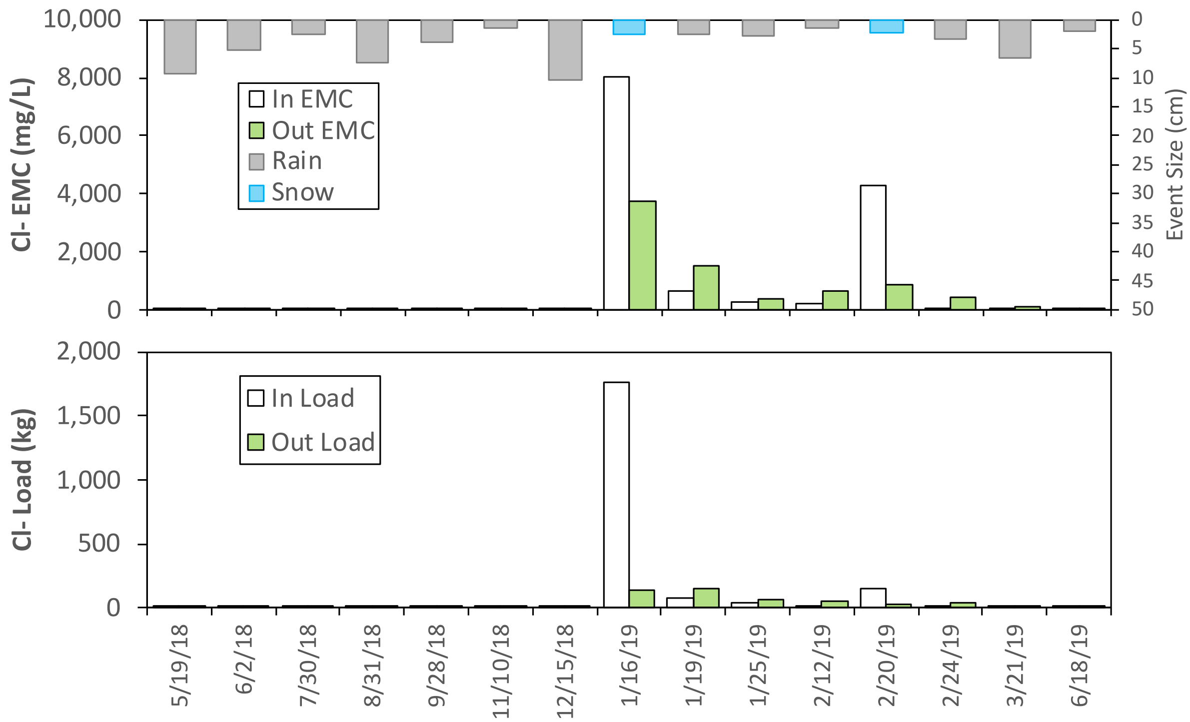

Figure 3.3. Bioswale inlet and outlet Cl^- EMCs (top) and loads (bottom) for 15 monitored rain and snowmelt events. White and green bars show loads or concentrations going in and out of the bioretention, respectively, and correspond to the left y-axis. Grey and blue bars show rain and snow, respectively, and correspond to the right inverted y-axis.

Na^+ concentrations and loads in and out of the bioswale follow a very similar pattern to Cl^- over the monitoring period (**Appendix B Figures B5 & B6**). Inlet bioswale Na^+ EMCs ranged from 17 mg/L (12/15/2018) to 4,976 mg/L (1/16/2019), while outlet Na^+ EMCs were between 27 mg/L (11/10/2018) and 3,501 mg/L (1/16/2019). Mean bioswale inlet Na^+ EMC (524 mg/L ± 321) was higher than mean outlet Na^+ EMC (428 mg/L ± 210). Snow events had higher inlet Na^+ concentrations than outlet, but higher outlet Na^+ concentrations than inlet for subsequent events. Winter, spring, summer, and fall events account for 97.2%, 1.8%, 0.8%, and 0.2% of the total Na^+ load into the bioswale and 85.6%, 7.0%, 6.5%, and 0.9% of the total load out, respectively. The single highest Na^+ load in (1/16/2019) accounts for 84% of the total Na^+ load in and 23% of the total load out over the entire monitoring period. The bioswale cumulative Na^+ surface water load reduction was 78%.

The percent change in average concentrations from inlet to outlet (concentration reduction) and cumulative load reductions of Cl^-, Na^+, K^+, Mg^{2+}, and Ca^{2+} for the bioretention and bioswale are displayed in **Table 3.1**. Both GI have positive average concentration reductions for Cl^- and Na^+, but negative reductions in K^+, Mg^{2+}, and Ca^{2+}. Both GI export of Mg^{2+} loads, and the bioswale exports K^+ and Ca^{2+} loads as well. When broken down by individual event, K^+, Mg^{2+}, and Ca^{2+} concentration and load export occur much more frequently in both GI during and after high salt inputs (**Appendix B Figures B3-B6**).

Table 3.1. Average concentrations, standard error (SE), and *p-values* of concentrations, and total loads of Cl^-, Na^+, K^+, Mg^{2+}, and Ca^{2+} in and out of the bioretention and bioswale. Average concentration reductions and total load reductions are calculated as percent change in vs. out. *p-values* approximately less than or equal to 0.05 are in bold.

	Concentration						**Load**		
	Average In (mg/L)	SE	Average Out (mg/L)	SE	*p-value* In vs. Out	**Average Reduction (%)**	Total In (kg)	Total Out (kg)	**Total Reduction (%)**
Bioretention									
n = 28									
Cl^-	552	277	329	139	0.188	**40**	14061	2869	**80**
Na^+	333	162	178	65	0.162	**47**	8686	1592	**82**
K^+	1.4	0.1	1.7	0.3	0.250	**-22**	45	18	**60**
Mg^{2+}	1.4	0.1	6.9	1.9	**0.007**	**-383**	45	80	**-77**
Ca^{2+}	13.3	2.2	33.6	11.2	**0.052**	**-152**	408	346	**15**
Bioswale									
n = 15									
Cl^-	918	562	878	457	0.856	**4**	2085	501	**76**
Na^+	557	341	452	222	0.510	**19**	1294	282	**78**
K^+	1.1	0.2	3.4	0.8	**0.005**	**-211**	2	3	**-39**
Mg^{2+}	0.9	0.2	11.8	3.9	**0.013**	**-1230**	2	10	**-385**
Ca^{2+}	11.0	3.8	74.0	32.6	**0.054**	**-573**	26	53	**-108**

3.3.2 Soil Observations

Extractible Cl^- in the bioretention ESM (**Figure 3.4.A**) remained relatively constant over approximately three years of monitoring (3.2 mg/kg in October-2016 and 3.4 mg/kg in July-2019), though a small seasonal uptick was observed in spring 2019 (17.6 mg/kg in April-2019). Extractible Na^+ showed a steady increase over time from 7.0 mg/kg (October-2019) to 196.2 mg/kg (July-2019). Increase in soil Na^+ was statistically significant over the monitoring period (between July 2018 and July 2019, 95% CI difference, $p = 0.002$). ESM base saturation percentages (**Figure 3.4.B**) of Na^+ and Ca^{2+} increased over time, Mg^{2+} decreased over time, and K^+ remained relatively constant (**Figure 3.4.B**). CEC gradually decreased over time (October-2016: 18 meq/100g, July-2018: 14, April-2019: 13, and July-2019: 12). Average bulk density of the ESM was 2.0 g/cm^3 in October-2019.

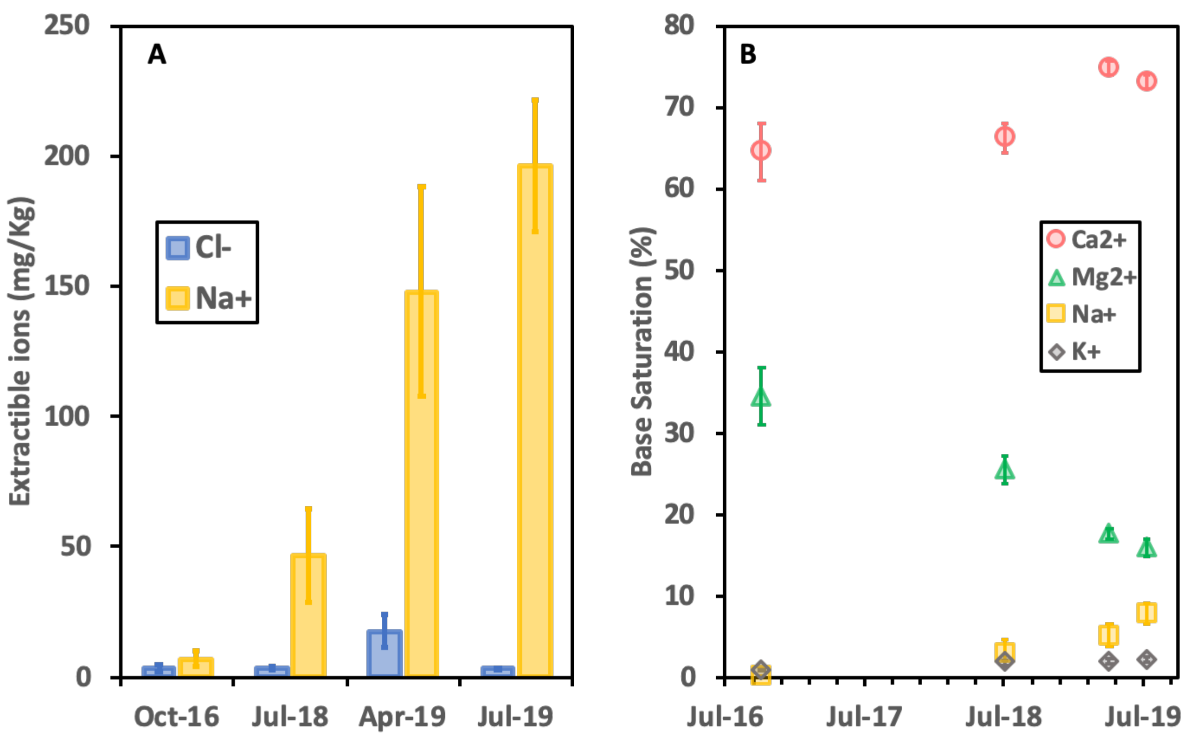

Figure 3.4. Bioretention soil extractible Cl^- and Na^+ concentrations (A) and base saturation of Na^+, K^+, Mg^{2+}, and Ca^{2+} (B) between October 2016 and July 2019. Error bars indicate +/- 1 standard error.

3.3.3 Groundwater Observations

Groundwater samples from the two shallow wells beside the forebay of the bioretention displayed high Cl^- and Na^+ concentrations (**Figure 3.5**). During dates where both wells were sampled, Well 1 (closer to the basin) had higher average Cl^- ($p = 0.004$) and Na^+ ($p = 0.0003$) concentrations (342 mg/L Cl^- and 193 mg/L Na^+) than Well 2 (184 mg/L Cl^- and 84 mg/L Na^+). Cl^- and Na^+ concentrations in Well 1 were highest in August and September 2018 and then decreased over time until increasing again in April 2019 (**Appendix B Figure B7**). Well 2 Cl^- and Na^+ concentrations were more stable over time. In both wells, Cl^- and Na^+ concentrations were an order of magnitude or more higher than Ca^{2+}, Mg^{2+}, and K^+. Average depth to groundwater was 133.5 cm for Well 1 and 120.1 cm for Well 2 (depths relative to the base of Well 1). Groundwater elevations were consistently higher in Well 2 than Well 1, although Well 1 levels displayed more variability and occasionally spiked above Well 2 during periods of heavy rain (**Appendix B Figure B8**).

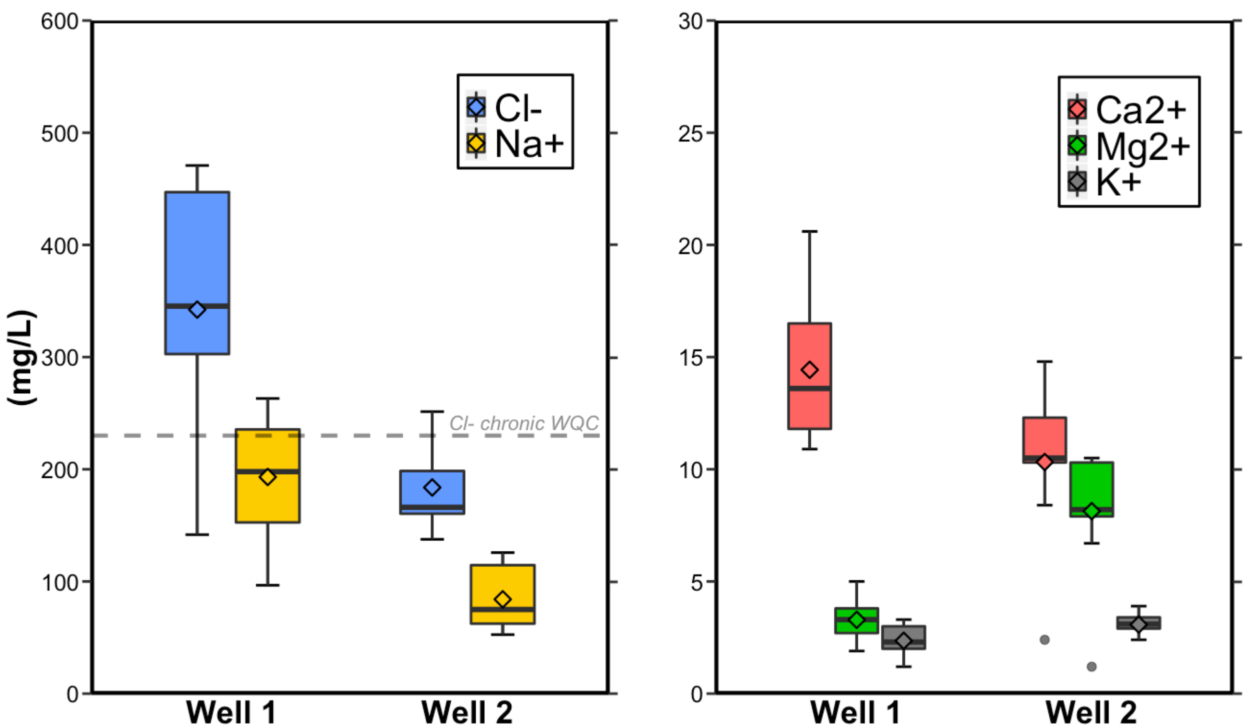

Figure 3.5. Groundwater concentrations of Cl^- and Na^+ (left) and Ca^{2+}, Mg^{2+}, K^+ (right) from two shallow wells next to the bioretention. Nine samples were collected from Well 1 and Well 2 between December 12, 2018 and October 11, 2019. Boxplots depict median values (thick black line), mean values (diamond), 25th to 75th percentiles (colored boxes), 1.5 times the interquartile range (whiskers), and outlier values (points). The dotted grey line indicates U.S. EPA Cl^- chronic freshwater quality criteria of 230 mg/L.

Average molar ratios of Na^+:Cl^- in groundwater were closer to 1 in Well 1 (0.89) than Well 2 (0.70)($p = 0.008$), though the slope of the linear regression line of molar Na^+ vs. Cl^- (**Figure 3.6**) for Well 1 (0.71) was lower than Well 2 (0.96)($p = 0.27$). The slopes of the molar Na^+ vs. Cl^- trendlines for the bioretention and bioswale inlet samples were both very close to 1 (bioretention = 0.90, bioswale = 0.94), while their respective outlet slopes were slightly lower (bioretention = 0.72, bioswale = 0.75). The slopes of Well 1 and Well 2 Na^+:Cl^- trendlines had no significant difference (based on 95% CI difference) from the inlet or outlet Na^+:Cl^- trendline slopes of both GI.

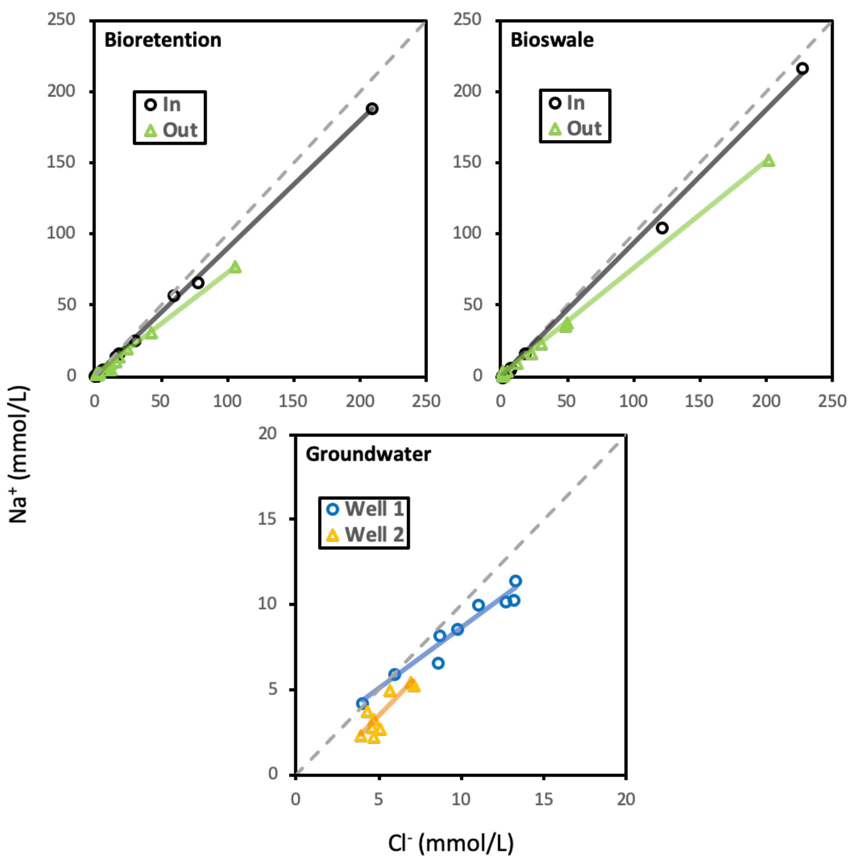

Figure 3.6. Molar Na^+ vs. Cl^- concentrations from bioretention, bioswale, and groundwater samples. Dotted grey lines indicate 1:1 molar ratio and colored lines are linear regressions.

3.4 Discussion

3.4.1 GI Salt Performance

We found high seasonal salt ion concentrations in stormwater entering both the bioretention and the bioswale, almost entirely in the form of NaCl (**Figure 3.1**). For both GI types, Cl^- and Na^+ concentrations in inlet stormwater were, on average, approximately two orders of magnitude higher in the winter than the summer, similar to ranges found in other studies [33,45]. Additionally, slopes of linear regression lines of molar Na^+ vs. Cl^- concentrations were very close to 1 for stormwater entering into both GI, indicating NaCl as the source (**Figure 3.6**). Both GI types displayed similarly high effluent surface load reductions of Cl^- and Na^+, despite differences in design between the bioretention and bioswale (**Table 3.1**). Due to high runoff reductions and limited concentration reductions during winter storms, stormwater runoff volume reduction by infiltration is thought to be the primary mechanism for the observed Cl^- and Na^+ load reduction. The bioretention and bioswale had overall runoff reductions of 61% and 37%, respectively, but 82% and 92% for the highest single salt load event (1/16/2019), which accounted for the vast majority of total inlet Cl^- and Na^+ (**Figures 3.2 and 3.3**).

The bioretention displayed moderate overall Cl^- and Na^+ average concentration reduction, while the bioswale had little concentration reduction of Cl^- and Na^+. Both GI partially reduced initial NaCl concentration shocks, likely by temporarily storing and/or infiltrating Cl^- and Na^+ into plants, soil, and groundwater. Concentration and load exports after high salt events suggest that some stored Cl^- and Na^+ is washed out by subsequent storms. Cl^- concentration and load reductions were slightly lower than Na^+, likely due to attenuation of Na^+ in soils via cation exchange (see below). Overall, both GI practices show ability to dampen surface water from high Cl^- and Na^+ stormwater runoff loads in the winter.

Stormwater data from both GI display evidence of soil cation exchange, with negative average concentration reductions of K^+, Mg^{2+}, and Ca^{2+} and negative cumulative load reductions of Mg^{2+} (bioswale had negative load reductions of K^+, Mg^{2+}, and Ca^{2+}). The export of K^+, Mg^{2+}, and Ca^{2+} occurred largely during and after storms with high Na^+ input (**Appendix B Figures B3-B6**). These results are consistent with other studies on cation exchange in soils receiving high salt inputs [32,45–47]. Export of Mg^{2+} was particularly high for both GI. The higher overall K^+, Mg^{2+}, and Ca^{2+} percentage concentration and load exports in the bioswale are largely due to the lower overall stormwater runoff reduction of the system and the higher percentage of winter storms that make up the data set.

3.4.2 Uptake by Vegetation

The influence of vegetation was not directly observed, but may have played a role in Cl^- and Na^+ storage. Most vegetation was observed to be dormant during the winter season (**Appendix B Figures B1 and B2**), which accounted for the vast majority of salt loading into the GI. It is possible that vegetation at both the bioretention and bioswale contributed slightly to storage of Cl^- and Na^+, but the size of that contribution is estimated to be small based on the relatively short contact time of the ions with plant roots, the limited capacity of plant uptake, and the lack of known halophytic vegetation in both GI [38,39]. Additionally, vegetation salt uptake may only result in short term removal as salt would remobilize as vegetation decays. While traditionally employed vegetation may have limited ability for winter salt removal, it is certainly important for other GI functions, and those functions may be impaired if vegetation is inhibited by salt loading [37,48]. Therefore, it is important that salt tolerant vegetation is used for GI. The extent to which GI vegetation is impaired by salt and the ability of halophytic vegetation to store significant salt loads in GI are suggested for future study.

3.4.3 Bioretention Soil Changes Over Time

The ESM within the bioretention basin displayed significant long-term accumulation of Na^+ but not Cl^-, adding evidence of Na^+ cation exchange (**Figure 3.4.A**). A minor increase in extractible Cl^- in the spring is likely the result of leftover Cl^- temporarily stored in soil porewater [32]. Over the long term, however, there was no significant change in ESM Cl^- concentration. Gradual increases in Na^+ base saturation coupled with gradual decreases in Mg^{2+} suggests that Na^+ primarily exchanges with Mg^{2+} in the bioretention ESM (**Figure 3.4.B)**.

Cation exchange in the ESM could possibly induce remobilization of other soil ions, such as metals. Metal remobilization in soils associated with salt addition has been found to occur under certain salt and soil conditions as a result of cation exchange, pH change, and Cl^- complexation [49–53]. Additionally, the observed seasonal peaks in the ratio of Na^+ to other base cations (SAR) in stormwater influent has been associated with soil media clogging, lower infiltration rates, and particle erosion [54–56]. Particle erosion (in the form of soil fines washing-out) may be responsible for the observed reduction in soil CEC over time. Reduction in CEC decreases the soil's ability to sorb pollutants, which can diminish GI performance over time and may lead to increased maintenance efforts to manage and/or replace the ESM of older GI. The bioretention ESM is relatively young and soil monitoring only spans approximately 3 years. Future research should look into how ESM Na^+ and CEC levels continue to change as well as the development of more resilient ESM to deicing salt ions.

Assuming uniform distribution of Cl^- and Na^+ average soil concentrations and soil bulk density, the entire volume of ESM in the bioretention basin is calculated to have stored (long-term) 0% of the Cl^- and 3.1% of the Na^+ load reduced by the bioretention from July 2018 to July 2019. Assuming that plant uptake of Cl^- and Na^+ is minor, the vast majority of Cl^- and Na^+ removed from surface water by the bioretention (and very likely the bioswale too) infiltrates into groundwater. This means that as much as 80% of Cl^- and 79% of Na^+ bioretention stormwater influent loads end up in groundwater.

3.4.4 Infiltration into Groundwater

We found elevated Cl^- and Na^+ concentrations year-round in two shallow monitoring wells beneath the forebay of the bioretention (**Figure 3.5**). Groundwater Cl^- levels, however, were not as high as those found under stormwater ponds by Snodgrass et al. [33]. The slope of the regression line of molar Na^+ vs. Cl^- concentrations for Well 1 (0.71) was statistically indistinguishable from the slope of the outlet of the bioretention (0.72), suggesting infiltrating stormwater as the source of Na^+ and Cl^- to Well 1 (**Figure 3.6**). Well 2 had consistently lower levels of Cl^- and Na^+, likely because it is further from the infiltration basin and generally upstream of the hydraulic gradient. Well 1's greater groundwater level fluctuations during heavy rainfall (**Appendix B Figure B8**) suggest it is influenced more by infiltrating stormwater from the bioretention basin than Well 2. Na^+ concentrations were, on average, an order of magnitude higher than other base cations, further suggesting NaCl from infiltrating stormwater. Well 1 groundwater Cl^- and Na^+ concentrations didn't spike until April 2019, a five month lag time from the first snow event in November 2018 (**Appendix B Figure B7)**. This delayed release of salt ions is consistent a Robinson et al. (2017) study that observed soils to slowly release Cl^- and Na^+ over several months following salt application [32]. The initial decreasing trend in Cl^- and Na^+ concentrations in Well 1 from August 2018 to March 2019 may have been a recovery from salting from previous winters [32,45]. Temporal trends in groundwater Cl^- and Na^+ levels suggest slower, longer term transport of salt into groundwater, beyond the time scale of this study. The residence time of Cl^- and Na^+ ions in groundwater is unknown and it is likely some ions eventually re-enter back into surface water systems. However, even temporary storage in groundwater can help buffer surface waters from wintertime shocks of high Cl^- and Na^+ surface water loads [15]. A more detailed and longer-term study into the movement of salt ions in groundwater underlying infiltration GI is suggested for future research.

While transfer of Cl^- and Na^+ to groundwater may help seasonally protect surface waters, it will also increasingly impair slower-moving groundwater over time. This tradeoff between surface water and groundwater salt loading should be an important consideration for urban/transportation planners and engineers. For this reason, infiltration GI may not be the best choice for drainage areas with high deicing salt loading near groundwater drinking water sources. However, for locations with high salt loading that do not rely on groundwater for drinking water, infiltration GI may be a good choice to seasonally buffer surface waters from high salt concentrations/loads. For the many drainage areas with high salt loading that already employ infiltration GI, better management of winter salt application is suggested to alleviate the negative effects of deicing salt ions on GI performance and the surrounding environment.

3.5 Conclusions

Both the bioretention and bioswale received high winter stormwater loads of Cl^- and Na^+ and were able to significantly reduced those loads in effluent surface water by minor retention in soils and infiltration into groundwater. Changes in bioretention soil chemistry indicate a small percentage of Na^+ was stored long-term by ion exchange, but no long-term Cl^- storage was observed. Limited observed soil storage, assumed limited vegetation storage, and groundwater Cl^- and Na^+ observations suggest the majority of salt removed from stormwater by the bioretention infiltrates into groundwater. Infiltration GI have ability to buffer surface waters from salt, but their primary mechanism for doing so is salt transfer from surface water to groundwater.

Results indicate that infiltration GI plays an important role in deicing salt transport. Stormwater managers can utilize infiltration GI to reduce surface water winter deicing salt loading, but should recognize the increased threat to groundwater resources in doing so. Further investigation is suggested into the viability of halophytic vegetation as a deicing salt sink, long-term changes and improved deicing salt resilience in engineered soil media, and fate/transport of deicing salts in groundwater underlying infiltration GI.

Supplementary Data: Appendix B

3.6 References

(1) Dhakal, K. P.; Chevalier, L. R. Urban Stormwater Governance: The Need for a Paradigm Shift. *Environ. Manage.* **2016**, *57* (5), 1112–1124. https://doi.org/10.1007/s00267-016-0667-5.

(2) Ahiablame, L. M.; Engel, B. A.; Chaubey, I. Effectiveness of Low Impact Development Practices in Two Urbanized Watersheds: Retrofitting with Rain Barrel/Cistern and Porous Pavement. *J. Environ. Manage.* **2013**, *119*, 151–161. https://doi.org/10.1016/j.jenvman.2013.01.019.

(3) Wardynski, B. J.; Winston, R. J.; Line, D. E.; Hunt, W. F. Metrics for Assessing Thermal Performance of Stormwater Control Measures. *Ecol. Eng.* **2014**, *71*, 551–562. https://doi.org/10.1016/J.ECOLENG.2014.07.068.

(4) Walsh, C. J.; Roy, A. H.; Feminella, J. W.; Cottingham, P. D.; Groffman, P. M.; Morgan Ii, R. P. The Urban Stream Syndrome: Current Knowledge and the Search for a Cure. *Benthol. Soc* **2005**, *24* (3), 706–723.

(5) Spromberg, J. A.; Baldwin, D. H.; Damm, S. E.; Mcintyre, J. K.; Huff, M.; Sloan, C. A.; Anulacion, B. F.; Davis, J. W.; Scholz, N. L. EDITOR'S CHOICE: Coho Salmon Spawner Mortality in Western US Urban Watersheds: Bioinfiltration Prevents Lethal Storm Water Impacts. *J. Appl. Ecol.* **2016**, *53* (2), 398–407. https://doi.org/10.1111/1365-2664.12534.

(6) Coffman, L. *Low-Impact Development Design Strategies An Integrated Design Approach*; Prince George's County, Maryland, 2000.

(7) Vogel, J. R.; Moore, T. L.; Coffman, R. R.; Rodie, S. N.; Hutchinson, S. L.; McDonough, K. R.; McLemore, A. J.; McMaine, J. T. Critical Review of Technical Questions Facing Low Impact Development and Green Infrastructure: A Perspective from the Great Plains. *Water Environ. Res.* **2015**, *87* (9), 849–862.

https://doi.org/10.2175/106143015X14362865226392.
(8) Morse, N. R.; Mcphillips, L. E.; Shapleigh, J. P.; Walter, M. T.; Wrigley, J. A. The Role of Denitrification in Stormwater Detention Basin Treatment of Nitrogen. *Environ. Sci. Technol. 2017,* **2017**, *51*, 7928−7935. https://doi.org/10.1021/acs.est.7b01813.
(9) Kramer, M. G. *Enhancing Sustainable Communities with Green Infrastructure (EPA 100-R-14-006)*; 2014.
(10) McIntyre, J. K.; Davis, J. W.; Hinman, C.; Macneale, K. H.; Anulacion, B. F.; Scholz, N. L.; Stark, J. D. Soil Bioretention Protects Juvenile Salmon and Their Prey from the Toxic Impacts of Urban Stormwater Runoff. *Chemosphere* **2015**, *132*, 213–219. https://doi.org/10.1016/j.chemosphere.2014.12.052.
(11) McIntyre, J. K.; Davis, J. W.; Incardona, J. P.; Stark, J. D.; Anulacion, B. F.; Scholz, N. L. Zebrafish and Clean Water Technology: Assessing Soil Bioretention as a Protective Treatment for Toxic Urban Runoff. *Sci. Total Environ.* **2014**, *500*, 173–180. https://doi.org/10.1016/j.scitotenv.2014.08.066.
(12) Pennino, M. J.; McDonald, R. I.; Jaffe, P. R. Watershed-Scale Impacts of Stormwater Green Infrastructure on Hydrology, Nutrient Fluxes, and Combined Sewer Overflows in the Mid-Atlantic Region. *Sci. Total Environ.* **2016**, *565*, 1044–1053. https://doi.org/10.1016/j.scitotenv.2016.05.101.
(13) Henderson, D.; Smith, J. A.; Fitch, G. M. Impact of Vegetation Management on Vegetated Roadsides and Their Performance as a Low-Impact Development Practice for Linear Transportation Infrastructure. *Transp. Res. Rec. J. Transp. Res. Board* **2016**, *2588*, 172–180. https://doi.org/10.3141/2588-19.
(14) Henderson, D. A.; Moruza, G.; Burgis, C. R.; Smith, J. A. Low Impact Development Technologies for Highway Stormwater Runoff. In *Encyclopedia of Water: Science, Technology, and Society.*; Wiley, 2019.
(15) Ledford, S. H.; Lautz, L. K.; Stella, J. C. Hydrogeologic Processes Impacting Storage, Fate, and Transport of Chloride from Road Salt in Urban Riparian Aquifers. *Environ. Sci. Technol.* **2016**, *50* (10), 4979–4988. https://doi.org/10.1021/acs.est.6b00402.
(16) Perera, N.; Gharabaghi, B.; Howard, K. Groundwater Chloride Response in the Highland Creek Watershed Due to Road Salt Application: A Re-Assessment after 20years. *J. Hydrol.* **2013**, *479*, 159–168. https://doi.org/10.1016/j.jhydrol.2012.11.057.
(17) Corsi, S. R.; De Cicco, L. A.; Lutz, M. A.; Hirsch, R. M. River Chloride Trends in Snow-Affected Urban Watersheds: Increasing Concentrations Outpace Urban Growth Rate and Are Common among All Seasons. *Sci. Total Environ.* **2015**, *508*, 488–497. https://doi.org/10.1016/J.SCITOTENV.2014.12.012.
(18) Kaushal, S. S.; Groffman, P. M.; Likens, G. E.; Belt, K. T.; Stack, W. P.; Kelly, V. R.; Band, L. E.; Fisher, G. T. Increased Salinization of Fresh Water in the Northeastern United States. *Proc. Natl. Acad. Sci. U. S. A.* **2005**, *102* (38), 13517–13520. https://doi.org/10.1073/pnas.0506414102.
(19) Haq, S.; Kaushal, S. S.; Duan, S. Episodic Salinization and Freshwater Salinization Syndrome Mobilize Base Cations, Carbon, and Nutrients to Streams across Urban Regions. *Biogeochemistry* **2018**, *141* (3), 463–486. https://doi.org/10.1007/s10533-018-0514-2.
(20) Corsi, S. R.; Graczyk, D. J.; Geis, S. W.; Booth, N. L.; Richards, K. D. A Fresh Look at Road Salt: Aquatic Toxicity and Water-Quality Impacts on Local, Regional, and National Scales. *Environ. Sci. Technol.* **2010**, *44* (19), 7376–7382.

https://doi.org/10.1021/es101333u.
(21) Kelly, V. R.; Lovett, G. M.; Weathers, K. C.; Findlay, S. E. G.; Strayer, D. L.; Burns, D. J.; Likens, G. E. Long-Term Sodium Chloride Retention in a Rural Watershed: Legacy Effects of Road Salt on Streamwater Concentration. *Environ. Sci. Technol.* **2008**, *42* (2), 410–415. https://doi.org/10.1021/es071391l.
(22) Trowbridge, P. R.; Kahl, J. S.; Sassan, D. A.; Heath, D. L.; Walsh, E. M. Relating Road Salt to Exceedances of the Water Quality Standard for Chloride in New Hampshire Streams. *Environ. Sci. Technol.* **2010**, *44* (13), 4903–4909. https://doi.org/10.1021/es100325j.
(23) Müller, A.; Österlund, H.; Marsalek, J.; Viklander, M. The Pollution Conveyed by Urban Runoff: A Review of Sources. *Sci. Total Environ.* **2020**, *709*, 136125. https://doi.org/10.1016/J.SCITOTENV.2019.136125.
(24) U.S. Geological Survey. *MINERAL COMMODITY SUMMARIES 2019*; 2019. https://doi.org/https://doi.org/10.3133/70202434.
(25) Howard, K. W. F.; Haynes, J. Groundwater Contamination Due to Road De-Icing Chemicals - Salt Balance Implications. *Geosci. Canada* **1993**, *20* (1), 1–8. https://doi.org/10.1016/0169-7722(93)90010-P.
(26) Jones, D. K.; Mattes, B. M.; Hintz, W. D.; Schuler, M. S.; Stoler, A. B.; Lind, L. A.; Cooper, R. O.; Relyea, R. A. Investigation of Road Salts and Biotic Stressors on Freshwater Wetland Communities. **2017**. https://doi.org/10.1016/j.envpol.2016.11.060.
(27) Equiza, M. A.; Calvo-Polanco, M.; Cirelli, D.; Señorans, J.; Wartenbe, M.; Saunders, C.; Zwiazek, J. J. Long-Term Impact of Road Salt (NaCl) on Soil and Urban Trees in Edmonton, Canada. *Urban For. Urban Green.* **2017**, *21*, 16–28. https://doi.org/10.1016/j.ufug.2016.11.003.
(28) Hintz, W. D.; Mattes, B. M.; Schuler, M. S.; Jones, D. K.; Stoler, A. B.; Lind, L.; Relyea, R. A. Salinization Triggers a Trophic Cascade in Experimental Freshwater Communities with Varying Food-Chain Length. *Ecol. Appl.* **2017**, *27* (3), 833–844. https://doi.org/10.1002/eap.1487.
(29) Kaushal, S. S.; Likens, G. E.; Pace, M. L.; Utz, R. M.; Haq, S.; Gorman, J.; Grese, M. Freshwater Salinization Syndrome on a Continental Scale. *Proc. Natl. Acad. Sci. U. S. A.* **2018**, *115* (4), E574–E583. https://doi.org/10.1073/pnas.1711234115.
(30) US EPA. National Recommended Water Quality Criteria - Aquatic Life Criteria Table https://www.epa.gov/wqc/national-recommended-water-quality-criteria-aquatic-life-criteria-table (accessed Feb 10, 2020).
(31) EPA. *Drinking Water Advisory: Consumer Acceptability Advice and Health Effects Analysis on Sodium*; Washington, DC, 2003.
(32) Robinson, H. K.; Hasenmueller, E. A.; Chambers, L. G. Soil as a Reservoir for Road Salt Retention Leading to Its Gradual Release to Groundwater. *Appl. Geochemistry* **2017**, *83*, 72–85. https://doi.org/10.1016/J.APGEOCHEM.2017.01.018.
(33) Snodgrass, J. W.; Moore, J.; Lev, S. M.; Casey, R. E.; Ownby, D. R.; Flora, R. F.; Izzo, G. Influence of Modern Stormwater Management Practices on Transport of Road Salt to Surface Waters. *Environ. Sci. Technol.* **2017**, *51* (8), 4165–4172. https://doi.org/10.1021/acs.est.6b03107.
(34) Denich, C.; Bradford, A.; Drake, J. Bioretention: Assessing Effects of Winter Salt and Aggregate Application on Plant Health, Media Clogging and Effluent Quality. *Water Qual. Res. J.* **2013**, *48* (4), 387–399. https://doi.org/10.2166/wqrjc.2013.065.

(35) Interstate Commission on the Potomac River Basin. *Chloride TMDLs for the Accotink Creek Watershed, Fairfax County, Virginia*; 2017.
(36) Minnesota Pollution Control Agency. *Twin Cities Metropolitan Area Chloride Management Plan*; 2016.
(37) Fay, L.; Shi, X. Environmental Impacts of Chemicals for Snow and Ice Control: State of the Knowledge. *Water, Air, Soil Pollut.* **2012**, *223* (5), 2751–2770. https://doi.org/10.1007/s11270-011-1064-6.
(38) Morteau, B.; Triffault-Bouchet, G.; Galvez, R.; Martel, L. Nutrient and Removal Kinetics Impacts on Salt Phytoremediation by Atriplex Patula and Typha Angustifolia. *J. Environ. Eng.* **2015**, *141* (2), 04014059. https://doi.org/10.1061/(ASCE)EE.1943-7870.0000889.
(39) Hasanuzzaman, M.; Nahar, K.; Alam, M. M.; Bhowmik, P. C.; Hossain, M. A.; Rahman, M. M.; Prasad, M. N. V.; Ozturk, M.; Fujita, M. Potential Use of Halophytes to Remediate Saline Soils. *Biomed Res. Int.* **2014**, *2014*, 589341. https://doi.org/10.1155/2014/589341.
(40) VDOT Maintenance Division. *Maintenance Best Practices*; Richmond, VA, 2015.
(41) VDOT. *AVERAGE DAILY TRAFFIC VOLUMES with VEHICLE CLASSIFICATION DATA on INTERSTATE, ARTERIAL and PRIMARY ROUTES*; 2018.
(42) Beisch, W. D. *Final Design Hydrologic and Hydraulic Summary Lorton Road Widening, Project 4YP213*; 2012.
(43) Hayes, G. M.; Burgis, C.; Zhang, W.; Henderson, D.; Smith, J. A. Runoff Reduction by Four Green Stormwater Infrastructure Systems in a Shared Environment. *J. Sustain. Water Built Environ. (under Rev.*
(44) Oster, J. D.; Sposito, G. The Gapon Coefficient and the Exchangeable Sodium Percentage-Sodium Adsorption Ratio Relation. *Soil Sci. Soc. Am. J.* **1980**, *44* (2), 258–260. https://doi.org/10.2136/sssaj1980.03615995004400020011x.
(45) Mullins, A. R.; Bain, D. J.; Pfeil-McCullough, E.; Hopkins, K. G.; Lavin, S.; Copeland, E. Seasonal Drivers of Chemical and Hydrological Patterns in Roadside Infiltration-Based Green Infrastructure. *Sci. Total Environ.* **2020**, 136503. https://doi.org/10.1016/j.scitotenv.2020.136503.
(46) Norrström, A. .; Jacks, G. Concentration and Fractionation of Heavy Metals in Roadside Soils Receiving De-Icing Salts. *Sci. Total Environ.* **1998**, *218* (2–3), 161–174. https://doi.org/10.1016/S0048-9697(98)00203-4.
(47) Kaushal, S. S.; Likens, G. E.; Pace, M. L.; Haq, S.; Wood, K. L.; Galella, J. G.; Morel, C.; Doody, T. R.; Wessel, B.; Kortelainen, P.; et al. Novel 'Chemical Cocktails' in Inland Waters Are a Consequence of the Freshwater Salinization Syndrome. *Philos. Trans. R. Soc. B Biol. Sci.* **2019**, *374* (1764). https://doi.org/10.1098/rstb.2018.0017.
(48) Muerdter, C. P.; Wong, C. K.; LeFevre, G. H. Emerging Investigator Series: The Role of Vegetation in Bioretention for Stormwater Treatment in the Built Environment: Pollutant Removal, Hydrologic Function, and Ancillary Benefits. *Environ. Sci. Water Res. Technol.* **2018**, *4* (5), 592–612. https://doi.org/10.1039/C7EW00511C.
(49) Bäckström, M.; Karlsson, S.; Bäckman, L.; Folkeson, L.; Lind, B. Mobilisation of Heavy Metals by Deicing Salts in a Roadside Environment. *Water Res.* **2004**, *38* (3), 720–732. https://doi.org/10.1016/J.WATRES.2003.11.006.
(50) Huber, M.; Hilbig, H.; Badenberg, S. C.; Fassnacht, J.; Drewes, J. E.; Helmreich, B. Heavy Metal Removal Mechanisms of Sorptive Filter Materials for Road Runoff Treatment and Remobilization under De-Icing Salt Applications. *Water Res.* **2016**, *102*, 453–463. https://doi.org/10.1016/J.WATRES.2016.06.063.

(51) Muthanna, T. M.; Viklander, M.; Blecken, G.; Thorolfsson, S. T. Snowmelt Pollutant Removal in Bioretention Areas. *Water Res.* **2007**, *41* (18), 4061–4072. https://doi.org/10.1016/J.WATRES.2007.05.040.
(52) Norrström, A. C. Metal Mobility by De-Icing Salt from an Infiltration Trench for Highway Runoff. *Appl. Geochemistry* **2005**, *20* (10), 1907–1919. https://doi.org/10.1016/J.APGEOCHEM.2005.06.002.
(53) Søberg, L. C.; Viklander, M.; Blecken, G.-T. Do Salt and Low Temperature Impair Metal Treatment in Stormwater Bioretention Cells with or without a Submerged Zone? *Sci. Total Environ.* **2017**, *579*, 1588–1599. https://doi.org/10.1016/J.SCITOTENV.2016.11.179.
(54) Flanagan, K.; Branchu, P.; Boudahmane, L.; Caupos, E.; Demare, D.; Deshayes, S.; Dubois, P.; Meffray, L.; Partibane, C.; Saad, M.; et al. Retention and Transport Processes of Particulate and Dissolved Micropollutants in Stormwater Biofilters Treating Road Runoff. *Sci. Total Environ.* **2019**, *656*, 1178–1190. https://doi.org/10.1016/J.SCITOTENV.2018.11.304.
(55) Norrström, A.-C.; Bergstedt, E. The Impact of Road De-Icing Salts (NaCl) on Colloid Dispersion and Base Cation Pools in Roadside Soils. *Water. Air. Soil Pollut.* **2001**, *127* (1/4), 281–299. https://doi.org/10.1023/A:1005221314856.
(56) Shainberg, I.; Letey, J. Response of Soils to Sodic and Saline Conditions. *Hilgardia* **1984**, *52* (2), 1–57. https://doi.org/10.3733/hilg.v52n02p057.

Chapter 4: Tracking Denitrification in Green Stormwater Infrastructure with Nitrate Stable Isotopes

One publication has been created from this chapter and is ready for submission.

Burgis, C.R., Hayes, G., Zhang, W., Henderson, D.A., Macko, S.A., Smith, J.A. (2020)

"Tracking Denitrification in Green Stormwater Infrastructure with Dual Nitrate Stable Isotopes."

(*manuscript in preparation*)

4.1 Introduction

Changes in human land use over the past century have altered the nitrogen cycle, leading to significantly increased watershed nitrogen export [1–4]. Excess nitrogen input can lead to eutrophication, harmful algae blooms, hypoxia, and a loss of biodiversity and habitat in aquatic systems [5–7]. Urbanized areas in particular have become significant vectors of non-point source nitrogen pollution, including nitrogen from fossil fuel combustion, fertilizer application, combined sewer overflows, and leaky sanitary sewers [8–14]. As population growth intensifies urbanization, strategies to mitigate urban watershed nitrogen export will be critical in protecting and improving water resources [15,16].

Green infrastructure (GI) stormwater management techniques (e.g. bioretention) are designed to return an area to pre-development hydrology by slowing, spreading, and infiltrating stormwater runoff before discharging it to receiving waters. GI mimics natural landscape features, employing physical (e.g. settling and filtration) and biological (e.g. plant uptake and microbial cycling) processes to remove pollutants from stormwater. GI is increasingly designed into urban landscapes to protect waterways from detrimental effects of urban stormwater, while also potentially providing economic, social, and public health benefits to urban communities [17–22]. However, GI is a relatively new and still developing technology with many performance knowledge gaps.

GI has shown ability to remove nitrogen from stormwater, but the mechanism of removal is often unclear [18,23–26]. Physical mechanisms have proven ineffective for GI dissolved nitrogen removal, but biological mechanisms (plant uptake and denitrification) have shown potential [27–29]. GI may also act as a nitrogen conduit from surface to groundwater through infiltration, a setting for nitrogen transformation through nitrification, or even a source of export by leaching of stored nitrogen from soil media and plants [18,23,25,30–32]. Denitrification, the microbially mediated conversion of nitrate (NO_3^-) to nitrous oxide (N_2O) and N_2 gas, is the only mechanism that results in permanent removal of dissolved nitrogen by GI [33].

Previous studies have looked for evidence of denitrification in GI. Bettez and Groffman (2012) found higher denitrification potential in GI sediments than in natural riparian buffer areas and suggest that bioretention practices may have high denitrification potential [34]. Morse et al. (2017) found wet basins were capable of denitrifying 58% of incoming dissolved inorganic nitrogen (DIN), while dry basins were only capable of denitrifying 1%. Payne et al. (2014) used stable isotope methods to track denitrification and plant uptake in laboratory bioretention columns, finding that plant uptake was the dominant nitrate removal mechanism, with denitrification only accounting for 0-8% of nitrate removal [28]. These studies suggest that GI may have varying degrees of denitrification potential, but few field experiments have tracked the occurrence of denitrification in operational GI.

Dual nitrogen and oxygen stable isotope analysis of nitrate ($\delta^{15}N\text{-}NO_3^-$ and $\delta^{18}O\text{-}NO_3^-$) has become a useful tool for both the identification of denitrification and sources of nitrate in water [35–38]. Denitrifying microbes prefer to denitrify nitrate with lighter nitrogen and oxygen isotopes, leaving residual nitrate enriched in $\delta^{15}N\text{-}NO_3^-$ and $\delta^{18}O\text{-}NO_3^-$. Shifting isotope ratios left behind by this microbial preference can be used as a footprint of denitrification.

In this study, we monitor the year-round field performance of a roadside infiltration GI practice (bioretention basin) in Northern Virginia to investigate the transport of nitrogen and the occurrence and contribution of denitrification. Stormwater runoff volumes, nitrogen concentrations, and nitrate isotope ratios ($\delta^{15}N\text{-}NO_3^-$ and $\delta^{18}O\text{-}NO_3^-$) were measured at the inlet and outlet of the bioretention during 24 storm events in all seasons over 14 months. We use this information to gain insight into nitrogen removal and transport within bioretention, including determining when denitrification is taking place, how much nitrogen removal denitrification is responsible for, what sources of nitrogen are involved, and what other removal mechanisms are taking place. We also suggest ways to encourage denitrification in future GI designs. To our knowledge, this is the first field experiment using dual nitrate stable isotope analysis to track denitrification within an operational bioretention basin.

4.2 Materials and Methods

4.2.1 Study Site

The study site and stormwater field monitoring methods have been described elsewhere [30,39]. Briefly, a bioretention basin (hereafter bioretention) was monitored directly north of Lorton Road, in Fairfax County, Virginia. The bioretention was designed for a 1 year, 24 hour frequency storm and its construction was completed in spring 2017. Maintenance was performed bi-annually (once in spring and once in fall) to remove trash, mow roadside grass slopes, clear decaying vegetation, and maintain mulch levels. Lorton Road is a four-lane divided road with an average daily traffic volume of 100,000 vehicles/day[40] and is part of the Giles Run watershed, within the Chesapeake Bay watershed.

The bioretention (pictured in **Figure 2.2**) design specifications are presented in **Table 4.1**. Concentrated stormwater from Lorton Road is conveyed to the bioretention via a curb and gutter sewer. Stormwater first flows into a forebay before traveling into a basin where it filters through engineered soil media and underlying gravel. An underdrain at the top of the gravel layer drains the basin. For larger than designed precipitation events, a channel in the forebay allows overflow stormwater to bypass the basin. The engineered soil media is a highly permeable mix of sand, topsoil, and leaf compost. Both the basin and the forebay have a variety of grasses, wildflowers, trees, and shrubs (**Appendix A Table A1 and Appendix B Figure B1**).

Table 4.1. Engineering specifications of the Lorton Road bioretention study site.

		Bioretention
Contributing drainage area (CDA)	m^2	47,753
Impervious drainage area	%	35
Bioretention area (forebay + basin)	m^2	1,012
CDA:bioretention area	ratio	47.2
Storage volume	m^3	447
Ponding depth	cm	15.2
CDA land use		roadway, residential properties, and woods
Stormwater inflow		curb and gutter sewer
Stormwater outflow		10 cm diameter basin underdrain + bypass channel
Basin mulch depth	cm	5
Basin engineered soil depth	cm	76
Basin underlying gravel depth	cm	40
Engineered soil makeup		sand, topsoil, compost (5%)
Engineered soil particle distribution		91.2% sand, 5.6% silt, 3.2% clay
Vegetation type		trees, shrubs, grasses, and wildflowers (see Table S1 for species)

4.2.2 Stormwater Field Monitoring

We monitored 24 rain and snow events at the bioretention between April 2018 and June 2019. A tipping bucket rain gauge next to the bioretention recorded 10-minute precipitation data with a 0.025 cm measurement resolution. Only events with more than 0.25 cm of precipitation were monitored and at least 12 hours of dry conditions preceded and followed each event. If the rain gauge malfunctioned, publicly available weather data from the nearest weather station were used.

Stormwater runoff flow volumes and nitrogen concentrations were determined to calculate the mass of different forms of nitrogen traveling in and out of the bioretention. Runoff flow rates were measured using custom sized flumes at each monitoring location to intercept stormwater flow from the culvert, pipe, or channel based on Hayes (2020) [39]. Flow rate data over time were used to calculate volume of water passing through each monitoring location per storm. The bioretention had three monitoring points (inlet culvert, basin outlet underdrain, and bypass channel; **Figure 2.2**). All three monitoring points were used to calculate runoff and nitrogen load reductions (load reduction = inlet – outlet – bypass).

Autosamplers collected flow-weighted composite stormwater samples (i.e. one composite sample per monitoring location per storm event) throughout each storm event at preprogrammed volume increments. For each storm, subsamples at each monitoring location spanned as much stormwater volume as possible to makeup flow-weighted composite samples (number and spread of sub-samples in **Appendix A Equation A5 & Table A2**). Samples were taken within the flumes, stored in 9.5 L glass jars on ice within each autosampler, and collected within 24 hours of each storm event for lab analysis. Autosamplers operated with purge/withdrawal cycles for each sample. All flumes, sample lines, and bottles were cleaned between storms and field blanks were taken to ensure equipment was clean. Concentrations in flow-weighted composite samples were used as event mean concentrations (EMCs) for each monitoring location. Nitrogen loads through each monitoring station were determined by multiplying EMC values by total stormwater volume over a monitoring period.

Grab samples were taken from the bioretention outlet underdrain at the tail end of each event's hydrograph (when outlet flow rate had dropped below peak-flow conditions). Five grab samples (from events on 6/2/2018, 7/30/2018, 8/31/2018, 9/28/2018, and 10/11/2018) whose nitrate concentrations were lower than their respective inlet flow-weighted composite sample concentrations were selected for additional isotope analysis. A rain sample was collected during the 3/21/19 event in a 9.5 L glass jar positioned on top of the bioretention outlet monitoring equipment.

4.2.3 Sample Water Quality Analysis

Concentrations of nitrate, nitrite, and ammonium in all samples were determined using ion chromatography (IC). Samples were filtered (0.45 µm PTFE) before IC analysis (Dionex ICS-5000). IC runs included blanks which were all below relevant detection limits. When sample ion concentrations were higher than the upper range of calibration, samples were diluted and re-run within calibration range. Total dissolved nitrogen (TDN) and dissolved organic carbon (DOC) were analyzed by a Shimadzu TOC-L with a coupled TNM-L analyzer. Stormwater samples were acidified to 2% HCL and filtered (0.45 µm PTFE) before TOC-L/TDN analysis.

4.2.4 Isotopic Analysis

Stable isotope analysis of all samples was done at the Stable Isotope Facility at UC Davis. Filtered (0.1 µm PTFE) frozen samples were analyzed for $\delta^{15}N\text{-}NO_3^-$ and $\delta^{18}O\text{-}NO_3^-$ by the bacterial denitrifier method. Briefly, denitrifying bacteria (*Pseudomonas aureofaciens*) are used to convert dissolved NO_3^- in water samples to N_2O gas, which is then analyzed by isotope ratio mass spectrometry (IRMS) [41–47]. Samples are normalized to reference standards USGS32, USGS34, USGS35, and IAEA-NO-3 and isotopic ratios are reported in per mil (‰) relative to atmospheric N_2 for $\delta^{15}N$ and Vienna Standard Mean Ocean Water for $\delta^{18}O$ based on **Equation 4.1**:

$$\delta(‰) = \frac{R_{sample} - R_{standard}}{R_{standard}} \times 1000 \qquad (4.1)$$

where R is the ratio of the heavy to light isotope (e.g. $^{15}N/^{14}N$ or $^{18}O/^{16}O$). One in every ten samples was analyzed in duplicate and measurement error was within ± 0.4‰ for $\delta^{15}N$ and ± 0.5‰ for $\delta^{18}O$ for duplicate reference standards. The nitrate range of isotope quantification was 2 – 1500 uM.

4.2.5 Identification and Quantification of Denitrification

Decreasing NO_3^- concentrations with increasing $\delta^{15}N$-NO_3^- and $\delta^{18}O$-NO_3^- along a linear slope between 0.5 and 1 ($\delta^{18}O$-NO_3^-/ $\delta^{15}N$-NO_3^-) in stormwater samples from bioretention inlet to outlet was used to indicate the presence of denitrification [35–38,48–50]. Rayleigh curves were used to determine the percentage contribution of denitrification among other nitrogen removal mechanisms [49,51–53]. For storms that displayed isotopic evidence of denitrification, enrichment factors (ε) were calculated based on the **Equation 4.2:**

$$\varepsilon = \frac{\delta^{15}N_{out} - \delta^{15}N_{in}}{\ln(f)} \qquad (4.2)$$

where $\delta^{15}N_{out}$ and $\delta^{15}N_{in}$ represent the $\delta^{15}N$-NO_3^- of the outlet and inlet flow-weighted composite samples from a given storm and f is the fraction of NO_3^- concentration remaining. A Rayleigh curve with ε = -17‰ was used to represent a system where 100% of nitrate concentration reduction was from denitrification and a Rayleigh curve with ε = 0‰ was used to represent a system with 0% denitrification [51,54].

4.2.6 Statistical Analysis

Statistical analysis was preformed using the software R (version 3.6.1). P values were calculated by paired t-tests with 95% confidence intervals ($\alpha = 0.05$).

4.3 Results

4.3.1 Stormwater monitoring conditions

24 precipitation events (22 rain and 2 snow) were monitored between April 16th, 2018 and June 18th, 2019. Storm events ranged from 0.7 to 10.5 cm. All 24 events totaled 119.0 cm with a mean event size of 5.0 cm. Total precipitation over the same time period at nearby Ronald Reagan Airport Weather Station was 198.0 cm. Monitored bioretention events accounted for 61% of the

total rain from the weather station. Weather conditions for each of the 24 monitored events (e.g. event size, intensity, duration, temperature) are displayed in **Appendix C Table C1.**

4.3.2 Stormwater Quality

Stormwater samples were found to have detectable levels of nitrate, TDN, and DOC, but no detectable nitrite or ammonium was measured in any stormwater samples. EMCs from bioretention inlet and outlet samples displayed seasonal variability throughout the monitoring period (**Figure 4.1 and Appendix C Table C2**). Inlet nitrate concentrations ranged from 0.14 to 0.85 mg/L as N, outlet nitrate ranged from 0.02 to 1.05 mg/L as N, and bypass nitrate ranged from 0.00 to 0.29 mg/L as N. Mean inlet nitrate EMC (0.43 mg/L as N ± 0.04 standard error) was higher than mean outlet nitrate EMC (0.35 mg/L as N ± 0.06), but means were not significantly different (p = 0.12). Relative nitrate concentrations between the inlet and outlet (concentration reduction) displayed a seasonal trend, with inlet nitrate concentrations generally higher than outlet in the warmer months and outlet concentrations higher than inlet in the colder months. The positive relationship between concentration reduction and average daily temperature (**Appendix C Figure C1**) has a statistically significant positive linear regression (R^2 = 0.41, p = 0.0007). Of the 24 storms monitored, 16 had a reduction in nitrate concentration, while 8 had an increase in nitrate concentration from inlet to underdrain outlet. Both inlet and outlet nitrate concentrations were generally higher in the fall and winter months and lower in the spring and summer.

Inlet TDN concentrations ranged from 0.36 to 1.75 mg/L as N, outlet TDN ranged from 0.00 to 1.30 mg/L as N, and bypass TDN ranged from 0.00 to 0.80 mg/L as N. Mean inlet TDN EMC (0.81 mg/L as N ± 0.06) was statistically higher (p = 0.02) than mean outlet TDN EMC (0.66

mg/L as N ± 0.06). Inlet and outlet TDN concentrations and TDN concentration reductions were more consistent throughout the monitoring period (**Figure 4.1 and Appendix C Figure C2).**

Inlet DOC concentrations ranged from 3.27 to 9.60 mg/L, outlet DOC ranged from 2.30 to 13.36 mg/L, and bypass DOC ranged from 0.00 to 9.67 mg/L. Mean inlet DOC EMC (5.4 mg/L ± 0.25) was statistically lower (p = 0.008) than outlet DOC EMC (7.0 mg/L ± 0.63). DOC inlet concentrations were relatively stable throughout the monitoring period but outlet concentrations were higher in the spring, summer, and fall than the winter (**Figure 4.1).** There was a negative relationship between DOC concentration reduction and average daily temperature (**Appendix C Figure C3**) with a statistically significant linear regression (R^2 = 0.37, p = 0.0015).

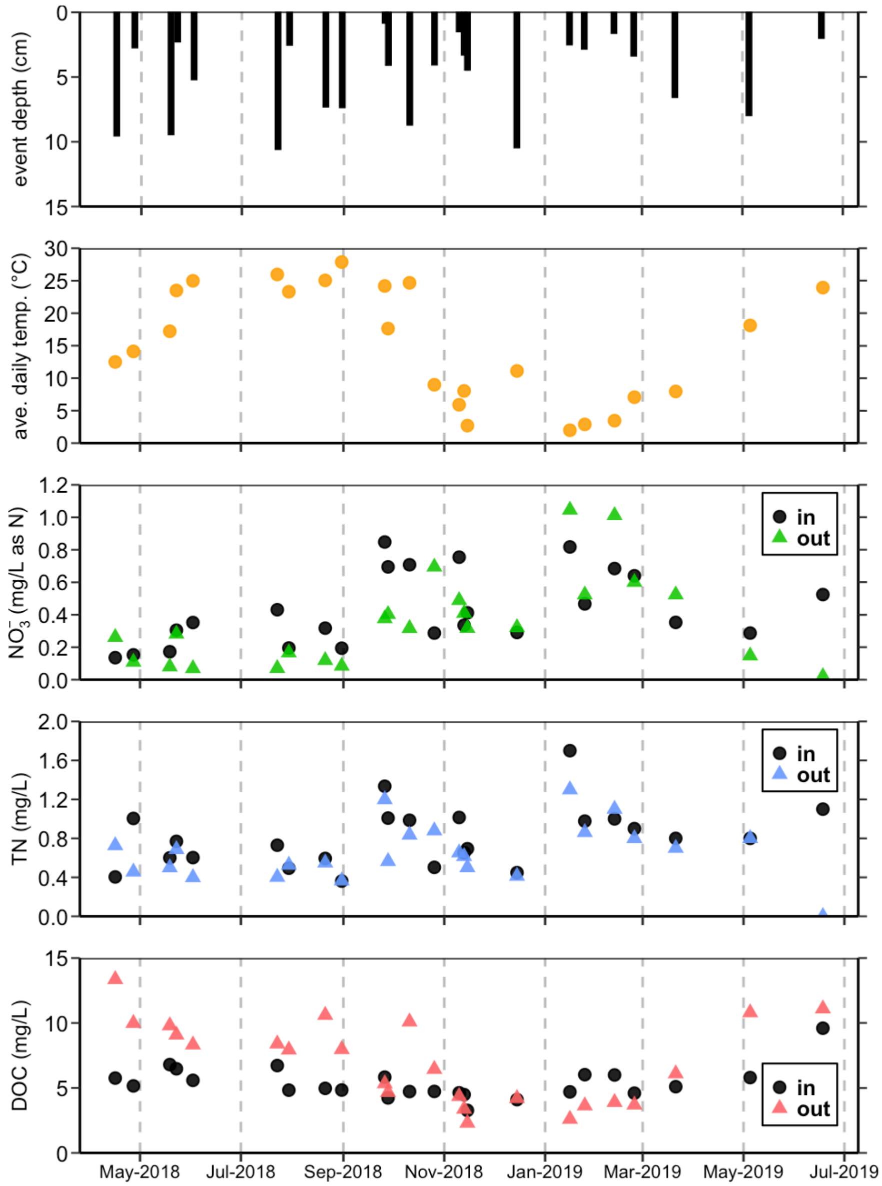

Figure 4.1. Bioretention weather conditions and water quality results from the 24 monitored events. From top to bottom: rain/snow event depths, average daily temperature for each event, and nitrate, TDN, and DOC concentrations in EMC inlet and outlet samples. Average daily temperature data is from the nearby Ronald Reagan Airport Weather Station.

4.3.3 Overall Bioretention Performance

A summary of the overall performance of the bioretention with respect to total stormwater runoff and average concentrations and total loads of nitrate, TDN, and DOC is presented in **Figure 4.2**. Cumulative runoff reduction over the monitoring period was 60%, with 76% of total surface effluent exiting through the underdrain outlet and 24% exiting through the bypass channel. Monitored stormwater volumes and runoff reductions per event are in **Appendix C Table C3**. Overall average concentration reductions were 19% for both nitrate and TDN, but -30% for DOC.

Factoring stormwater concentrations and runoff volumes together resulted in total surface effluent load reductions of 73%, 70%, and 50% for nitrate, TDN, and DOC, respectively (**Figure 4.2**). Only 13%, 17%, and 18% of nitrate, TDN, and DOC surface effluent loads were bypassed, respectively, while the remaining nitrate, TDN, and DOC surface effluent loads exited the bioretention through the underdrain outlet. The inlet and outlet had similar percentages of nitrate that made up TDN (55% and 51% of TDN load, respectively), while bypass nitrate was only 37% of the TDN load. Nitrate, TDN, and DOC loads and nitrate/TDN percentages by storm event are in **Appendix C Table C4**.

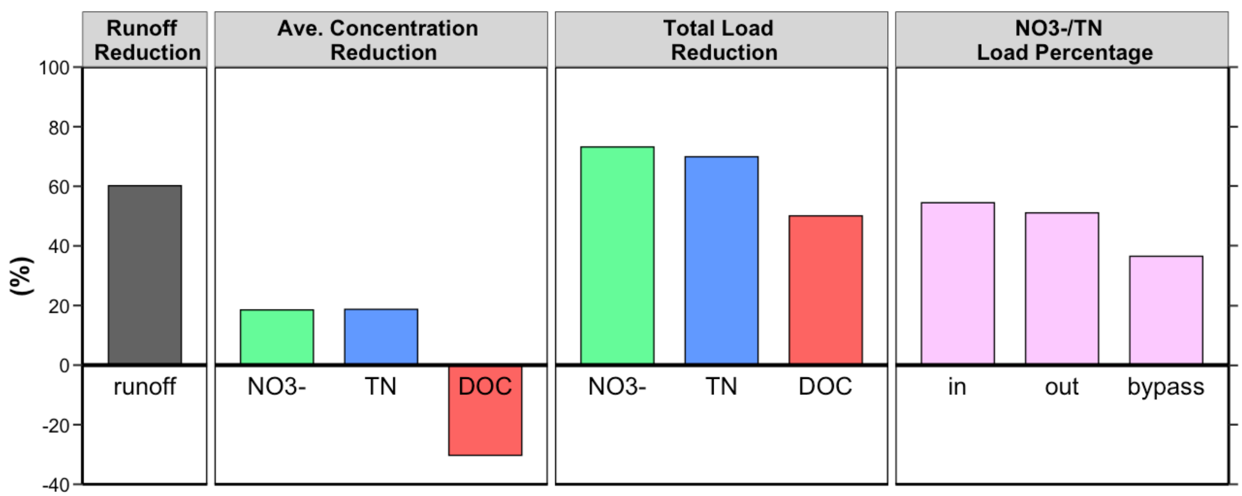

Figure 4.2. Bioretention stormwater management performance over the 14 month monitoring period. From left to right: total stormwater runoff reduction, average concentration reductions (in vs. out), total load reductions, and the percentage of nitrate that made up the TDN load at each monitoring location.

4.3.4 Stable Isotopes

$\delta^{15}N-NO_3^-$ and $\delta^{18}O-NO_3^-$ of the 24 inlet flow-weighted composite stormwater samples ranged between -0.8‰ and 7.7‰ (mean 4.8‰ ± 0.46) and 3.0‰ and 31.7‰ (mean 13.9‰ ±

1.37), respectively. $\delta^{15}N\text{-}NO_3^-$ and $\delta^{18}O\text{-}NO_3^-$ of the 24 underdrain outlet flow-weighted composite stormwater samples ranged between -2.5‰ and 9.3‰ (mean 5.2‰ ± 0.53) and 3.6‰ and 11.4‰ (mean 8.0‰ ± 0.41), respectively. Inlet and outlet sample means $\delta^{15}N\text{-}NO_3^-$ were not statistically different but mean inlet $\delta^{18}O\text{-}NO_3^-$ was statistically higher than mean inlet $\delta^{18}O\text{-}NO_3^-$ ($p = 0.0003$).

Inlet sample $\delta^{15}N\text{-}NO_3^-$ and $\delta^{18}O\text{-}NO_3^-$ ranges are indicative of a variable mix of sources between soil, fertilizer, and atmospheric nitrate (**Figure 4.3**) [35]. Outlet sample $\delta^{15}N\text{-}NO_3^-$ and $\delta^{18}O\text{-}NO_3^-$ are in line with expected values from soil nitrate sources and show less influence from fertilizer and atmospheric nitrate compared to inlet samples. Bioretention nitrate concentration reduction had a marginally significant positive linear relationship with change in $\delta^{15}N\text{-}NO_3^-$ from inlet to outlet ($R^2 = 0.18$, $p = 0.04$) but an insignificant relationship with change in $\delta^{18}O\text{-}NO_3^-$ (**Appendix C Figure C4**). Inlet samples had had a marginally significant negative linear relationship between $\delta^{15}N\text{-}NO_3^-$ and $\delta^{18}O\text{-}NO_3^-$ ($R^2 = 0.20$, $p = 0.03$), but outlet samples had an insignificant $\delta^{15}N\text{-}NO_3^-$ and $\delta^{18}O\text{-}NO_3^-$ relationship (**Appendix C Figure C5**).

$\delta^{15}N\text{-}NO_3^-$ and $\delta^{18}O\text{-}NO_3^-$ of the five underdrain outlet tail grab stormwater samples ranged between 9.0‰ and 14.8‰ (mean 12.6‰ ± 0.99) and 5.6‰ and 9.2‰ (mean 7.1‰ ± 0.62), respectively. The underdrain outlet tail grab samples (taken at the tail end of the outflow hydrograph after the outlet flow-weighted composite sample) showed significant $\delta^{15}N\text{-}NO_3^-$ enrichment ($p = 0.01$) but similar $\delta^{18}O\text{-}NO_3^-$ values compared to outlet composite samples. These outlet tail grab samples were in the range of manure/wastewater/compost nitrate sources. The rain sample had $\delta^{15}N\text{-}NO_3^-$ and $\delta^{18}O\text{-}NO_3^-$ values of -1.4‰ and 60.1‰, putting it in the expected range for atmospheric nitrate. The rain sample had a nitrate concentration of 0.09 mg/L as N, an ammonium concentration of 0.04 mg/L as N, and no detectable nitrite.

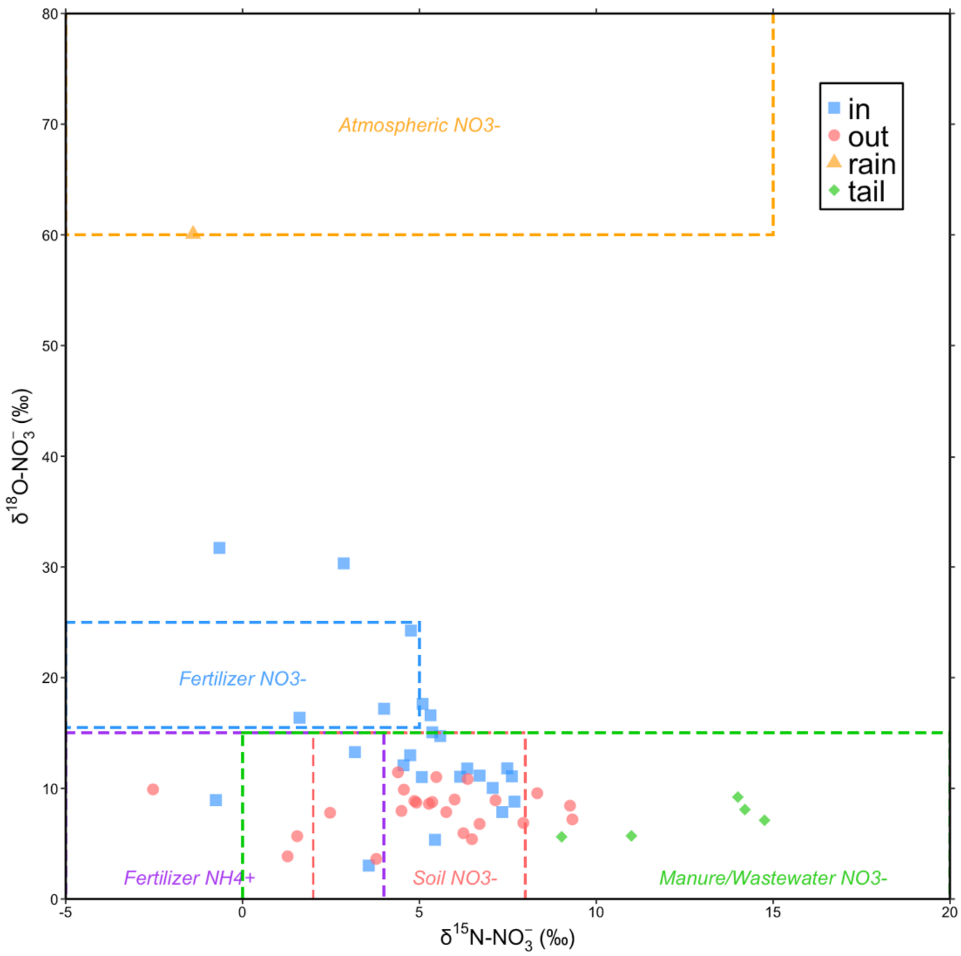

Figure 4.3. Dual $\delta^{15}N$-NO_3^- and $\delta^{18}O$-NO_3^- plots of bioretention stormwater from the inlet (blue), outlet (red), and outlet tail grab samples (green), as well as a rain sample from the 3/21/2019 event (orange). Boxes represent typical $\delta^{15}N$-NO_3^- and $\delta^{18}O$- NO_3^- ranges from different nitrate sources from Kendall et al. (2007) [35].

When broken down by storm event, bioretention inlet to outlet EMC $\delta^{15}N$-NO_3^- and $\delta^{18}O$-NO_3^- changes displayed a variety of trends throughout the monitoring period (**Figure 4.4**). Only two of the 24 monitored events (7/23/2018 and 10/11/2018) met the criteria for presence of denitrification (reduction in nitrate concentration and enrichment in $\delta^{15}N$-NO_3^- and $\delta^{18}O$-NO_3^- from inlet to outlet with a slope between 0.5 and 1) [35,49]. The slope of $\delta^{15}N$-NO_3^- and $\delta^{18}O$-NO_3^- enrichment between inlet and outlet samples was 0.81 for the 10/11/2018 event and 0.82 for the 7/30/2018 event. Four of the 24 storms (4/16/2018, 10/26/2018, 2/12/2019, and 3/21/2019) displayed trends associated with nitrification (increase in nitrate concentration and depletion of

$\delta^{15}N\text{-}NO_3^-$ and $\delta^{18}O\text{-}NO_3^-$ from inlet to outlet) [35,49]. Generally, winter storms displayed less isotopic change from inlet to outlet compared to the rest of the year. The 6/18/2019 outlet sample had a nitrate concentration (0.02 mg/L as N) below the limit of quantification for $\delta^{15}N\text{-}NO_3^-$ and $\delta^{18}O\text{-}NO_3^-$ analysis.

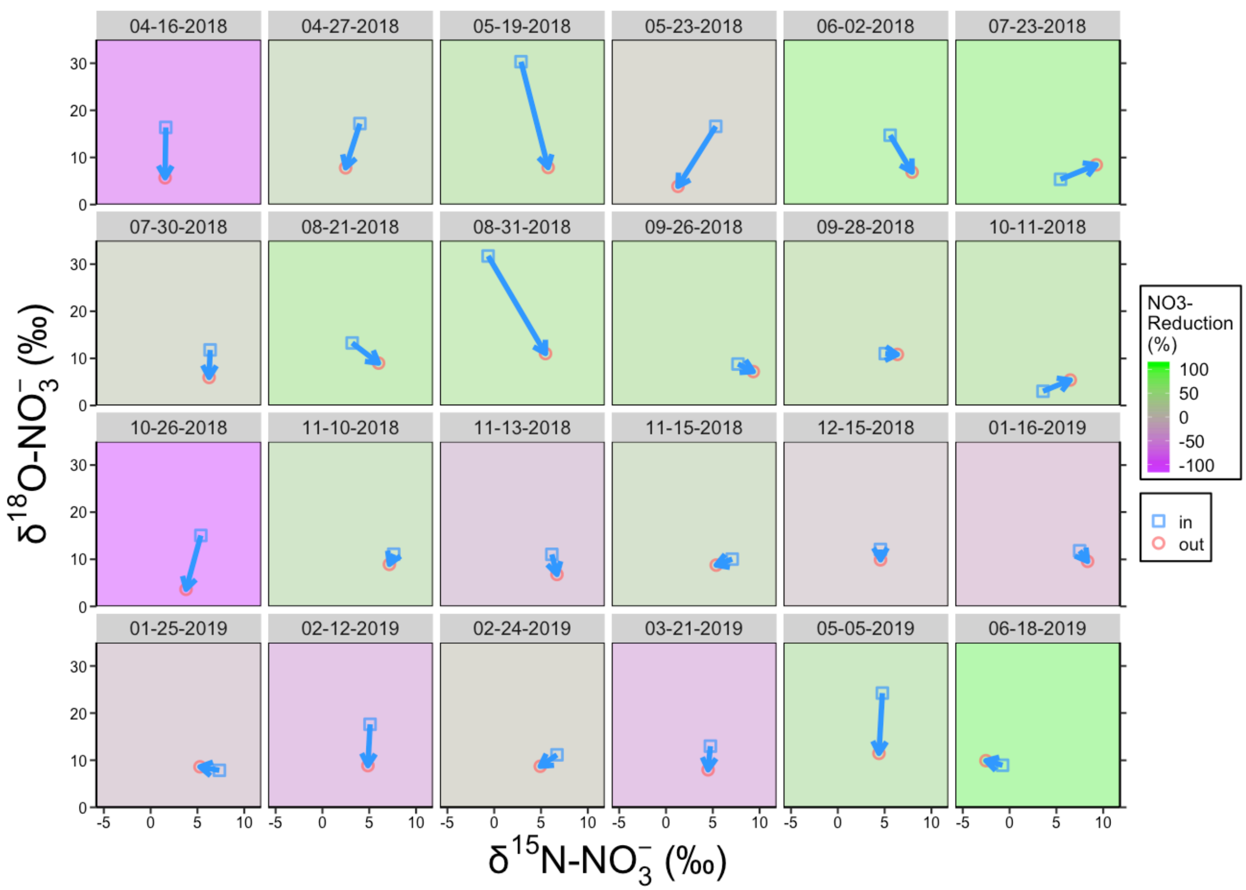

Figure 4.4. Dual $\delta^{15}N\text{-}NO_3^-$ and $\delta^{18}O\text{-}NO_3^-$ plots of bioretention stormwater inlet and outlet EMC samples broken up by storm event. Blue arrows show the directional shift in isotope signatures from inlet to outlet samples. Background color gradient indicates nitrate concentration reduction between the inlet and outlet.

The five underdrain outlet tail grab samples all displayed enrichment of $\delta^{15}N\text{-}NO_3^-$ relative to their corresponding outlet composite samples but differing $\delta^{18}O\text{-}NO_3^-$ trends (**Figure 4.5**). Of the five storm events, only the 10/11/2018 had outlet grab sample enrichment of $\delta^{15}N\text{-}NO_3^-$ and $\delta^{18}O\text{-}NO_3^-$ relative to its inlet sample, though both the 10/11/2018 and 7/30/2018 storms had outlet grab sample enrichment $\delta^{15}N\text{-}NO_3^-$ and $\delta^{18}O\text{-}NO_3^-$ relative to their outlet composite samples. The slope of $\delta^{15}N\text{-}NO_3^-$ and $\delta^{18}O\text{-}NO_3^-$ enrichment between outlet composite and outlet grab samples was 0.51 for the 10/11/2018 event and 0.14 for the 7/30/2018 event.

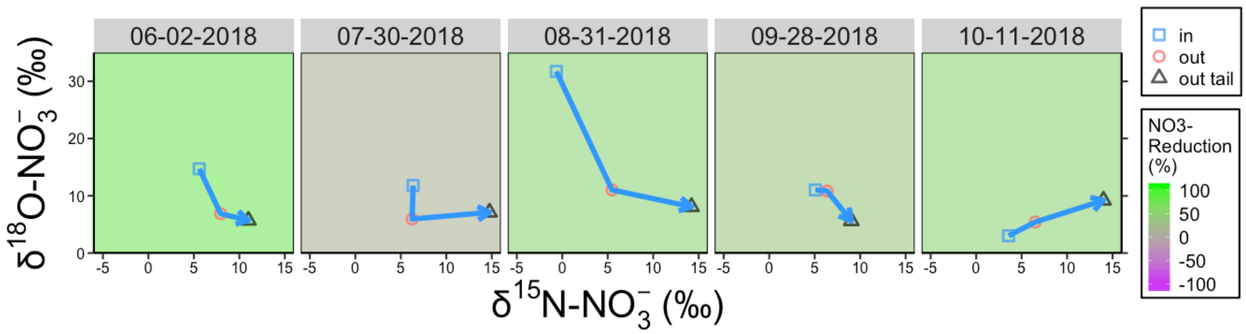

Figure 4.5. Dual $\delta^{15}N\text{-}NO_3^-$ and $\delta^{18}O\text{-}NO_3^-$ plots of five bioretention stormwater inlet and outlet EMCs with corresponding outlet tail grab samples broken up by storm event. Blue arrows show the directional shift in isotope signatures from inlet to outlet to outlet tail grab samples. Background color gradient indicates nitrate concentration reduction between the inlet and outlet.

Rayleigh curve analysis was performed for the 7/23/2018 and 10/11/2018 events with observed denitrification trends. Enrichment factors were calculated to be ε = -2.1‰ and ε = -3.6‰ for the 7/23/2018 and 10/11/2018 events, respectively. Assuming ε = -17‰ for 100% denitrification and ε = 0‰ for 0% denitrification, the percent of denitrification responsible for nitrate concentration change was calculated to be 24% and 28% for the 7/23/2018 and 10/11/2018 events, respectively (**Figure 4.6**). These calculations are further detailed in **Appendix C Figure C6**.

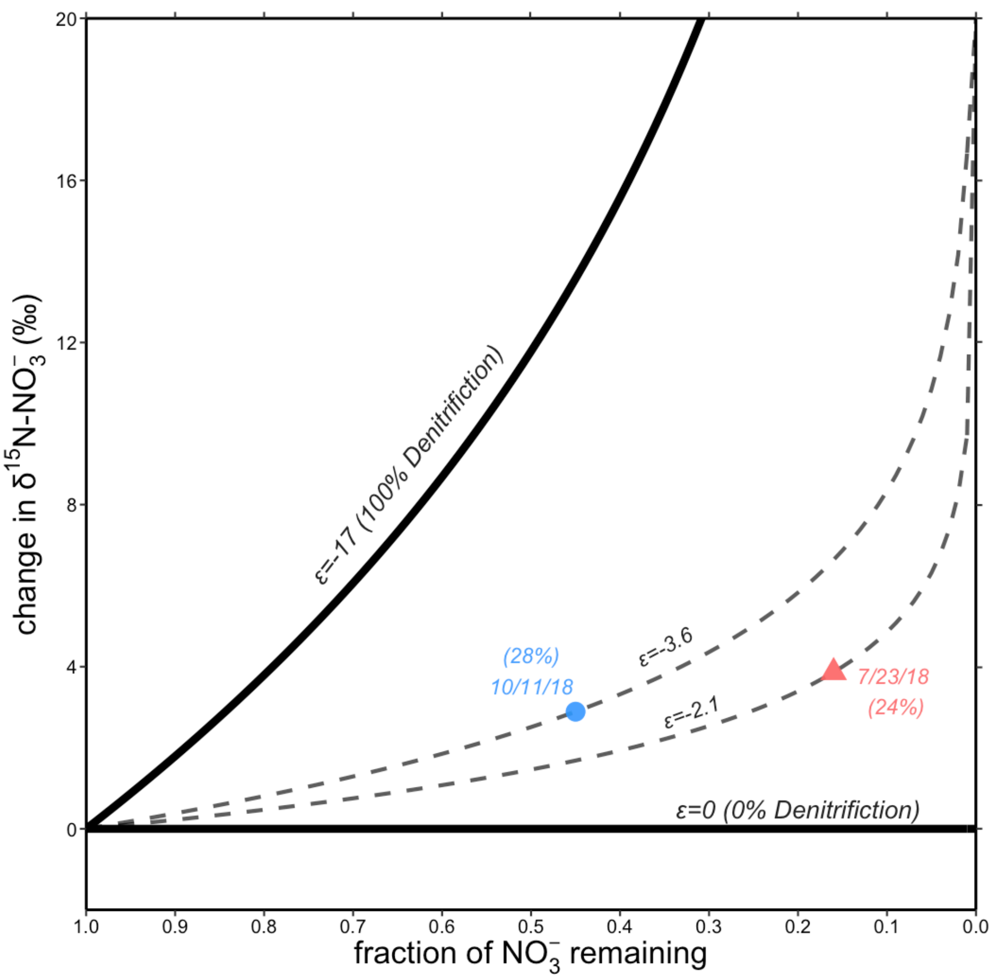

Figure 4.6. Relation between the fraction of nitrate concentration remaining in water and the enrichment of δ^{15}N-NO_3^- in systems with different enrichment factors (ε). These curves are used to estimate the percentage of nitrate concentration reduction that denitrification is responsible for. The blue circle and red triangle show the two events with denitrification isotope trends with their calculated denitrification percentages in parenthesis.

4.4 Discussion

4.4.1 Bioretention Surface Water Nitrogen Removal

The Lorton Road bioretention displayed high cumulative surface water effluent load reductions of both nitrate and TDN (73% and 70%, respectively), but only moderate overall differences in concentrations (19% for both nitrate and TDN; **Figure 4.2**). Because cumulative stormwater runoff reduction was 60% over the monitoring period, runoff volume reduction had a much greater effect on mass reductions than concentration differences, suggesting volume reduction as the primary nitrogen surface water removal pathway. This is expected as the bioretention is designed to reduce stormwater volumes by infiltration. Overall bioretention nitrate load and concentration reductions are similar to those found in another bioretention with a conventional underdrain by Hunt et al. 2006 [23].

Significant seasonal changes in bioretention nitrate concentration reductions were positively correlated to temperature (**Figure 4.1 and Appendix Figure C1**), suggesting the presence of a nitrate removal mechanism associated with temperature (e.g. assimilation and/or denitrification) [28,29,55]. Assimilation has been reported to be an important nitrogen removal mechanism in bioretention. Payne et al. reported that 88-99% of nitrate entering bioretention columns ended up in plant matter but may only remain there temporarily as organic matter decomposes [28]. Given the limited occurrence of denitrification (see below) in the Lorton Road bioretention, it is suggested that assimilation primarily accounts for seasonal nitrate concentration reduction as plants are more active during warmer storm events and dormant/decaying during colder events. Observed seasonal nitrate concentration reduction differences highlight the need for year-round monitoring in accounting for nitrogen transport.

4.4.2 Denitrification Identification

Only two of the 24 monitored precipitation events displayed evidence of denitrification, based on nitrate concentration, $\delta^{15}N\text{-}NO_3^-$, and $\delta^{18}O\text{-}NO_3^-$ trends in bioretention inlet and outlet samples (**Figure 4.4**). This result indicates that, although bioretention has potential for denitrification to occur (as pointed out by other researchers), it is happening infrequently and other (less desirable) nitrogen removal mechanisms (i.e. assimilation, infiltration) are primarily responsible for nitrogen reductions [27,56,57]. The two storms with denitrification trends (7/23/2018 and 10/11/2018) were two of the largest precipitation events occurring during warmer times of the year (**Appendix C Table C1**). Denitrification happens in consistently water logged soils and larger precipitation events saturate the soils of the bioretention for a longer period of time, allowing more time for denitrification to occur [33,34]. Additionally, denitrification rates are higher at warmer temperatures, which further encourages denitrification to take place in the limited time stormwater is saturating the bioretention basin [55]. Other weather conditions, such as antecedent moisture and event duration and intensity had a less discernable effect on the timing of the two monitored denitrification events.

Rayleigh curve calculations estimated that 24% and 28% of the bioretention nitrate concentration reductions for the 7/23/2018 and 10/11/2018 events, respectively, were attributable to denitrification. So, even when denitrification trends were detected, the contribution of denitrification on nitrate reduction was relatively minor. By calculating the nitrate load reduced by the estimated fractional contribution of denitrification on concentration reduction during the 7/23/2018 and 10/11/2018 events, we found that only about 1.4% of the total nitrate surface effluent load (or 0.8 % of TDN load) over the entire monitoring period was reduced by denitrification. The finding that denitrification is infrequent and a low contributor to nitrogen reduction in bioretention is in agreement with column studies by Payne et al (2014) [28]. The Lorton Road bioretention is a relatively young system (about one year old during the start of monitoring). Future studies should look into denitrification occurrence in more mature systems.

4.4.3 Sources of Nitrate

Nitrate isotope analysis also revealed information about the source of both incoming and outgoing nitrate. Nitrate in stormwater entering into the bioretention had a variable mix of $\delta^{15}N-NO_3^-$ and $\delta^{18}O-NO_3^-$ values indicative of a combination of soil, fertilizer, and atmospheric nitrate [35]. Inlet nitrate $\delta^{15}N-NO_3^-$ and $\delta^{18}O-NO_3^-$ was similar to nitrate from an urban watersheds outside of Baltimore, Maryland in Kaushal et al. (2011) and different from a more atmospheric nitrate influenced low-density residential watershed outside of Tampa, Florida in Yang and Toor (2016) [36,37]. Nitrate outlet $\delta^{15}N\text{-}NO_3^-$ and $\delta^{18}O\text{-}NO_3^-$ values match with soil nitrate sources, though outlet grab samples taken at the tail end of outlet hydrographs were significantly more enriched in $\delta^{15}N\text{-}NO_3^-$ (**Figure 4.3**).

Differences in nitrate isotopes from inlet to outlet are consistent with mixing of inlet nitrate sources with additional nitrate sources within the bioretention basin [36]. Inlet stormwater can mix with soil nitrogen and compost amendment as it infiltrates though the bioretention soil media. In particular, the outlet tail grab samples taken during periods of low stormwater flow appear to be most impacted by nitrate from within the bioretention basin, with their enriched $\delta^{15}N\text{-}NO_3^-$ values that are indicative of the plant-based compost used in the bioretention soil media [35]. Additionally, four monitored events (all with very low antecedent moisture conditions) also displayed possible nitrification trends (increase in nitrate concentration and depletion of $\delta^{15}N\text{-}NO_3^-$ and $\delta^{18}O\text{-}NO_3^-$ from inlet to outlet), though because no ammonium was measured in stormwater inlet samples, nitrification is not thought to be a major factor for this bioretention. Nitrification is another way the bioretention soil can export nitrate. These results affirm what other studies have found: bioretention can be both a source and sink for nitrogen [25,57,58].

Exported nitrate from bioretention soil media may have interfered with the detection of denitrification $\delta^{15}N\text{-}NO_3^-$ and $\delta^{18}O\text{-}NO_3^-$ trends between the inlet and outlet samples. If a significant amount of exporting nitrate from the bioretention soil media mixed with inlet stormwater, isotopic ratios could shift in a direction that masks relatively smaller enrichments of $\delta^{15}N\text{-}NO_3^-$ and $\delta^{18}O\text{-}NO_3^-$ from denitrification. However, considering the high loading ratio of the bioretention (CDA : size of the basin = 47) and reduction in nitrate concentration during most events, it is likely that the load of nitrate infiltrating through the bioretention from incoming stormwater is significantly more than what would be exported from the soil media during a precipitation event. Nevertheless, future studies utilizing stable nitrate methods for identifying denitrification in GI should monitor enrichment in $\delta^{15}N\text{-}NO_3^-$ and $\delta^{18}O\text{-}NO_3^-$ in multiple outlet samples over the course of each precipitation event (instead of only comparing flow-weighted composite inlet to outlet samples) to get further insight into potential masking effects of exporting nitrate.

4.4.4 Fate of Nitrogen in Bioretention

The limited occurrence and contribution of denitrification, along with evidence of high stormwater volume reduction and seasonal assimilation by vegetation, suggests infiltration as the major nitrogen surface effluent removal mechanism with assimilation serving as a seasonal nitrogen sink. As nitrogen infiltrates further through natural soils underlying bioretention, its transport may be site specific, but nitrate will generally have higher denitrification potential during its longer residence time within anoxic groundwater than its short stay with only periodically anoxic bioretention media [33,59]. Given the concentration export of DOC, it is likely that conditions beneath the Lorton Road bioretention would be suitable for subsurface denitrification [59]. Vegetation assimilation appears to help achieve seasonal concentration reductions and storage of nitrate. However, most vegetation storage is often short-term and maintenance efforts are necessary to prevent decaying vegetation from seasonally exporting stored nitrogen [27–29]. Overall, findings suggest that the conventionally designed bioretention in this study primarily reduced surface effluent nitrogen loads not by permanent removal (denitrification) but instead by redirecting nitrogen from stormwater to groundwater, plants, and soil.

4.4.5 Encouraging Denitrification in Future GI Designs

Denitrification trends were found during two of the largest monitored storm events, suggesting larger precipitation events were needed to saturate the soils of the bioretention long enough for denitrification to occur. Increasing the hydraulic residence time (HRT) of the bioretention (and other GI) is suggested to allow denitrifying bacteria more time to act in saturated soil [27,33,34]. Therefore, bioretention design parameters (e.g. underdrain size, storage volume, infiltration rate, ponding depth) may be modified to increase HRT in order to promote denitrification. Furthermore, outlet control mechanisms encouraging bioretention internal water storage have been reported to improve nitrogen removal [24,60–62].

4.5 Conclusions

This is the first known field study using dual nitrate stable isotope analysis to track denitrification within an operational bioretention basin. Nitrogen monitoring through the bioretention during 24 storm events over 14 months revealed seasonal trends in nitrate concentration reductions, with significantly higher reductions happening in warmer months. Cumulative bioretention nitrate and total nitrogen load reductions were 73% and 70%, respectively. General inlet to outlet nitrate isotope differences are consistent with mixing of inlet nitrate sources with additional nitrate sources within the bioretention basin, suggesting that bioretention acts as both a sink and source for nitrogen. Two out of 24 monitored events displayed denitrification isotope trends, indicating that although bioretention has denitrification potential, it is infrequent in only temporarily saturated soils and other nitrogen removal mechanisms (i.e. infiltration and plant uptake) are primarily responsible for nitrogen reductions. Only approximately 1.4% of the total reduced nitrate surface effluent load over the monitoring period was attributable to denitrification. These results characterize denitrification contribution in a young bioretention and future studies should characterize later stage bioretention denitrification. Because denitrification did occur during two of the largest monitored events, future GI designs should consider increasing HRT to encourage the important ecosystem service denitrification provides.

Supplementary Data: Appendix C

4.6 References

(1) Galloway, J. N.; Aber, J. D.; Erisman, J. W.; Seitzinger, S. P.; Howarth, R. W.; Cowling, E. B.; Cosby, B. J. The Nitrogen Cascade. *Am. Inst. Biol. Sci.* **2003**, *53* (4), 341. https://doi.org/10.1641/0006-3568(2003)053[0341:TNC]2.0.CO;2.

(2) Galloway, J. N.; Townsend, A. R.; Erisman, J. W.; Bekunda, M.; Cai, Z.; Freney, J. R.; Martinelli, L. A.; Seitzinger, S. P.; Sutton, M. A. Transformation of the Nitrogen Cycle: Recent Trends, Questions, and Potential Solutions. *Science* **2008**, *320* (5878), 889–892. https://doi.org/10.1126/science.1136674.

(3) Vitousek, P. M.; Aber, J. D.; Howarth, R. W.; Likens, G. E.; Matson, P. A.; Schindler, D. W.; Schlesinger, W. H.; Tilman, D. G. HUMAN ALTERATION OF THE GLOBAL NITROGEN CYCLE: SOURCES AND CONSEQUENCES. *Ecol. Appl.* **1997**, *7* (3), 737–750. https://doi.org/10.1890/1051-0761(1997)007[0737:HAOTGN]2.0.CO;2.

(4) Howarth, R. W.; Billen, G.; Swaney, D.; Townsend, A.; Jaworski, N.; Lajtha, K.; Downing, J. A.; Elmgren, R.; Caraco, N.; Jordan, T.; et al. Regional Nitrogen Budgets and Riverine N & P Fluxes for the Drainages to the North Atlantic Ocean: Natural and Human Influences. *Biogeochemistry* **1996**, *35* (1), 75–139. https://doi.org/10.1007/BF02179825.

(5) Howarth, R. W. Coastal Nitrogen Pollution: A Review of Sources and Trends Globally and Regionally. *Harmful Algae* **2008**, *8* (1), 14–20. https://doi.org/10.1016/j.hal.2008.08.015.

(6) McKinney, M. L. Effects of Urbanization on Species Richness: A Review of Plants and Animals. *Urban Ecosyst.* **2008**, *11* (2), 161–176. https://doi.org/10.1007/s11252-007-0045-4.

(7) Paerl, H. W.; Scott, J. T. Throwing Fuel on the Fire: Synergistic Effects of Excessive Nitrogen Inputs and Global Warming on Harmful Algal Blooms. *Environ. Sci. Technol.* **2010**, *44* (20), 7756–7758. https://doi.org/10.1021/es102665e.

(8) Walsh, C. J.; Roy, A. H.; Feminella, J. W.; Cottingham, P. D.; Groffman, P. M.; Morgan Ii, R. P. The Urban Stream Syndrome: Current Knowledge and the Search for a Cure. *Benthol. Soc* **2005**, *24* (3), 706–723.

(9) Redling, K.; Elliott, E.; Bain, D.; Sherwell, J. Highway Contributions to Reactive Nitrogen Deposition: Tracing the Fate of Vehicular NOx Using Stable Isotopes and Plant Biomonitors. *Biogeochemistry* **2013**, *116* (1–3), 261–274. https://doi.org/10.1007/s10533-013-9857-x.

(10) Bettez, N. D.; Groffman, P. M. Nitrogen Deposition in and near an Urban Ecosystem. *Environ. Sci. Technol.* **2013**, *47* (11), 6047–6051. https://doi.org/10.1021/es400664b.

(11) E. M. Elliott, *,†,‡; C. Kendall, †; S. D. Wankel, †; D. A. Burns, §; E. W. Boyer, ∥; K. Harlin, ⊥; D. J. Bain, † and; Butler#, T. J. Nitrogen Isotopes as Indicators of NOx Source Contributions to Atmospheric Nitrate Deposition Across the Midwestern and Northeastern United States. **2007**. https://doi.org/10.1021/ES070898T.
(12) Law, N.; Band, L.; Grove, M. Nitrogen Input from Residential Lawn Care Practices in Suburban Watersheds in Baltimore County, MD. *J. Environ. Plan. Manag.* **2004**, *47* (5), 737–755. https://doi.org/10.1080/0964056042000274452.
(13) Sercu, B.; Werfhorst, L. C. Van De; Murray, J.; Holden, P. A. Storm Drains Are Sources of Human Fecal Pollution during Dry Weather in Three Urban Southern California Watersheds. *Environ. Sci. Technol.* **2009**, *43* (2), 293–298. https://doi.org/10.1021/es801505p.
(14) Gasperi, J.; Gromaire, M. C.; Kafi, M.; Moilleron, R.; Chebbo, G. Contributions of Wastewater, Runoff and Sewer Deposit Erosion to Wet Weather Pollutant Loads in Combined Sewer Systems. *Water Res.* **2010**, *44* (20), 5875–5886. https://doi.org/10.1016/J.WATRES.2010.07.008.
(15) UN Department of Economic and Social Affairs. *United Nations World Population Prospects 2019: Highlights*; 2019.
(16) Kaushal, S. S.; Groffman, P. M.; Band, L. E.; Shields, C. A.; Morgan, R. P.; Palmer, M. A.; Belt, K. T.; Swan, C. M.; Findlay, S. E. G.; Fisher, G. T. Interaction between Urbanization and Climate Variability Amplifies Watershed Nitrate Export in Maryland. *Environ. Sci. Technol.* **2008**, *42* (16), 5872–5878. https://doi.org/10.1021/es800264f.
(17) Henderson, D. A.; Moruza, G.; Burgis, C. R.; Smith, J. A. Low Impact Development Technologies for Highway Stormwater Runoff. In *Encyclopedia of Water: Science, Technology, and Society.*; Wiley, 2019.
(18) Pennino, M. J.; McDonald, R. I.; Jaffe, P. R. Watershed-Scale Impacts of Stormwater Green Infrastructure on Hydrology, Nutrient Fluxes, and Combined Sewer Overflows in the Mid-Atlantic Region. *Sci. Total Environ.* **2016**, *565*, 1044–1053. https://doi.org/10.1016/j.scitotenv.2016.05.101.
(19) McIntyre, J. K.; Davis, J. W.; Hinman, C.; Macneale, K. H.; Anulacion, B. F.; Scholz, N. L.; Stark, J. D. Soil Bioretention Protects Juvenile Salmon and Their Prey from the Toxic Impacts of Urban Stormwater Runoff. *Chemosphere* **2015**. https://doi.org/10.1016/j.chemosphere.2014.12.052.
(20) Kramer, M. G. *Enhancing Sustainable Communities with Green Infrastructure (EPA 100-R-14-006)*; 2014.
(21) Coffman, L. *Low-Impact Development Design Strategies An Integrated Design Approach*; Prince George's County, Maryland, 2000.
(22) Vogel, J. R.; Moore, T. L.; Coffman, R. R.; Rodie, S. N.; Hutchinson, S. L.; McDonough, K. R.; McLemore, A. J.; McMaine, J. T. Critical Review of Technical Questions Facing Low Impact Development and Green Infrastructure: A Perspective from the Great Plains. *Water Environ. Res.* **2015**, *87* (9), 849–862. https://doi.org/10.2175/106143015X14362865226392.
(23) Hunt, W. F.; Jarrett, A. R.; Smith, J. T.; Sharkey, L. J. Evaluating Bioretention Hydrology and Nutrient Removal at Three Field Sites in North Carolina. *J. Irrig. Drain. Eng.* **2006**, *132* (6), 600–608. https://doi.org/10.1061/(ASCE)0733-9437(2006)132:6(600).
(24) Brown, R. A.; Hunt, W. F. Underdrain Configuration to Enhance Bioretention Exfiltration to Reduce Pollutant Loads. *J. Environ. Eng.* **2011**, *137* (11), 1082–1091.

https://doi.org/10.1061/(ASCE)EE.1943-7870.0000437.
(25) Li, L.; Davis, A. P. Urban Stormwater Runoff Nitrogen Composition and Fate in Bioretention Systems. *Environ. Sci. Technol.* **2014**, *48* (6), 3403–3410. https://doi.org/10.1021/es4055302.
(26) Henderson, D.; Smith, J. A.; Fitch, G. M. Impact of Vegetation Management on Vegetated Roadsides and Their Performance as a Low-Impact Development Practice for Linear Transportation Infrastructure. *Transp. Res. Rec. J. Transp. Res. Board* **2016**, *2588*, 172–180. https://doi.org/10.3141/2588-19.
(27) Morse, N. R.; Mcphillips, L. E.; Shapleigh, J. P.; Walter, M. T.; Wrigley, J. A. The Role of Denitrification in Stormwater Detention Basin Treatment of Nitrogen. *Environ. Sci. Technol. 2017,* **2017**, *51*, 7928−7935. https://doi.org/10.1021/acs.est.7b01813.
(28) Payne, E. G. I.; Fletcher, T. D.; Russell, D. G.; Grace, M. R.; Cavagnaro, T. R.; Evrard, V.; Deletic, A.; Hatt, B. E.; Cook, P. L. M. Temporary Storage or Permanent Removal? The Division of Nitrogen between Biotic Assimilation and Denitrification in Stormwater Biofiltration Systems. *PLoS One* **2014**, *9* (3), e90890. https://doi.org/10.1371/journal.pone.0090890.
(29) Payne, E. G. I.; Pham, T.; Deletic, A.; Hatt, B. E.; Cook, P. L. M.; Fletcher, T. D. Which Species? A Decision-Support Tool to Guide Plant Selection in Stormwater Biofilters. *Adv. Water Resour.* **2018**, *113*, 86–99. https://doi.org/10.1016/j.advwatres.2017.12.022.
(30) Burgis, C. R.; Hayes, G. M.; Henderson, D. A.; Zhang, W.; Smith, J. A. Green Stormwater Infrastructure Buffers Surface Water from Deicing Salt Loading. *Sci. Total Environ.* **2020**, *(under review)*.
(31) Bremner, J. M.; Blackmer, A. M. Nitrous Oxide: Emission from Soils during Nitrification of Fertilizer Nitrogen. *Science* **1978**, *199* (4326), 295–296. https://doi.org/10.1126/science.199.4326.295.
(32) Hatt, B. E.; Fletcher, T. D.; Deletic, A. Hydrologic and Pollutant Removal Performance of Stormwater Biofiltration Systems at the Field Scale. *J. Hydrol.* **2009**, *365* (3–4), 310–321. https://doi.org/10.1016/J.JHYDROL.2008.12.001.
(33) Seitzinger, S.; Harrison, J. A.; Böhlke, J. K.; Bouwman, A. F.; Lowrance, R.; Peterson, B.; Tobias, C.; Van Drecht, G. Denitrification across Landscapes and Waterscapes: A Synthesis. *Ecol. Appl.* **2006**, *16* (6), 2064–2090. https://doi.org/10.1890/1051-0761(2006)016[2064:dalawa]2.0.co;2.
(34) Bettez, N. D.; Groffman, P. M. Denitrification Potential in Stormwater Control Structures and Natural Riparian Zones in an Urban Landscape. *Environ. Sci. Technol.* **2012**, *46* (20), 10909–10917. https://doi.org/10.1021/es301409z.
(35) Kendall, C.; Elliott, E. M.; Wankel, S. D. Stable Isotopes in Ecology and Environmental Science. In *Stable Isotopes in Ecology and Environmental Science*; Michener, R., Lajtha, K., Eds.; Blackwell Publishing Ltd, 2007; pp 375–449. https://doi.org/10.1002/9780470691854.ch12.
(36) Kaushal, S. S.; Groffman, P. M.; Band, L. E.; Elliott, E. M.; Shields, C. A.; Kendall, C. Tracking Nonpoint Source Nitrogen Pollution in Human-Impacted Watersheds. *Environ. Sci. Technol.* **2011**. https://doi.org/10.1021/es200779e.
(37) Yang, Y.-Y.; Toor, G. S. Δ15N and Δ18O Reveal the Sources of Nitrate-Nitrogen in Urban Residential Stormwater Runoff. *Environ. Sci. Technol.* **2016**, *50* (6), 2881–2889. https://doi.org/10.1021/acs.est.5b05353.
(38) Divers, M. T.; Elliott, E. M.; Bain, D. J. Quantification of Nitrate Sources to an Urban

Stream Using Dual Nitrate Isotopes. *Environ. Sci. Technol.* **2014**, *48* (18), 10580–10587. https://doi.org/10.1021/es404880j.
(39) Hayes, G. M.; Burgis, C.; Zhang, W.; Henderson, D.; Smith, J. A. Runoff Reduction by Four Green Stormwater Infrastructure Systems in a Shared Environment. *J. Sustain. Water Built Environ. (under Rev.*
(40) VDOT. *AVERAGE DAILY TRAFFIC VOLUMES with VEHICLE CLASSIFICATION DATA on INTERSTATE, ARTERIAL and PRIMARY ROUTES*; 2018.
(41) Sigman, D. M.; Casciotti, K. L.; Andreani, M.; Barford, C.; Galanter, M.; Böhlke, J. K. A Bacterial Method for the Nitrogen Isotopic Analysis of Nitrate in Seawater and Freshwater. *Anal. Chem.* **2001**, *73* (17), 4145–4153. https://doi.org/10.1021/ac010088e.
(42) Casciotti, K. L.; Sigman, D. M.; Hastings, M. G.; Böhlke, J. K.; Hilkert, A. Measurement of the Oxygen Isotopic Composition of Nitrate in Seawater and Freshwater Using the Denitrifier Method. *Anal. Chem.* **2002**, *74* (19), 4905–4912. https://doi.org/10.1021/ac020113w.
(43) Granger, J.; Sigman, D. M. Removal of Nitrite with Sulfamic Acid for Nitrate N and O Isotope Analysis with the Denitrifier Method. *Rapid Commun. Mass Spectrom.* **2009**, *23* (23), 3753–3762. https://doi.org/10.1002/rcm.4307.
(44) Knapp, A. N.; Sigman, D. M.; Lipschultz, F. N Isotopic Composition of Dissolved Organic Nitrogen and Nitrate at the Bermuda Atlantic Time-Series Study Site. *Global Biogeochem. Cycles* **2005**, *19* (1). https://doi.org/10.1029/2004GB002320.
(45) David Felix, J.; Elliott, E. M.; Gish, T. J.; McConnell, L. L.; Shaw, S. L. Characterizing the Isotopic Composition of Atmospheric Ammonia Emission Sources Using Passive Samplers and a Combined Oxidation-Bacterial Denitrifier Approach. *Rapid Commun. Mass Spectrom.* **2013**, *27* (20), 2239–2246. https://doi.org/10.1002/rcm.6679.
(46) Böhlke, J. K.; Mroczkowski, S. J.; Coplen, T. B. Oxygen Isotopes in Nitrate: New Reference Materials for ^{18}O: ^{17}O: ^{16}O Measurements and Observations on Nitrate-Water Equilibration. *Rapid Commun. Mass Spectrom.* **2003**, *17* (16), 1835–1846. https://doi.org/10.1002/rcm.1123.
(47) Rock, L.; Ellert, B. H. Nitrogen-15 and Oxygen-18 Natural Abundance of Potassium Chloride Extractable Soil Nitrate Using the Denitrifier Method. *Soil Sci. Soc. Am. J.* **2007**, *71* (2), 355–361. https://doi.org/10.2136/sssaj2006.0266.
(48) Burns, D. A.; Boyer, E. W.; Elliott, E. M.; Kendall, C. Sources and Transformations of Nitrate from Streams Draining Varying Land Uses: Evidence from Dual Isotope Analysis. *J. Environ. Qual.* **2009**, *38* (3), 1149–1159. https://doi.org/10.2134/jeq2008.0371.
(49) Lehmann, M. F.; Reichert, P.; Bernasconi, S. M.; Barbieri, A.; McKenzie, J. A. Modelling Nitrogen and Oxygen Isotope Fractionation during Denitrification in a Lacustrine Redox-Transition Zone. *Geochim. Cosmochim. Acta* **2003**, *67* (14), 2529–2542. https://doi.org/10.1016/S0016-7037(03)00085-1.
(50) Böttcher, J.; Strebel, O.; Voerkelius, S.; Schmidt, H.-L. Using Isotope Fractionation of Nitrate-Nitrogen and Nitrate-Oxygen for Evaluation of Microbial Denitrification in a Sandy Aquifer. *J. Hydrol.* **1990**, *114* (3–4), 413–424. https://doi.org/10.1016/0022-1694(90)90068-9.
(51) Søvik, A. K.; Mørkved, P. T. Use of Stable Nitrogen Isotope Fractionation to Estimate Denitrification in Small Constructed Wetlands Treating Agricultural Runoff. *Sci. Total Environ.* **2008**, *392* (1), 157–165. https://doi.org/10.1016/J.SCITOTENV.2007.11.014.
(52) Lund, L. J.; Horne, A. J.; Williams, A. E. Estimating Denitrification in a Large

Constructed Wetland Using Stable Nitrogen Isotope Ratios. *Ecol. Eng.* **1999**. https://doi.org/10.1016/S0925-8574(99)00020-8.
(53) Mariotti, A.; Germon, J. C.; Hubert, P.; Kaiser, P.; Letolle, R.; Tardieux, A.; Tardieux, P. Experimental Determination of Nitrogen Kinetic Isotope Fractionation: Some Principles; Illustration for the Denitrification and Nitrification Processes. *Plant Soil* **1981**, *62* (3), 413–430. https://doi.org/10.1007/BF02374138.
(54) Blackmer, A. M.; Bremner, J. M. Nitrogen Isotope Discrimination in Denitrification of Nitrate in Soils. *Soil Biol. Biochem.* **1977**, *9*, 73–77.
(55) Dawson, R. N.; Murphy, K. L. The Temperature Dependency of Biological Denitrification. *Water Res.* **1972**, *6* (1), 71–83. https://doi.org/10.1016/0043-1354(72)90174-1.
(56) Peterson, I. J.; Igielski, S.; Davis, A. P.; Asce, F. Enhanced Denitrification in Bioretention Using Woodchips as an Organic Carbon Source. **2015**. https://doi.org/10.1061/JSWBAY.0000800.
(57) Chen, X.; Peltier, E.; Sturm, B. S. M.; Young, C. B. Nitrogen Removal and Nitrifying and Denitrifying Bacteria Quantification in a Stormwater Bioretention System. *Water Res.* **2013**, *47* (4), 1691–1700. https://doi.org/10.1016/J.WATRES.2012.12.033.
(58) Chahal, M. K.; Shi, Z.; Flury, M. Nutrient Leaching and Copper Speciation in Compost-Amended Bioretention Systems. *Sci. Total Environ.* **2016**, *556*, 302–309. https://doi.org/10.1016/J.SCITOTENV.2016.02.125.
(59) Rivett, M. O.; Buss, S. R.; Morgan, P.; Smith, J. W. N.; Bemment, C. D. Nitrate Attenuation in Groundwater: A Review of Biogeochemical Controlling Processes. *Water Res.* **2008**, *42* (16), 4215–4232. https://doi.org/10.1016/J.WATRES.2008.07.020.
(60) Li, M.-H.; Swapp, M.; Kim, M. H.; Chu, K.-H.; Sung, C. Y. Comparing Bioretention Designs With and Without an Internal Water Storage Layer for Treating Highway Runoff. *Water Environ. Res.* **2014**, *86* (5), 387–397. https://doi.org/10.2175/106143013X13789303501920.
(61) Lucas, W. C.; Greenway, M. Hydraulic Response and Nitrogen Retention in Bioretention Mesocosms with Regulated Outlets: Part II-Nitrogen Retention. *Water Environ. Res.* **2011**, *83* (8), 703–713. https://doi.org/10.2175/106143011X12989211840936.
(62) Patel, D.; Johnston, J.; Lucas, W.; McCamman, K. Bioretention System Enhancements for Nutrient Removal. *J. Sustain. Water Built Environ.* **2020**, *6* (2), 04020006. https://doi.org/10.1061/JSWBAY.0000901.

Chapter 5: Conclusions and Future Study

This dissertation explored the water quality performance of field-operational green infrastructure (GI) over an annual range of weather conditions along a road in Northern Virginia. Four distinct GI designs along the same road were compared in terms of traditional stormwater quality criteria as they received the same storm event conditions. Additionally, the mitigation of deicing salt by two infiltration-based GI was evaluated to highlight the transport of an emerging stormwater contaminant through GI. Finally, an innovative stable isotope method was used to monitor the occurrence and contribution of denitrification in bioretention.

The four different GI designs had a wide range of performances with respect to traditional stormwater quality criteria, some acting as pollutant sinks and others as pollutant sources. The bioretention and GC had significantly higher total load reduction averages of all water quality parameters than the CAGC and bioswale. Of the GI studied, bioretention and GC are the best choices for nutrient, DOC, and TSS water quality performance and work well together for the needs of the transportation environment. More complex GI designs did not necessarily have better performance than simple GI and small differences in design (e.g. compost amendment) significantly altered GI performance. Future research is needed in long-term GI performance and maintenance.

In the deicing salt study, the infiltration-based GI (bioretention and bioswale) received high winter stormwater loads of Cl^- and Na^+ and were able to significantly reduce those loads in effluent surface water, primarily by infiltration into groundwater. Changes in bioretention soil chemistry indicated a small percentage of Na^+ was stored long-term by ion exchange, but no long-term Cl^- storage was observed. Limited soil storage, assumed limited vegetation storage, and groundwater Cl^- and Na^+ concentrations suggest the majority of salt removed from stormwater by the GI infiltrates into groundwater. Stormwater managers can use infiltration GI to reduce surface water winter deicing salt loading, but should recognize the increased threat to groundwater resources in doing so. Further investigation is suggested into the viability of halophytic vegetation as a deicing salt sink, long-term changes and improved deicing salt resilience in engineered soil media, and fate/transport of deicing salts in groundwater underlying infiltration GI.

The denitrification study is the first known field study using dual nitrate stable isotope analysis to track denitrification within an operational bioretention basin. Nitrogen monitoring revealed seasonal trends in nitrate concentration reductions, with significantly higher reductions happening in warmer months. Cumulative bioretention nitrate and total nitrogen load reductions were 73% and 70%, respectively, but only two out of 24 monitored events displayed denitrification isotope trends, indicating that other nitrogen removal mechanisms (i.e. infiltration and plant uptake) are primarily responsible for nitrogen reductions. Only approximately 1.4% of the total reduced nitrate surface effluent load over the monitoring period was attributable to denitrification. Inlet to outlet nitrate isotope differences also indicated additional nitrate sources within the bioretention basin, suggesting that bioretention is both a sink and source for nitrogen. Future studies should look for denitrification in older bioretentions and bioretentions with internal water storage. Future GI designs should consider increasing HRT to encourage the important ecosystem service denitrification provides.

As population growth drives urbanization and other land use changes, strategies to mitigate watershed pollution export are critical in protecting and improving water resources. When designed well, GI is an effective stormwater management strategy, but when designed poorly it may have unintended consequences. By continuing to explore and expand upon the ability of GI, we can incorporate the ecosystem services nature uses into our water resource management strategies. There is still much to learn, as GI is young and developing, but monitoring results from this dissertation can help future GI designs achieve their full potential.

Appendix A

<u>Summary</u>
5 tables
5 equations

2.2 Materials and Methods:

2.2.1 Study Site

Table A1. Vegetation planting palette for Lorton Road GI.

Bioretention		Grass Channel	Compost-Amended Grass Channel	Bioswale
Species	Location	Species	Species	Species
Trees and Shrubs		**Grasses & Wildflowers**	**Trees and Shrubs**	**Trees and Shrubs**
Canadian Serviceberry	Forebay	Common yarrow	Cockspur Hawthorn	Cockspur Hawthorn
Winterberry	Forebay	Partridge pea	Sweetbay	**Grasses, Sedges & Wildflowers**
Buttonbush	Forebay	Lanceleaf tickseed	**Grasses & Wildflowers**	Upland Bentgrass
Sweetbay	Basin	Golden tickseed	Upland bentgrass	Deertongue
Red-Osier Dogwood	Basin	Sheep fescue	Rough bentgrass	Swamp Milkweed
Buttonbush	Basin	Italian ryegrass	Partridge pea	Blue Wild Indigo
Winterberry	Basin	Blackeyed susan	Lanceleaf tickseed	Squarrose Sedge
Sedges & Wildflowers			Deertongue	Fox Sedge
Fox Sedge	Forebay		Purple coneflower	Indian Woodoats
Dense Blazing Star	Basin		Canada wildrye	Lanceleaf Tickseed
Blue Wild Indigo	Basin		Virginia wildrye	Purple Coneflower
Talus Slope Penstemon	Basin		Dense blazing star	Riverbank Wildrye
Marsh Marigold	Basin		Italian ryegrass	Dense Blazing Star
			Wild bergamot	Wild Bergamot
			Talus slope penstemon	Talus Slope Penstemon
			Blackeyed susan	Blackeyed Susan
			Little bluestem	Little Bluestem
			Indiangrass	American Senna
			Purpletop tridens	Flat-Top Goldentop
				New England Aster
				Bluejacket
				Swamp Verbena
				Golden Zizia

2.2.2 Stormwater Field Monitoring

Ultrasonic sensors measured the height of water in each flume and stormwater flow rates were calculated by solar powered Hach AS950 autosamplers based on an empirically derived equation (**Equation A1**) relating water height in each flume to flow rate.

$$Q = a + b * h^{0.5} + c * h^{1.5} + d * h^{2.5} \qquad \text{(A1)}$$

In Equation A1, Q = flowrate, h = stormwater height, and a, b, c, and d are empirically derived constants specific to each flume size.

To monitor sheet flow entering into the bioswale, a 9.1 m long sheet flow collection gutter was used to channel sheet flow (adjacent to the swales CDA) from Lorton Road into a flume. An impervious roadside area extrapolation was used to calculate the volume of water expected from the impervious roadside CDA of the swales based on the volume of water measured from the 9.1 meter sheet flow collector CDA (**Equation A2**). To account for the pervious CDA of the swales not included in road sheet flow (a relatively small fraction of the total inflow), the Soil Conservation Service (SCS) curve number method was used.

$$V_{in} = V_{SF} * \frac{A_{imperv}}{A_{SF}} + V_{Perv} \qquad \text{(A2)}$$

In Equation A2, V_{in} = total volume of runoff estimated into the swales, V_{SF} = volume of runoff measured in the sheet flow collector, A_{imperv} = impervious CDA for each swale, A_{SF} = CDA for the sheet flow collector, and V_{perv} = volume of runoff estimated from the pervious CDA based on SCS curve number method (**Equation A3 and A4**)[1].

$$V_{Perv} = A_{perv} * \frac{(P-0.2S)^2}{P-0.8S} \qquad \text{(A3)}$$

$$S = \frac{1000}{CN} - 10 \qquad \text{(A4)}$$

In Equation A3 and A4, V_{perv} = volume of runoff estimated into a swale from the pervious CDA, A_{perv} = pervious CDA for a swale, P = rainfall depth, S = maximum soil moisture retention volume, and CN = runoff curve number (estimated based on land use).

For seven high intensity storm events (5/19/2018, 6/2/2018, 8/31/2018, 12/15/2018, 1/25/2019, 2/24/2019, and 3/21/2019), flow rate data from the bioswale outlet were corrected for flume flooding by setting the maximum flow rate to the empirically observed max flow rate of the bioretention outlet pipe (same diameter as bioswale outlet). This procedure is further detailed in Hayes et al. (2020)[2].

For stormwater sampling quality control purposes, we calculated how well each flow-weighted composite sample represented the total flow through each monitoring station over each storm event. **Equation A5** was used to calculate sample “representation percentage”.

$$R\% = \frac{n*P}{V_t} * 100 \qquad \text{(A5)}$$

In Equation A5, $R\%$ = representation percentage for a flow-weighted composite sample, n = number of successful samples taken, P = sampler pacing volume, V_t = the total volume of stormwater monitored at a monitoring location over a storm event. Nearly all flow-weighted composite samples included subsamples spanning first flush through peak flow rate at each monitoring location, with the exception of 3/20/18 bioretention outlet (which sampled peak flow but missed first flush), 12/15/18 bioretention bypass, and 1/19/19 bioretention inlet. For the 12/15/18 and 9/26/18 events with bioretention bypass sample failure, the bioretention bypass inlet sample concentrations were used for the bypass.

Table A2. Storm sample representation percentages (**Equation A5**) and number of samples in each flow-weighted composite sample at each of the five monitoring locations for each storm. * indicates a grab sample.

	Bioretention						Grass Channel				Compost-Amended Grass Channel				Bioswale			
Storm Date	**Inlet (%)**	**# Samples**	**Outlet (%)**	**# Samples**	**Bypass (%)**	**# Samples**	**Inlet (%)**	**# Samples**	**Outlet (%)**	**# Samples**	**Inlet (%)**	**# Samples**	**Outlet (%)**	**# Samples**	**Inlet (%)**	**# Samples**	**Outlet (%)**	**# Samples**
4/16/18	68	85	90	64	6	80												
4/27/18	92	51	110	55	51	49												
5/19/18	99	100	94	139	84	86									57	147	69	145
5/23/18	94	42	89	43	64	49	81	32	22	117	81	32	61	129				
6/2/18	65	88	98	99	77	25	99	101	77	22	99	101	99	144	99	101	79	113
7/23/18	91	76	93	72	15	122												
7/30/18	91	52	94	94	40	52					46	32	74	29	46	32	90	33
8/21/18	57	101	99	130	34	85												
8/31/18	52	59	99	100	48	22	22	33	10	119	22	33	68	180	22	33	63	72
9/26/18	116	29	103	18	30	5					100	13	81	17				
9/28/18	73	81	88	117	57	90	95	83	63	127	95	83	98	293	95	83	86	173
10/11/18	95	54	95	35	48	97	89	26	84	57	89	26	88	56				
10/26/18	94	64	92	45	77	13	61	44	84	85	61	44	89	33				
11/10/18	96	47	85	41	43	11	71	22	65	66	71	22	81	24	71	22	78	27
11/13/18	80	75	101	109	69	55	62	57	63	114	62	57	95	143				
11/15/18	51	76	66	156	42	61												
12/15/18	58	115	63	102	0	0	51	125	60	117					51	125	34	134
1/16/19	64	127	74	77	19	9									29	228	53	79
1/19/19	0	0	86	56	40	30	77	55	81	27	77	55	47	89	77	55	81	96
1/25/19	88	79	92	64	51	37	76	86	78	36	76	86	70	129	76	86	63	77
2/12/19	96	72	95	54	32	19	60	9	64	11	60	9	87	54	60	9	83	35
2/20/19	86	124	NA	1*	35	67	51	92	11	84	51	92	64	348	51	92	57	108
2/24/19	89	121	68	98	41	95	68	75	74	108	68	75	68	225	68	75	35	111
3/21/19	96	70	96	71	82	53	79	87	81	64	79	87	90	93	79	87	84	57
4/26/19	100	27	97	16	26	2												
5/5/19	94	38	95	50	63	26	84	83	79	25								
6/18/19	92	13	94	18	74	8	57	10	69	7	57	10	87	6	57	10	89	6

2.3. Results

2.3.1 Stormwater monitoring conditions

Table A3. Weather conditions from monitored precipitation events. * indicates missing data.

Date	Precipitation Type	Storm Depth (cm)	Ave. Storm Intensity (cm/hr)	Max intensity (cm/10min)	Duration (hrs)	Ave. Daily Temp. (C)	Antecedant Moisture Conditions (PPT depth in past 5 days) (cm)	Source
4/16/18	Rain	9.4	0.44	1.19	21.8	12.5	0.1	rain gauge
4/27/18	Rain	2.6	0.34	0.56	7.7	14.1	2.8	rain gauge
5/19/18	Rain	9.3	0.10	0.25	91.5	17.2	0.0	rain gauge
5/23/18	Rain	2.2	0.21	0.74	10.7	23.5	4.5	rain gauge
6/2/18	Rain	5.1	0.10	0.30	51.3	25.0	0.0	rain gauge
7/23/18	Rain	10.5	0.21	1.02	51.0	26.0	4.3	rain gauge
7/30/18	Rain	2.4	0.28	0.48	8.7	23.3	5.0	rain gauge
8/21/18	Rain	7.2	0.42	1.63	17.2	25.1	0.2	rain gauge
8/31/18	Rain	7.3	0.97	2.46	7.5	27.9	0.0	rain gauge
9/26/18	Rain	0.7	0.22	0.13	3.3	24.2	7.1	rain gauge
9/28/18	Rain	4.0	0.21	0.46	18.8	17.6	4.3	rain gauge
10/11/18	Rain	8.6	0.48	1.24	17.8	24.7	0.1	rain gauge
10/26/18	Rain	4.0	0.19	0.15	21.2	9.0	0.0	rain gauge
11/10/18	Rain	1.4	0.10	0.20	13.7	5.9	6.7	rain gauge
11/13/18	Rain	3.2	0.25	0.13	12.7	8.0	1.4	rain gauge
11/15/18	Rain/Snow	4.4	0.22	0.25	19.5	2.7	3.2	rain gauge
12/15/18	Rain	10.4	0.22	0.25	47.0	11.1	0.0	rain gauge
1/16/19	Snow	2.4	*	*	*	2.0	0.5	weather station
1/19/19	Rain	2.4	0.19	0.15	13.0	3.9	0.4	rain gauge
1/25/19	Rain	2.7	0.23	0.18	11.8	2.9	2.4	rain gauge
2/12/19	Rain	1.5	0.04	0.25	35.0	3.5	0.1	rain gauge
2/20/19	Rain/Snow	2.3	*	*	*	0.5	1.2	weather station
2/24/19	Rain	3.3	0.15	0.43	21.5	7.1	0.0	rain gauge
3/21/19	Rain	6.5	0.25	0.23	26.2	8.0	0.0	rain gauge
4/26/19	Rain	1.0	0.23	0.51	4.3	18.5	0.0	rain gauge
5/5/19	Rain	7.9	0.43	1.02	18.4	18.1	1.2	weather station
6/18/19	Rain	1.9	0.35	0.99	5.5	23.9	7.1	rain gauge
	Average	**4.6**	**0.27**	**0.61**	**22.3**	**14.3**	**2.0**	
	Total	**124.7**						

2.3.2 Stormwater Runoff Reduction

Table A4. Monitored and calculated stormwater runoff volumes at all monitoring locations and calculated runoff reductions for each GI during each monitored event.

	Bioretention					Grass Channel			CA Grass Channel			Bioswale		
Event Date	Inflow Volume (L)	Outlet Underdrain Volume (L)	Outlet Bypass Volume (L)	Runoff Reduction (%)	% Outflow as Bypass (%)	Inflow Volume (L)	Outlet Underdrain Volume (L)	Runoff Reduction (%)	Inflow Volume (L)	Outlet Underdrain Volume (L)	Runoff Reduction (%)	Inflow Volume (L)	Outlet Underdrain Volume (L)	Runoff Reduction (%)
6/2/18	2104107	479156	39168	75.4	7.6	184535	28274	84.7	238993	138003	42.3	163297	152350	6.7
8/31/18	854816	304521	35006	60.3	10.3	185223	88017	52.5	246466	144707	41.3	165259	33555	79.7
9/28/18	1049641	412432	35738	57.3	8.0	104687	48250	53.9	137441	121027	11.9	93436	64771	30.7
11/10/18	464948	127431	13549	69.7	9.6	26175	15264	41.7	33174	15712	52.6	23018	14411	37.4
1/19/19	1093804	358227	25587	64.9	6.7	130284	17748	86.4	163924	92457	43.6	114042	83885	26.4
1/25/19	1005210	370685	19636	61.2	5.0	174524	17390	90.0	219171	82666	62.3	152566	78564	48.5
2/12/19	1398073	421623	21954	68.3	4.9	74612	14265	80.9	92946	81676	12.1	64984	47907	26.3
2/24/19	1599442	538750	38746	63.9	6.7	108893	27584	74.7	140320	101704	27.5	96415	107138	-11.1
3/21/19	2117413	577944	148593	65.7	20.5	243941	59708	75.5	316153	195960	38.0	215522	128584	40.3
6/18/19	376315	145377	69345	42.9	32.3	40944	5400	86.8	52681	18272	65.3	36316	10212	71.9
Total	12063769	3736145	447323	**65.3**	10.7	1273820	321899	**74.7**	1641269	992183	**39.5**	1124855	721376	**35.9**

2.3.3 Stormwater Quality

Table A5. Calculated loads of nitrate, TDN, DOC, phosphate, TP, and TSS travelling through each monitoring location per storm event as well as load reductions for each GI.

	Bioretention nitrate					GC nitrate			CAGC nitrate			Bioswale nitrate		
Date	Load In (Kg)	Load Out Underdrain (Kg)	Load Out Bypass (Kg)	Load Reduction (%)	% Outflow Load Bypassed (%)	Load In (Kg)	Load Out (Kg)	Load Reduction (%)	Load In (Kg)	Load Out (Kg)	Load Reduction (%)	Load In (Kg)	Load Out (Kg)	Load Reduction (%)
6/2/18	0.74	0.033	0.001	95.3	3.4	0.0096	0.0000	100.0	0.0125	0.0000	100.0	0.0085	0.0036	57.6
8/31/18	0.17	0.026	0.006	80.7	19.7	0.0168	0.0067	60.4	0.0224	0.0206	8.0	0.0150	0.0044	70.6
9/28/18	0.73	0.166	0.002	77.0	1.1	0.0118	0.0021	82.5	0.0155	0.0039	75.1	0.0105	0.0067	36.8
11/10/18	0.35	0.062	0.000	82.1	0.6	0.0011	0.0004	60.4	0.0014	0.0003	76.5	0.0009	0.0015	-56.7
1/25/19	0.47	0.194	0.000	58.7	0.0	0.0000	0.0000	N/A	0.0000	0.0000	N/A	0.0000	0.0173	N/A
2/12/19	0.96	0.427	0.000	55.4	0.0	0.0000	0.0000	N/A	0.0000	0.0000	N/A	0.0000	0.0099	N/A
2/24/19	1.02	0.323	0.003	68.1	1.0	0.0100	0.0011	89.3	0.0128	0.0000	100.0	0.0088	0.0074	16.3
3/21/19	0.75	0.303	0.038	54.4	11.1	0.0161	0.0018	89.1	0.0209	0.0172	17.7	0.0143	0.0138	2.9
6/18/19	0.20	0.003	0.004	96.5	56.7	0.0082	0.0001	98.2	0.0105	0.0003	97.5	0.0073	0.0004	94.9
Total Load	**5.38**	**1.54**	**0.05**	**70.4**	**3.4**	**0.07**	**0.01**	**83.5**	**0.10**	**0.04**	**56.0**	**0.07**	**0.06**	**0.7**

	Bioretention TDN					GC TDN			CAGC TDN			Bioswale TDN		
Date	Load In (Kg)	Load Out Underdrain (Kg)	Load Out Bypass (Kg)	Load Reduction (%)	% Outflow Load Bypassed (%)	Load In (Kg)	Load Out (Kg)	Load Reduction (%)	Load In (Kg)	Load Out (Kg)	Load Reduction (%)	Load In (Kg)	Load Out (Kg)	Load Reduction (%)
6/2/18	1.27	0.191	0.018	83.5	8.8	0.0462	0.0112	75.8	0.0598	0.1252	-109.2	0.0409	0.0888	-117.2
8/31/18	0.31	0.111	0.014	59.4	11.5	0.0816	0.0743	8.9	0.1086	0.1988	-83.1	0.0728	0.0309	57.6
9/28/18	1.06	0.233	0.000	78.0	0.0	0.0334	0.0257	23.1	0.0439	0.1336	-204.4	0.0298	0.0298	0.1
11/10/18	0.47	0.083	0.000	82.4	0.0	0.0057	0.0069	-21.2	0.0073	0.0113	-55.4	0.0050	0.0057	-14.1
1/25/19	0.98	0.319	0.000	67.5	0.0	0.1690	0.0000	100.0	0.2122	0.0000	100.0	0.1477	0.0407	72.4
2/12/19	1.40	0.464	0.007	66.4	1.4	0.0224	0.0043	80.9	0.0279	0.0408	-46.5	0.0195	0.0240	-22.9
2/24/19	1.44	0.431	0.012	69.3	2.6	0.0218	0.0055	74.7	0.0281	0.0407	-45.0	0.0193	0.0429	-122.2
3/21/19	1.69	0.405	0.074	71.7	15.5	0.0732	0.0239	67.4	0.0948	0.1176	-24.0	0.0647	0.0514	20.5
6/18/19	0.41	0.000	0.055	86.6	100.0	0.0368	0.0054	85.3	0.0474	0.0183	61.5	0.0327	0.0082	75.0
Total Load	**9.03**	**2.24**	**0.18**	**73.2**	**7.5**	**0.49**	**0.16**	**67.9**	**0.63**	**0.69**	**-8.9**	**0.43**	**0.32**	**25.4**

	Bioretention DOC					GC DOC			CAGC DOC			Bioswale DOC		
Date	Load In (Kg)	Load Out Underdrain (Kg)	Load Out Bypass (Kg)	Load Reduction (%)	% Outflow Load Bypassed (%)	Load In (Kg)	Load Out (Kg)	Load Reduction (%)	Load In (Kg)	Load Out (Kg)	Load Reduction (%)	Load In (Kg)	Load Out (Kg)	Load Reduction (%)
6/2/18	11.76	3.988	0.320	63.4	7.4	0.9467	0.2719	71.3	1.2261	2.8134	-129.5	0.8378	1.8970	-126.4
8/31/18	4.14	2.427	0.224	35.9	8.5	1.2677	0.8690	31.4	1.6868	3.0753	-82.3	1.1310	0.4305	61.9
9/28/18	4.44	1.924	0.000	56.7	0.0	0.5007	0.5001	0.1	0.6574	2.6040	-296.1	0.4469	0.5624	-25.8
11/10/18	2.15	0.555	0.099	69.6	15.2	0.1210	0.1347	-11.3	0.1534	0.2343	-52.7	0.1064	0.1097	-3.1
1/25/19	6.05	1.347	0.142	75.4	9.5	1.4781	0.1186	92.0	1.8562	0.9744	47.5	1.2921	0.5060	60.8
2/12/19	8.39	1.644	0.147	78.6	8.2	0.2761	0.0970	64.9	0.3439	0.8331	-142.2	0.2404	0.2922	-21.5
2/24/19	7.36	1.993	0.147	70.9	6.9	0.3158	0.1186	62.4	0.4069	0.7221	-77.5	0.2796	0.6000	-114.6
3/21/19	10.80	3.525	0.832	59.6	19.1	0.8050	0.4299	46.6	1.0433	2.0576	-97.2	0.7112	0.8358	-17.5
6/18/19	3.61	1.614	0.576	39.4	26.3	0.3931	0.1053	73.2	0.5057	0.3600	28.8	0.3486	0.1644	52.8
Total Load	**46.94**	**15.03**	**2.17**	**63.4**	**12.6**	**5.16**	**2.37**	**54.0**	**6.65**	**10.86**	**-63.2**	**4.56**	**3.50**	**23.2**

	Bioretention phosphate					GC phosphate			CAGC phosphate			Bioswale phosphate		
Date	Load In (Kg)	Load Out Underdrain (Kg)	Load Out Bypass (Kg)	Load Reduction (%)	% Outflow Load Bypassed (%)	Load In (Kg)	Load Out (Kg)	Load Reduction (%)	Load In (Kg)	Load Out (Kg)	Load Reduction (%)	Load In (Kg)	Load Out (Kg)	Load Reduction (%)
6/2/18	0.149	0.055	0.004	60.3	7.3	0.0190	0.0032	83.1	0.0246	0.0319	-29.4	0.0168	0.0245	-45.6
8/31/18	0.071	0.020	0.005	64.6	21.9	0.0126	0.0245	-93.8	0.0168	0.0566	-236.6	0.0113	0.0068	40.0
9/28/18	0.072	0.037	0.004	43.6	9.8	0.0113	0.0045	60.6	0.0149	0.0361	-142.4	0.0101	0.0078	23.0
11/10/18	0.047	0.008	0.002	78.3	17.4	0.0034	0.0016	53.9	0.0043	0.0043	0.0	0.0030	0.0018	39.6
2/24/19	0.000	0.000	0.000	N/A	N/A	0.0000	0.0000	N/A	0.0000	0.0104	N/A	0.0000	0.0077	N/A
3/21/19	0.157	0.016	0.003	87.8	16.6	0.0039	0.0011	73.0	0.0051	0.0295	-484.4	0.0034	0.0062	-81.4
6/18/19	0.006	0.004	0.003	-18.8	45.8	0.0018	0.0001	97.2	0.0023	0.0014	40.4	0.0016	0.0005	71.0
Total Load	**0.5**	**0.1**	**0.0**	**67.9**	**13.5**	**0.05**	**0.03**	**33.1**	**0.07**	**0.17**	**-150.2**	**0.05**	**0.06**	**-19.5**

	Bioretention TP					GC TP			CAGC TP			Bioswale TP		
Date	Load In (Kg)	Load Out Underdrain (Kg)	Load Out Bypass (Kg)	Load Reduction (%)	% Outflow Load Bypassed (%)	Load In (Kg)	Load Out (Kg)	Load Reduction (%)	Load In (Kg)	Load Out (Kg)	Load Reduction (%)	Load In (Kg)	Load Out (Kg)	Load Reduction (%)
9/28/18	0.092	0.008	0.001	90.1	9.8	0.0089	0.0067	24.6	0.0117	0.0495	-323.7	0.0079	0.0087	-10.1
11/10/18	0.023	0.006	0.002	60.5	27.7	0.0040	0.0016	59.9	0.0051	0.0061	-19.9	0.0035	0.0027	24.4
Total Load	**0.1**	**0.0**	**0.0**	**84.3**	**18.7**	**0.01**	**0.01**	**35.6**	**0.02**	**0.06**	**-231.3**	**0.01**	**0.01**	**0.5**

	Bioretention TSS					GC TSS			CAGC TSS			Bioswale TSS		
Date	Load In (Kg)	Load Out Underdrain (Kg)	Load Out Bypass (Kg)	Load Reduction (%)	% Outflow Load Bypassed (%)	Load In (Kg)	Load Out (Kg)	Load Reduction (%)	Load In (Kg)	Load Out (Kg)	Load Reduction (%)	Load In (Kg)	Load Out (Kg)	Load Reduction (%)
6/2/18	35.770	4.792	0.979	83.9	17.0	19.3761	0.3110	98.4	25.0943	4.9681	80.2	17.1462	2.8946	83.1
8/31/18	18.806	7.004	0.525	60.0	7.0	23.7086	4.4009	81.4	31.5477	6.5118	79.4	21.1532	1.7448	91.8
9/28/18	25.191	1.237	0.715	92.3	36.6	7.1187	0.3860	94.6	9.3460	9.5611	-2.3	6.3536	0.7773	87.8
1/25/19	66.344	1.112	0.452	97.6	28.9	10.9950	0.2956	97.3	13.8078	3.3066	76.1	9.6117	1.3356	86.1
2/24/19	118.092	0.808	2.723	97.0	77.1	37.1326	0.7310	98.0	47.8491	8.5036	82.2	32.8774	1.5833	95.2
3/21/19	314.789	6.422	4.557	96.5	41.5	25.9391	2.1694	91.6	33.6176	14.8929	55.7	22.9172	2.1002	90.8
Total Load	**579.0**	**21.4**	**10.0**	**94.6**	**31.8**	**124.27**	**8.29**	**93.3**	**161.26**	**47.74**	**70.4**	**110.06**	**10.44**	**90.5**

References:

(1) Bosznay, M. Generalization of SCS Curve Number Method. *J. Irrig. Drain. Eng.* **1989**, *115* (1), 139–144. https://doi.org/10.1061/(ASCE)0733-9437(1989)115:1(139).

(2) Hayes, G. M.; Burgis, C.; Zhang, W.; Henderson, D.; Smith, J. A. Runoff Reduction by Four Green Stormwater Infrastructure Systems in a Shared Environment. *J. Sustain. Water Built Environ. (under Rev.*

Appendix B

<u>Summary</u>
4 tables
8 figures
1 equation

3.2 Materials and Methods

3.2.1 Study Site

Figure B1. Bioretention basin on January 16th, 2019 (left) and October 11th, 2019 (right). Both pictures facing east.

Figure B2. Bioswale on January 16th, 2019 (left) and October 11th, 2019 (right). Both pictures facing east.

3.2.2 Stormwater Field Monitoring

Table B1. Storm sample representation percentages (**Appendix A Equation A5**) and number of samples in each flow-weighted composite sample at each of the five monitoring locations for each storm. * indicates a grab sample.

	Bioretention						Bioswale			
Storm Date	Inlet (%)	# Samples	Outlet (%)	# Samples	Bypass (%)	# Samples	Inlet (%)	# Samples	Outlet (%)	# Samples
3/20/18	104	91	30	63	101	63				
4/16/18	68	85	90	64	6	80				
4/27/18	92	51	110	55	51	49				
5/19/18	99	100	94	139	84	86	57	147	69	145
5/23/18	94	42	89	43	64	49				
6/2/18	65	88	98	99	77	25	99	101	79	113
7/23/18	91	76	93	72	15	122				
7/30/18	91	52	94	94	40	52	46	32	90	33
8/21/18	57	101	99	130	34	85				
8/31/18	52	59	99	100	48	22	22	33	63	72
9/26/18	116	29	103	18	0	0				
9/28/18	73	81	88	117	57	90	95	83	86	173
10/11/18	95	54	95	35	48	97				
10/26/18	94	64	92	45	77	13				
11/10/18	96	47	85	41	43	11	71	22	78	27
11/13/18	80	75	101	109	69	55				
11/15/18	51	76	66	156	42	61				
12/15/18	58	115	63	102	0	0	51	125	34	134
1/16/19	64	127	74	77	19	9	29	228	53	79
1/19/19	0	0	86	56	40	30	77	55	81	96
1/25/19	88	79	92	64	51	37	76	86	63	77
2/12/19	96	72	95	54	32	19	60	9	83	35
2/20/19	86	124	NA	1*	35	67	51	92	57	108
2/24/19	89	121	68	98	41	95	68	75	35	111
3/21/19	96	70	96	71	82	53	79	87	84	57
4/26/19	100	27	97	16	26	2				
5/5/19	94	38	95	50	63	26				
6/18/19	92	13	94	18	74	8	57	10	89	6

3.2.3 Stormwater Analysis

$$SAR = \frac{Na^{+}}{\sqrt{\frac{1}{2}(Ca^{2+} + Mg^{2+})}} \qquad \text{(B1)}$$

In Equation B1, SAR = sodium adsorption ratio and Na^{+}, Ca^{2+}, Mg^{2+} = sodium, calcium, and magnesium concentrations in milliequivalents/liter[1].

3.3 Results

3.3.1 Stormwater

Table B2. Weather conditions from monitored precipitation events. * indicates missing data.

Date	Precipitation Type	Storm Depth (cm)	Ave. Storm Intensity (cm/hr)	Max intensity (cm/10min)	Duration (hrs)	Ave. Daily Temp. (C)	Antecedant Moisture Conditions (PPT depth in past 5 days) (cm)	Source
3/20/18	Rain/Snow	6.1	0.29	0.13	13.0	1.7	0.0	rain gauge
4/16/18	Rain	9.4	0.44	1.19	21.8	12.5	0.1	rain gauge
4/27/18	Rain	2.6	0.34	0.56	7.7	14.1	2.8	rain gauge
5/19/18	Rain	9.3	0.10	0.25	91.5	17.2	0.0	rain gauge
5/23/18	Rain	2.2	0.21	0.74	10.7	23.5	4.5	rain gauge
6/2/18	Rain	5.1	0.10	0.30	51.3	25.0	0.0	rain gauge
7/23/18	Rain	10.5	0.21	1.02	51.0	26.0	4.3	rain gauge
7/30/18	Rain	2.4	0.28	0.48	8.7	23.3	5.0	rain gauge
8/21/18	Rain	7.2	0.42	1.63	17.2	25.1	0.2	rain gauge
8/31/18	Rain	7.3	0.97	2.46	7.5	27.9	0.0	rain gauge
9/26/18	Rain	0.7	0.22	0.13	3.3	24.2	7.1	rain gauge
9/28/18	Rain	4.0	0.21	0.46	18.8	17.6	4.3	rain gauge
10/11/18	Rain	8.6	0.48	1.24	17.8	24.7	0.1	rain gauge
10/26/18	Rain	4.0	0.19	0.15	21.2	9.0	0.0	rain gauge
11/10/18	Rain	1.4	0.10	0.20	13.7	5.9	6.7	rain gauge
11/13/18	Rain	3.2	0.25	0.13	12.7	8.0	1.4	rain gauge
11/15/18	Rain/Snow	4.4	0.22	0.25	19.5	2.7	3.2	rain gauge
12/15/18	Rain	10.4	0.22	0.25	47.0	11.1	0.0	rain gauge
1/16/19	Snow	2.4	*	*	*	2.0	0.5	weather station
1/19/19	Rain	2.4	0.19	0.15	13.0	3.9	0.4	rain gauge
1/25/19	Rain	2.7	0.23	0.18	11.8	2.9	2.4	rain gauge
2/12/19	Rain	1.5	0.04	0.25	35.0	3.5	0.1	rain gauge
2/20/19	Rain/Snow	2.3	*	*	*	0.5	1.2	weather station
2/24/19	Rain	3.3	0.15	0.43	21.5	7.1	0.0	rain gauge
3/21/19	Rain	6.5	0.25	0.23	26.2	8.0	0.0	rain gauge
4/26/19	Rain	1.0	0.23	0.51	4.3	18.5	0.0	rain gauge
5/5/19	Rain	7.9	0.43	1.02	18.4	18.1	1.2	weather station
6/18/19	Rain	1.9	0.35	0.99	5.5	23.9	7.1	rain gauge
	Average	**4.7**	**0.27**	**0.59**	**21.9**	**13.8**	**1.9**	
	Total	**130.8**						

Table B3. Stormwater runoff volumes at each monitoring location per precipitation event and runoff reductions (per event and cumulative).

	Bioretention					Bioswale		
Event Date	Inflow Volume (L)	Outlet Underdrain Volume (L)	Outlet Bypass Volume (L)	Runoff Reduction (%)	% Outflow as Bypass (%)	Inflow Volume (L)	Outlet Underdrain Volume (L)	Runoff Reduction (%)
3/20/18	722397	224815	25857	65.3	10.3			
4/16/18	1859925	726816	675227	24.6	48.2			
4/27/18	688256	182639	38135	67.9	17.3			
5/19/18	2425496	920185	87982	58.4	8.7	326079	261000	20.0
5/23/18	473641	145519	29845	63.0	17.0			
6/2/18	2104107	479156	39168	75.4	7.6	163297	152350	6.7
7/23/18	3813244	1087723	621570	55.2	36.4			
7/30/18	433288	188694	49162	45.1	20.7	59943	17430	70.9
8/21/18	1349767	426425	187099	54.5	30.5			
8/31/18	854816	304521	35006	60.3	10.3	165259	33555	79.7
9/26/18	237475	55976	3843	74.8	6.4			
9/28/18	1049641	412432	35738	57.3	8.0	93436	64771	30.7
10/11/18	2152335	417416	384465	62.7	47.9			
10/26/18	771667	221492	12786	69.6	5.5			
11/10/18	464948	127431	13549	69.7	9.6	23018	14411	37.4
11/13/18	886766	325407	24199	60.6	6.9			
11/15/18	1385135	579202	19650	56.8	3.3			
12/15/18	3369003	739206	551770	61.7	42.7	362545	302025	16.7
1/16/19	1139107	193074	9189	82.2	4.5	218983	18669	91.5
1/19/19	1093804	358227	25587	64.9	6.7	114042	83885	26.4
1/25/19	1005210	370685	19636	61.2	5.0	152566	78564	48.5
2/12/19	1398073	421623	21954	68.3	4.9	64984	47907	26.3
2/20/19						34426	17013	50.6
2/24/19	1599442	538750	38746	63.9	6.7	96415	107138	-11.1
3/21/19	2117413	577944	148593	65.7	20.5	215522	128584	40.3
4/26/19	204417	62300	5277	66.9	7.8			
5/5/19	1066765	397360	46825	58.4	10.5			
6/18/19	376315	145377	69345	42.9	32.3	36316	10212	71.9
Total	35042453	10630396	3220203	**60.5**	**23.2**	2126832	1337512	**37.1**

Table B4. Stormwater EMCs of Cl^-, Ca2$^+$, Mg^{2+}, and K^+ for each monitored event in the bioretention (top) and bioswale (bottom).

Bioretention	Cl- Concentration				Na+ Concentration				Ca2+ Concentration				Mg2+ Concentration				K+ Concentration			
Event Date	Inflow (mg/L)	Outlet Underdrain (mg/L)	Outlet Bypass (mg/L)	Concentration Reduction (%)	Inflow (mg/L)	Outlet Underdrain (mg/L)	Outlet Bypass (mg/L)	Concentration Reduction (%)	Inflow (mg/L)	Outlet Underdrain (mg/L)	Outlet Bypass (mg/L)	Concentration Reduction (%)	Inflow (mg/L)	Outlet Underdrain (mg/L)	Outlet Bypass (mg/L)	Concentration Reduction (%)	Inflow (mg/L)	Outlet Underdrain (mg/L)	Outlet Bypass (mg/L)	Concentration Reduction (%)
3/20/18	2080	113	131	95	1309	68	131	95	7.7	19.7	2.9	-157	0.7	5.5	2.7	-630	0.5	1.2	82.9	-115
4/16/18	35	550	48	-1471	33	247	35	-655	2.9	82.0	3.7	-2682	0.2	25.8	0.5	-11510	0.0	0.0	0.0	0
4/27/18	45	72	49	-60	51	59	40	-16	7.1	17.8	5.9	-151	1.0	4.3	1.1	-350	1.3	1.6	1.3	-21
5/19/18	41	43	52	-4	43	50	47	-15	9.0	12.1	9.6	-34	1.0	2.7	1.7	-165	1.4	1.4	1.9	3
5/23/18	50	50	18	0	49	69	32	-40	11.0	14.6	5.1	-33	1.5	3.4	0.9	-124	1.6	1.8	0.9	-11
6/2/18	51	38	29	25	41	55	41	-33	12.9	11.7	10.7	9	1.7	2.3	2.0	-37	1.7	1.5	1.4	14
7/23/18	22	26	6	-18	30	43	16	-43	11.4	9.9	4.8	13	1.7	1.9	0.9	-14	1.8	1.6	0.7	12
7/30/18	29	40	9	-40	29	55	17	-89	8.9	14.7	4.7	-66	1.1	2.7	0.8	-155	1.1	1.7	0.6	-51
8/21/18	12	17	5	-35	21	35	14	-72	5.9	12.4	3.1	-109	0.9	2.2	0.6	-157	0.7	1.1	0.5	-53
8/31/18	4	20	6	-413	15	37	15	-154	2.4	13.3	3.9	-456	0.6	2.3	0.7	-288	0.6	1.1	0.8	-95
9/26/18	61	52	*	16	48	51	*	-7	23.7	16.2	*	32	2.8	2.8	*	-3	2.5	2.0	*	18
9/28/18	22	25	20	-12	28	38	28	-35	15.2	14.6	13.2	4	1.8	2.7	2.7	-45	1.4	1.4	1.4	3
10/11/18	13	21	4	-62	22	31	14	-41	8.3	10.3	4.9	-25	0.9	1.6	0.6	-75	1.2	0.8	0.4	31
10/26/18	17	22	30	-26	21	31	28	-46	7.5	11.1	9.5	-47	0.8	1.9	2.0	-149	0.6	0.8	1.0	-42
11/10/18	44	32	22	29	38	36	28	3	15.1	11.8	11.7	22	1.7	1.9	2.3	-11	1.5	1.1	1.2	29
11/13/18	13	23	19	-74	19	31	23	-67	7.8	5.1	8.8	34	0.8	1.5	1.9	-78	0.7	0.8	1.0	-28
11/15/18	547	396	272	28	336	117	144	65	14.5	85.1	20.7	-486	1.5	24.9	5.3	-1602	2.0	2.5	2.4	-27
12/15/18	11	20	*	-81	17	31	*	-81	6.4	7.4	*	-16	0.9	1.2	*	-39	0.6	0.8	*	-50
1/16/19	7395	3748	411	49	4346	1789	195	59	59.8	311.8	62.6	-421	3.6	42.2	15.9	-1072	2.1	8.4	3.4	-306
1/19/19	642	1490	584	-132	390	721	323	-85	11.0	113.8	34.7	-932	1.1	26.2	8.6	-2326	2.2	4.7	2.8	-112
1/25/19	216	345	215	-60	129	186	123	-44	14.9	25.5	13.8	-71	1.9	7.6	3.4	-305	2.0	1.9	2.0	4
2/12/19	1056	618	274	41	599	334	144	44	22.4	27.5	15.5	-23	2.5	6.1	4.0	-139	1.7	2.0	1.6	-20
2/20/19	2744	865	2299	68	1527	458	1231	70	38.2	31.4	64.4	18	3.2	6.1	14.5	-92	2.2	2.5	2.3	-16
2/24/19	148	407	145	-175	98	214	92	-118	16.3	31.5	10.7	-94	1.3	8.5	1.5	-551	1.5	1.5	0.9	-5
3/21/19	46	75	56	-63	30	58	35	-94	6.6	5.5	6.3	17	0.8	1.3	0.9	-65	0.9	0.5	1.0	45
4/26/19	46	58	72	-27	27	72	46	-166	10.8	9.9	8.3	8	1.9	1.9	1.5	3	2.4	1.2	1.3	52
5/5/19	31	27	18	14	24	38	15	-60	7.6	8.3	5.1	-9	1.1	1.3	0.9	-20	1.3	0.8	0.9	42
6/18/19	26	19	4	27	19	34	3	-77	8.0	5.6	1.7	30	1.2	1.1	0.4	5	1.4	0.5	1.2	68
Average	552	329	185	**40**	333	178	110	**47**	13.3	33.6	13	**-152**	1.4	6.9	3	**-383**	1.4	1.7	4	**-22**

* missing sample
grab sample (blue shading)
bioswale inlet sample used (orange shading)

Bioswale	Cl- Concentration			Na+ Concentration			Ca2+ Concentration			Mg2+ Concentration			K+ Concentration		
Event Date	Inflow (mg/L)	Outlet Underdrain (mg/L)	Concentration Reduction (%)	Inflow (mg/L)	Outlet Underdrain (mg/L)	Concentration Reduction (%)	Inflow (mg/L)	Outlet Underdrain (mg/L)	Concentration Reduction (%)	Inflow (mg/L)	Outlet Underdrain (mg/L)	Concentration Reduction (%)	Inflow (mg/L)	Outlet Underdrain (mg/L)	Concentration Reduction (%)
5/19/18	52	23	56	44	31	30	8.9	15.5	-74	1.1	3.6	-239	1.8	1.8	1
6/2/18	25	29	-17	30	103	-250	4.9	41.3	-736	0.8	9.3	-1056	0.8	4.3	-403
7/30/18	19	28	-45	22	47	-114	3.5	23.3	-576	0.6	4.4	-654	0.8	2.3	-181
8/31/18	11	9	19	19	34	-77	3.1	12.4	-295	0.6	2.3	-308	0.7	1.2	-89
9/28/18	17	15	15	24	33	-33	9.3	25.6	-176	1.2	4.7	-295	1.1	2.1	-97
11/10/18	20	13	37	24	27	-13	6.6	16.8	-155	0.6	2.7	-361	0.9	1.1	-26
12/15/18	7	13	-91	17	32	-86	3.2	11.1	-248	0.4	1.9	-331	0.5	1.0	-86
1/16/19	8050	7112	12	4976	3501	30	63.7	524.5	-723	3.5	59.3	-1607	2.2	12.8	-487
1/19/19	642	1766	-175	390	863	-121	11.0	147.3	-1236	1.1	31.2	-2782	2.2	6.5	-194
1/25/19	241	808	-235	143	379	-165	8.0	69.7	-766	0.9	16.0	-1580	1.9	3.5	-89
2/12/19	231	1041	-352	129	539	-317	7.2	58.5	-716	0.9	11.9	-1292	1.0	3.5	-247
2/20/19	4270	1717	60	2420	823	66	22.6	109.2	-383	0.8	20.8	-2566	0.7	5.0	-660
2/24/19	64	402	-532	48	226	-367	6.2	29.8	-379	0.1	5.6	-4048	0.6	2.6	-334
3/21/19	65	141	-115	40	92	-130	3.0	10.1	-232	0.3	1.8	-480	0.4	1.4	-234
6/18/19	49	51	-6	26	50	-90	3.7	15.3	-315	0.5	2.2	-307	0.8	1.7	-120
Average	918	878	**4**	557	452	**19**	11.0	74.0	**-573**	0.9	11.8	**-1230**	1.1	3.4	**-211**

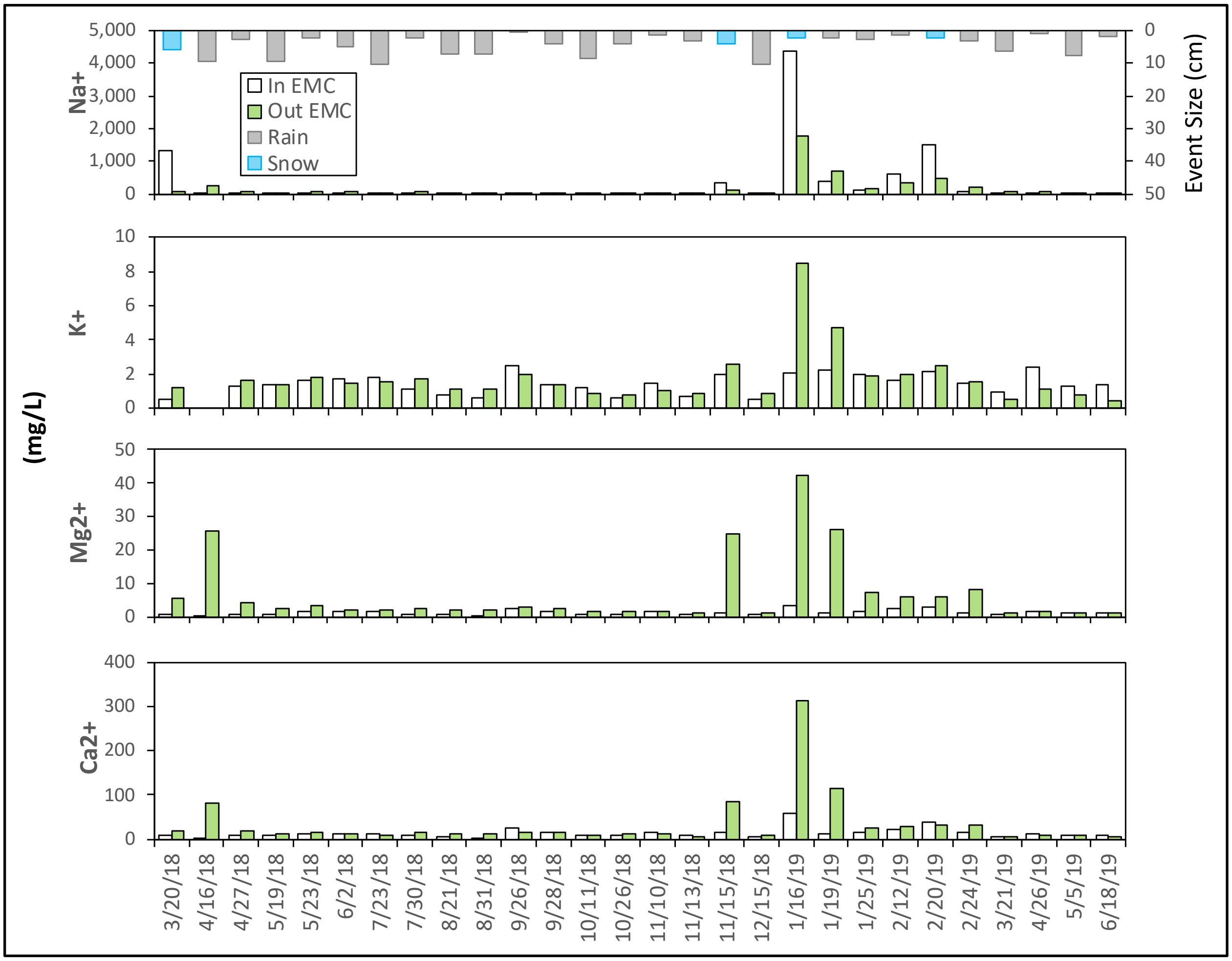

Figure B3. Bioretention inlet and outlet Na^{+}, K^{+}, Mg^{2+}, and Ca^{2+} EMCs for 28 monitored rain and snowmelt events. White and green bars show loads or concentrations going in and out of the bioretention (respectively) and correspond to the left y-axis. Grey and blue bars show rain and snow (respectively) and correspond to the right inverted y-axis. Bypass concentrations were not considered for the outlet concentrations. No outlet flow-weighted sample was collected on 2/20/19, but a grab sample was taken.

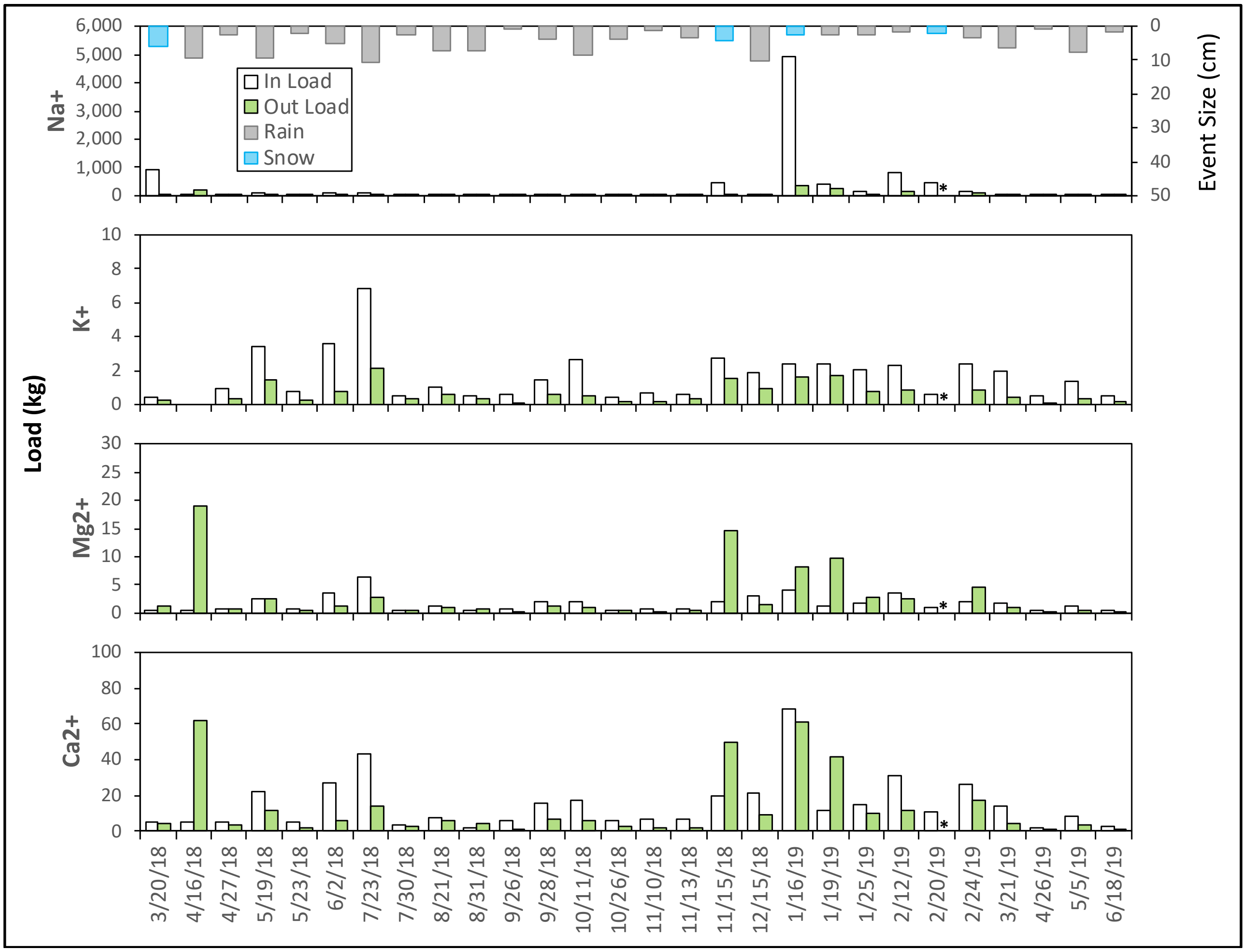

Figure B4. Bioretention inlet and outlet Na^+, K^+, Mg^{2+}, and Ca^{2+} loads for 28 monitored rain and snowmelt events. White and green bars show loads or concentrations going in and out of the bioretention (respectively) and correspond to the left y-axis. Grey and blue bars show rain and snow (respectively) and correspond to the right inverted y-axis. No outlet flow-weighted sample was collected on 2/20/19 (*).

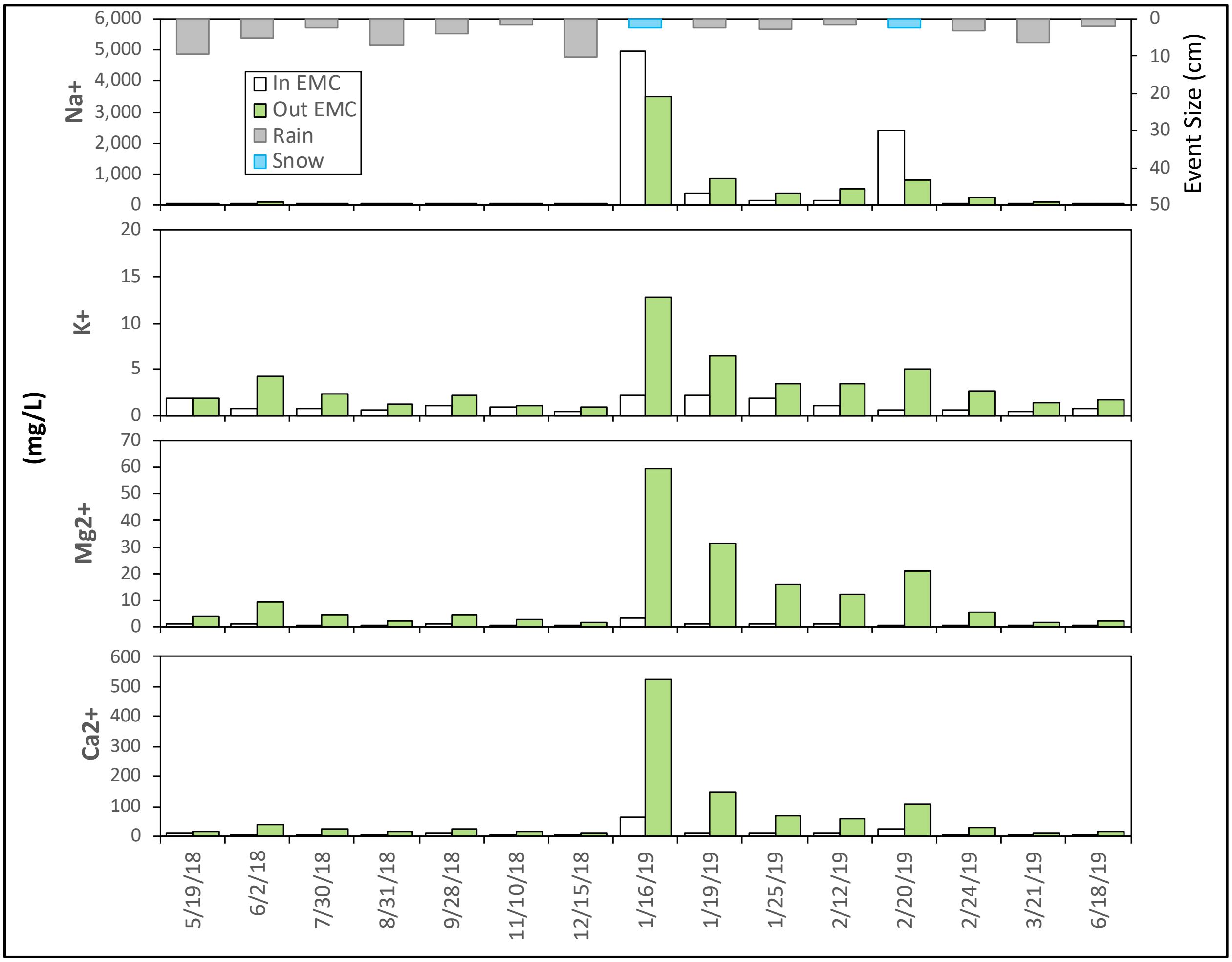

Figure B5. Bioswale inlet and outlet Na^{+}, K^{+}, Mg^{2+}, and Ca^{2+} EMCs for 15 monitored rain and snowmelt events. White and green bars show loads or concentrations going in and out of the bioretention (respectively) and correspond to the left y-axis. Grey and blue bars show rain and snow (respectively) and correspond to the right inverted y-axis.

Figure B6. Bioswale inlet and outlet Na^{+}, K^{+}, Mg^{2+}, and Ca^{2+} loads for 15 monitored rain and snowmelt events. White and green bars show loads or concentrations going in and out of the bioretention (respectively) and correspond to the left y-axis. Grey and blue bars show rain and snow (respectively) and correspond to the right inverted y-axis.

3.3.3 Groundwater Observations

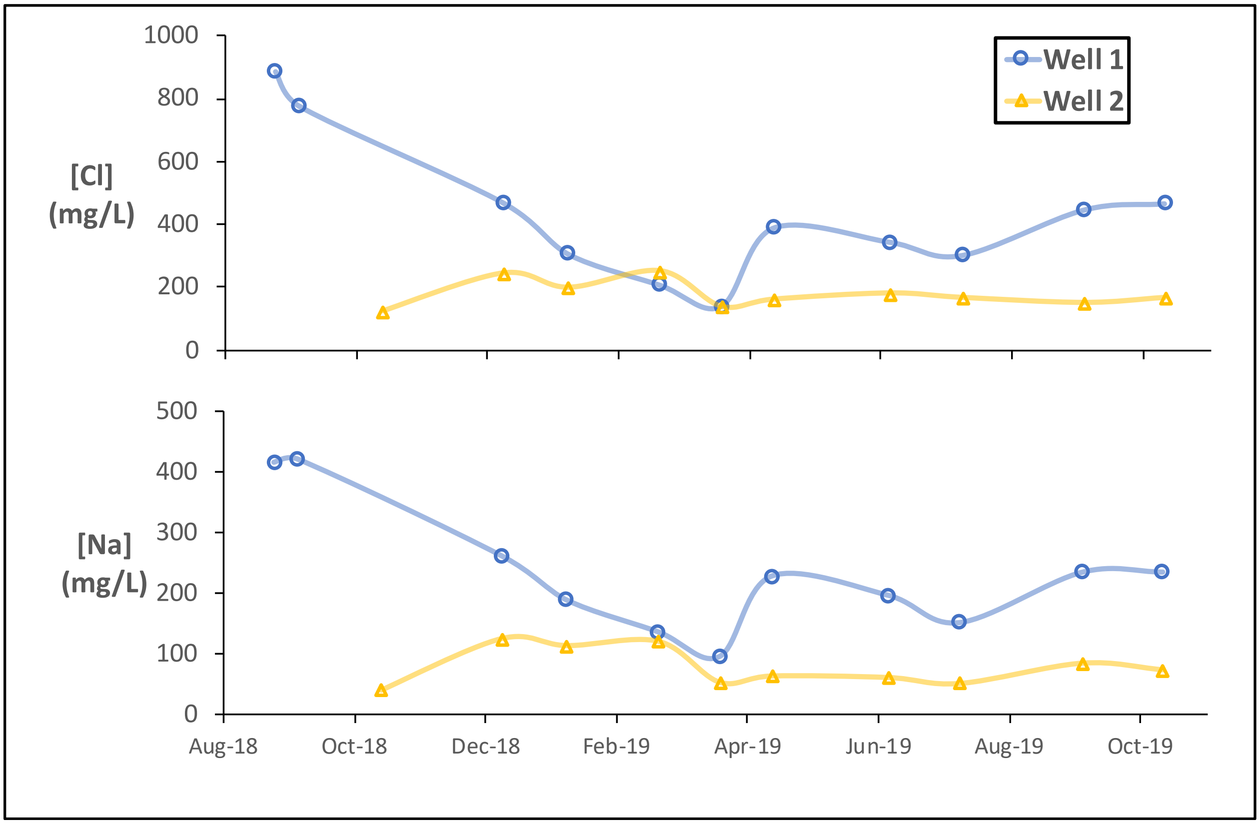

Figure B7. Groundwater Cl^- (top) and Na^+ (bottom) concentrations in two wells near the bioretention between August 2018 and October 2019. Well 1 was installed in August 2018 and Well 2 in October 2018.

Observed Groundwater Temporal Trends:

Groundwater chloride and sodium levels in Well 1 show more significant temporal trends than in Well 2 (**Figure B7).** Changes in concentrations over time may be the delayed result of seasonal road salt addition making its way into groundwater. Well 1 shows a gradual decline in chloride and sodium levels until April 2019, when levels spike. This spike may be from road salt additions in the winter of 2018/2019, which would be an approximately 5 month lag time from the first snow event in November 2018. Well 2 shows more consistent levels of chloride and sodium, showing an overall slight decreasing trend throughout the groundwater monitoring period.

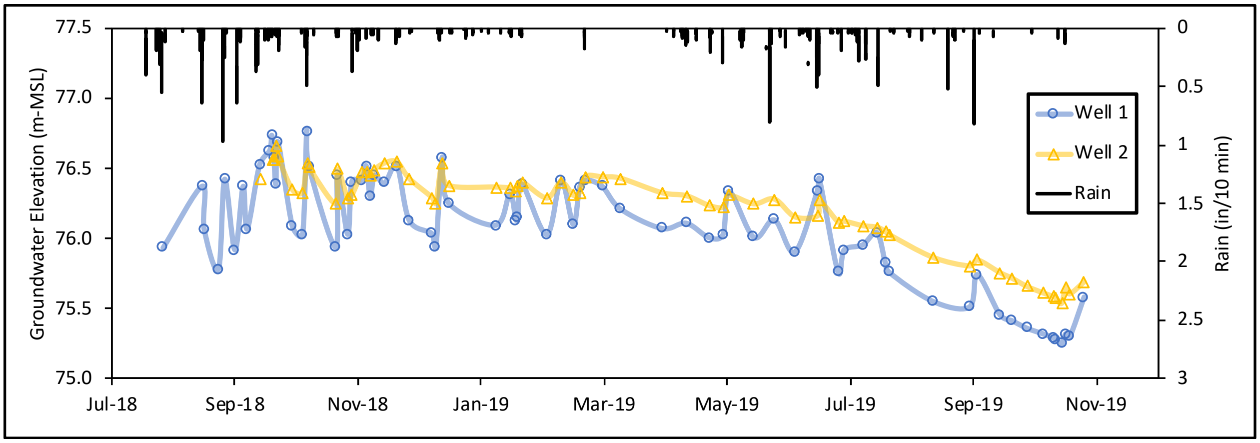

Figure B8. Groundwater elevations of Well 1 and 2 (left y-axis) and rain intensity (right y-axis) between August 2018 and October 2019. Levels are depths of groundwater relative to mean sea level. Rain intensity from March 2019 is missing.

References:

(1) Oster, J. D.; Sposito, G. The Gapon Coefficient and the Exchangeable Sodium Percentage-Sodium Adsorption Ratio Relation. *Soil Sci. Soc. Am. J.* **1980**, *44* (2), 258–260. https://doi.org/10.2136/sssaj1980.03615995004400020011x.

Appendix C

Summary
4 tables
6 figures

4.3 Results

4.3.1 Stormwater monitoring conditions

Table C1. Weather conditions from monitored precipitation events. * indicates missing data.

Date	Precipitation Type	Storm Depth (cm)	Ave. Storm Intensity (cm/hr)	Max intensity (cm/10min)	Duration (hrs)	Ave. Daily Temp. (C)	Antecedant Moisture Conditions (PPT depth in past 5 days) (cm)	Source
4/16/18	Rain	9.4	0.44	1.19	21.8	12.5	0.1	rain gauge
4/27/18	Rain	2.6	0.34	0.56	7.7	14.1	2.8	rain gauge
5/19/18	Rain	9.3	0.10	0.25	91.5	17.2	0.0	rain gauge
5/23/18	Rain	2.2	0.21	0.74	10.7	23.5	4.5	rain gauge
6/2/18	Rain	5.1	0.10	0.30	51.3	25.0	0.0	rain gauge
7/23/18	Rain	10.5	0.21	1.02	51.0	26.0	4.3	rain gauge
7/30/18	Rain	2.4	0.28	0.48	8.7	23.3	5.0	rain gauge
8/21/18	Rain	7.2	0.42	1.63	17.2	25.1	0.2	rain gauge
8/31/18	Rain	7.3	0.97	2.46	7.5	27.9	0.0	rain gauge
9/26/18	Rain	0.7	0.22	0.13	3.3	24.2	7.1	rain gauge
9/28/18	Rain	4.0	0.21	0.46	18.8	17.6	4.3	rain gauge
10/11/18	Rain	8.6	0.48	1.24	17.8	24.7	0.1	rain gauge
10/26/18	Rain	4.0	0.19	0.15	21.2	9.0	0.0	rain gauge
11/10/18	Rain	1.4	0.10	0.20	13.7	5.9	6.7	rain gauge
11/13/18	Rain	3.2	0.25	0.13	12.7	8.0	1.4	rain gauge
11/15/18	Rain/Snow	4.4	0.22	0.25	19.5	2.7	3.2	rain gauge
12/15/18	Rain	10.4	0.22	0.25	47.0	11.1	0.0	rain gauge
1/16/19	Snow	2.4	*	*	*	2.0	0.5	weather station
1/25/19	Rain	2.7	0.23	0.18	11.8	2.9	2.4	rain gauge
2/12/19	Rain	1.5	0.04	0.25	35.0	3.5	0.1	rain gauge
2/24/19	Rain	3.3	0.15	0.43	21.5	7.1	0.0	rain gauge
3/21/19	Rain	6.5	0.25	0.23	26.2	8.0	0.0	rain gauge
5/5/19	Rain	7.9	0.43	1.02	18.4	18.1	1.2	weather station
6/18/19	Rain	1.9	0.35	0.99	5.5	23.9	7.1	rain gauge
	Average	**5.0**	**0.28**	**0.63**	**23.5**	**15.1**	**2.1**	
	Total	**119.0**						

4.3.2 Stormwater Quality

Table C2. Concentrations of nitrate, TN, and DOC in all stormwater samples as well as concentration reductions and the nitrate percentage of TN concentration. * indicates missing data.

	NO3-				TN				NO3-/TN			DOC			
Date	Inflow (mg/L as N)	Outflow Underdrain (mg/L as N)	Outflow Bypass (mg/L as N)	Concentration Reduction (in vs underdrain; %)	Inflow (mg/L as N)	Outflow Underdrain (mg/L as N)	Outflow Bypass (mg/L)	Concentration Reduction (in vs underdrain; %)	In (%)	Out (%)	BP (%)	Inflow (mg/L as N)	Outflow Underdrain (mg/L as N)	Outflow Bypass (mg/L)	Concentration Reduction (in vs underdrain; %)
4/16/18	0.14	0.26	0.05	-93	0.40	0.73	0.30	-79.9	34	36	16	5.8	13.4	4.2	-132.0
4/27/18	0.15	0.11	0.02	29	1.00	0.46	0.34	54.6	15	24	7	5.2	10.0	6.0	-93.5
5/19/18	0.17	0.08	0.00	54	0.60	0.50	0.49	16.7	29	16	0	6.8	9.8	9.7	-44.1
5/23/18	0.30	0.28	0.08	8	0.77	0.69	0.53	10.7	40	41	15	6.5	9.1	7.1	-40.3
6/2/18	0.35	0.07	0.03	80	0.60	0.40	0.47	33.8	58	17	6	5.6	8.3	8.2	-49.0
7/23/18	0.43	0.07	0.11	84	0.73	0.40	0.44	44.9	59	18	25	6.7	8.4	5.3	-24.9
7/30/18	0.20	0.17	0.04	15	0.49	0.53	0.27	-6.6	40	32	16	4.8	7.9	4.1	-64.2
8/21/18	0.32	0.12	0.18	62	0.59	0.55	0.27	7.6	53	22	65	5.0	10.6	4.6	-113.3
8/31/18	0.19	0.08	0.18	56	0.36	0.36	0.41	-0.9	54	23	44	4.8	8.0	6.4	-64.7
9/26/18	0.85	0.38	*	56	1.33	1.20	*	10.2	64	31	*	5.8	5.3	*	8.5
9/28/18	0.69	0.40	0.05	42	1.01	0.56	0.00	44.0	69	71	100	4.2	4.7	0.0	-10.2
10/11/18	0.71	0.32	0.29	55	0.99	0.84	0.52	15.3	72	38	55	4.7	10.1	4.1	-113.7
10/26/18	0.29	0.69	0.04	-142	0.50	0.88	0.33	-74.8	57	79	13	4.7	6.4	9.3	-36.1
11/10/18	0.75	0.49	0.03	35	1.01	0.65	0.00	35.6	74	75	100	4.6	4.4	7.3	5.9
11/13/18	0.33	0.41	0.02	-22	0.65	0.62	0.28	5.6	51	67	5	4.5	3.4	5.7	24.8
11/15/18	0.41	0.32	0.03	23	0.69	0.50	0.21	27.8	59	63	13	3.3	2.3	3.6	29.7
12/15/18	0.29	0.32	*	-11	0.45	0.41	*	7.9	65	78	*	4.1	4.2	*	-2.4
1/16/19	0.82	1.05	0.03	-28	1.70	1.30	*	23.5	0	0	*	4.7	2.6	*	44.7
1/25/19	0.47	0.52	0.00	-12	0.98	0.86	0.00	11.8	48	61	N/A	6.0	3.6	7.2	39.7
2/12/19	0.68	1.01	0.00	-48	1.00	1.10	0.30	-10.0	68	92	0	6.0	3.9	6.7	35.0
2/24/19	0.64	0.60	0.08	6	0.90	0.80	0.30	11.1	71	75	28	4.6	3.7	3.8	19.6
3/21/19	0.35	0.52	0.25	-48	0.80	0.70	0.50	12.5	44	75	51	5.1	6.1	5.6	-19.6
5/5/19	0.29	0.15	0.09	49	0.80	0.80	0.50	0.0	36	18	19	5.8	10.8	7.6	-86.2
6/18/19	0.52	0.02	0.06	96	1.10	0.00	0.80	100.0	48	0	7	9.6	11.1	8.3	-15.6
Average	0.43	0.35	0.08	**19**	0.81	0.66	0.35	**19**	50	44	29	5.4	7.0	5.9	**-30**

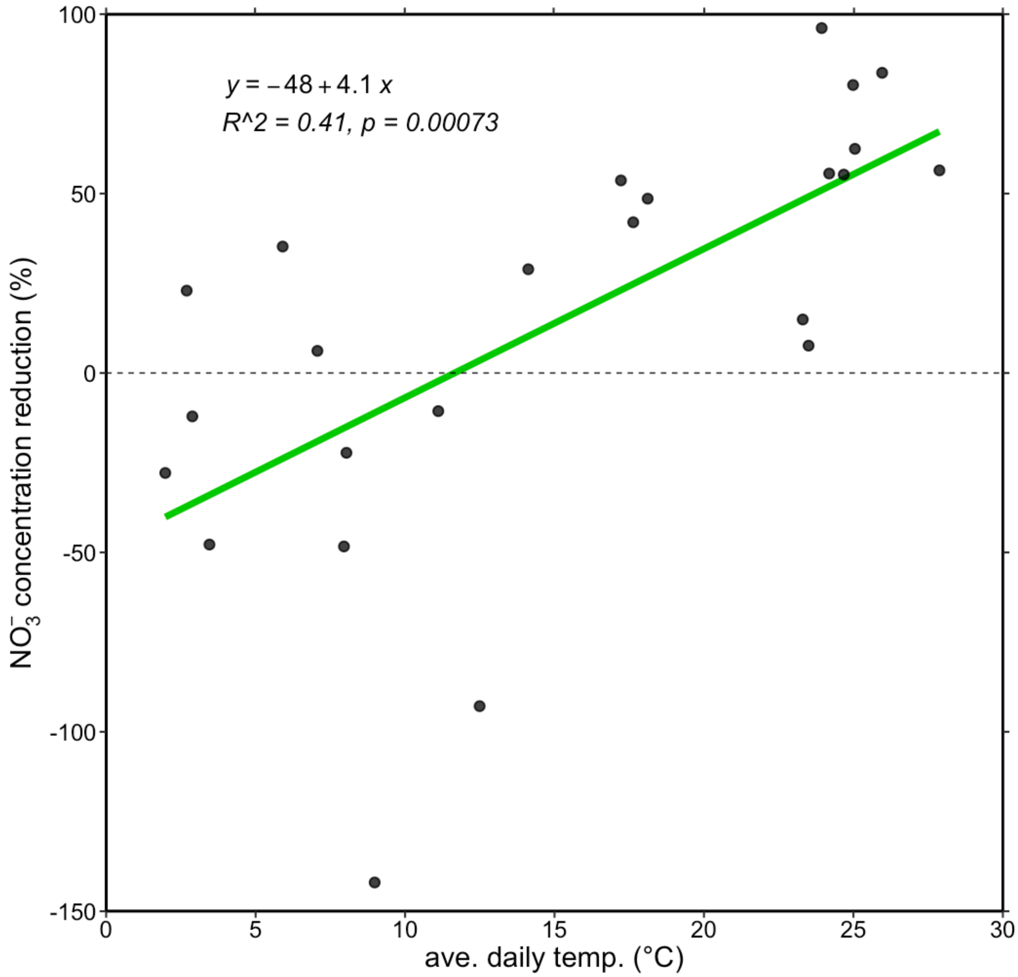

Figure C1. Relationship between nitrate concentration reduction between the bioretention inlet and underdrain outlet and average daily temperature during each monitored storm. The green line shows a linear regression with corresponding equation, R^2 and p values at the top of the figure.

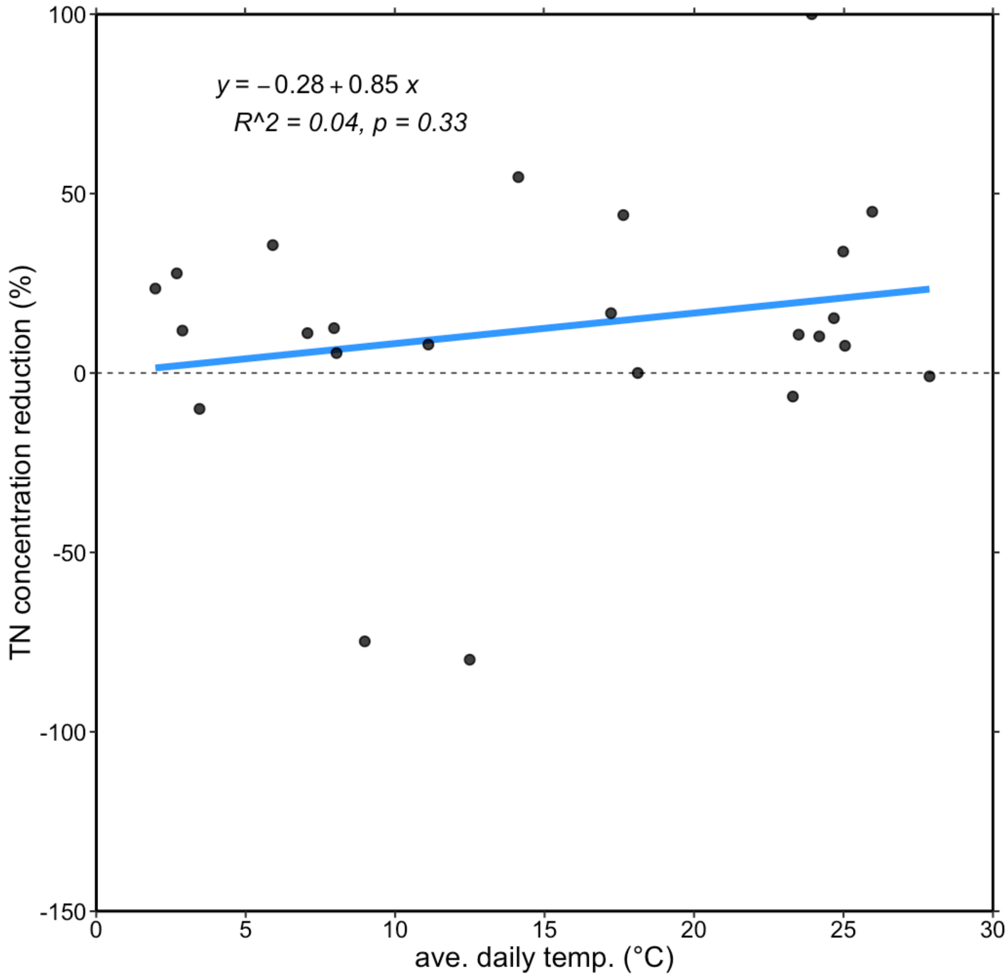

Figure C2. Relationship between TN concentration reduction between the bioretention inlet and underdrain outlet and average daily temperature during each monitored storm. The blue line shows a linear regression with corresponding equation, R^2 and p values at the top of the figure.

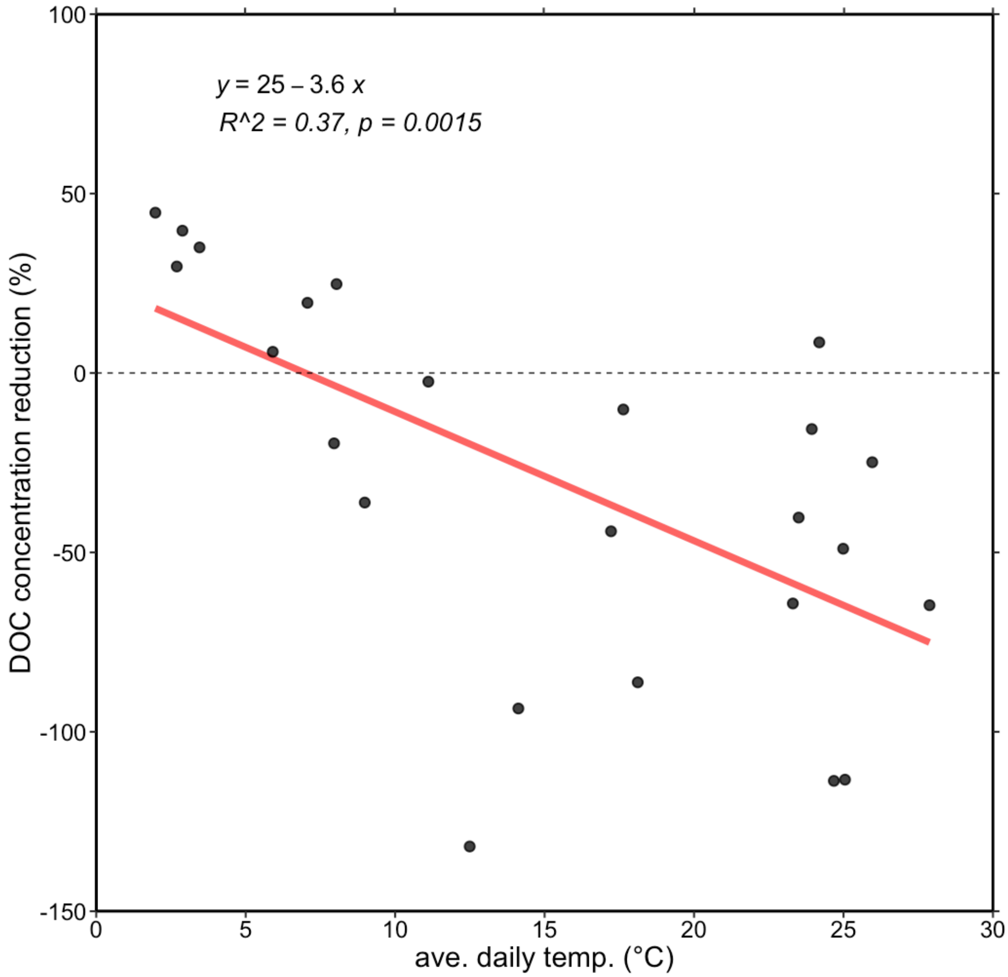

Figure C3. Relationship between DOC concentration reduction between the bioretention inlet and underdrain outlet and average daily temperature during each monitored storm. The blue line shows a linear regression with corresponding equation, R^2 and p values at the top of the figure.

4.3.3 Overall Bioretention Performance

Table C3. Stormwater runoff volumes at the three monitoring locations and calculated bioretention runoff reductions for each monitored event.

	Bioretention Stromwater Volumes				
Event Date	Inflow Volume (L)	Outlet Underdrain Volume (L)	Outlet Bypass Volume (L)	Runnoff Reduction (%)	% Outflow Bypassed (%)
4/16/18	1859925	726816	675227	24.6	48.2
4/27/18	688256	182639	38135	67.9	17.3
5/19/18	2425496	920185	87982	58.4	8.7
5/23/18	473641	145519	29845	63.0	17.0
6/2/18	2104107	479156	39168	75.4	7.6
7/23/18	3813244	1087723	621570	55.2	36.4
7/30/18	433288	188694	49162	45.1	20.7
8/21/18	1349767	426425	187099	54.5	30.5
8/31/18	854816	304521	35006	60.3	10.3
9/26/18	237475	55976	3843	74.8	6.4
9/28/18	1049641	412432	35738	57.3	8.0
10/11/18	2152335	417416	384465	62.7	47.9
10/26/18	771667	221492	12786	69.6	5.5
11/10/18	464948	127431	13549	69.7	9.6
11/13/18	886766	325407	24199	60.6	6.9
11/15/18	1385135	579202	19650	56.8	3.3
12/15/18	3369003	739206	551770	61.7	42.7
1/16/19	1139107	193074	9189	82.2	4.5
1/25/19	1005210	370685	19636	61.2	5.0
2/12/19	1398073	421623	21954	68.3	4.9
2/24/19	1599442	538750	38746	63.9	6.7
3/21/19	2117413	577944	148593	65.7	20.5
5/5/19	1066765	397360	46825	58.4	10.5
6/18/19	376315	145377	69345	42.9	32.3
Total	33021835	9985053	3163482	**60.2**	**24.1**

Table C4. Calculated loads of nitrate, TN, and DOC through each monitoring location over each storm as well as load reductions and the nitrate percentage of TN load. * indicates missing data.

	NO3-					TN					NO3-/TN			DOC				
Date	Load In (Kg)	Load Out Underdrain (Kg)	Load Out Bypass (Kg)	Load Reduction (%)	% Outflow Load Bypassed (%)	Load In (Kg)	Load Out Underdrain (Kg)	Load Out Bypass (Kg)	Load Reduction (%)	% Outflow Load Bypassed (%)	In (%)	Out (%)	BP (%)	Load In (Kg)	Load Out Underdrain (Kg)	Load Out Bypass (Kg)	Load Reduction (%)	% Outflow Load Bypassed (%)
4/16/18	0.25	0.190	0.033	11.7	14.7	0.75	0.528	0.199	3.2	27.4	34	36	16	10.7	9.7	2.9	-17.4	22.8
4/27/18	0.11	0.020	0.001	80.3	4.1	0.69	0.083	0.013	86.1	13.4	15	24	7	3.6	1.8	0.2	42.2	11.1
5/19/18	0.42	0.074	0.000	82.4	0.0	1.46	0.460	0.043	65.4	8.6	29	16	0	16.5	9.0	0.9	40.2	8.6
5/23/18	0.14	0.041	0.002	70.0	5.4	0.36	0.100	0.016	68.2	13.6	40	41	15	3.1	1.3	0.2	50.0	13.7
6/2/18	0.74	0.033	0.001	95.3	3.4	1.27	0.191	0.018	83.5	8.8	58	17	6	11.8	4.0	0.3	63.4	7.4
7/23/18	1.64	0.077	0.068	91.2	46.9	2.78	0.437	0.275	74.4	38.6	59	18	25	25.6	9.1	3.3	51.6	26.4
7/30/18	0.08	0.031	0.002	60.4	6.5	0.21	0.099	0.013	47.3	11.9	40	32	16	2.1	1.5	0.2	18.7	12.0
8/21/18	0.43	0.051	0.033	80.4	39.4	0.80	0.234	0.051	64.5	17.9	53	22	65	6.7	4.5	0.9	19.7	16.1
8/31/18	0.17	0.026	0.006	80.7	19.7	0.31	0.111	0.014	59.4	11.5	54	23	44	4.1	2.4	0.2	35.9	8.5
9/26/18	0.20	0.021	0.003	87.9	13.4	0.32	0.067	0.005	77.2	7.1	64	31	64	1.4	0.3	0.0	76.8	7.0
9/28/18	0.73	0.166	0.002	77.0	1.1	1.06	0.233	0.000	78.0	0.0	69	71	100	4.4	1.9	0.0	56.7	0.0
10/11/18	1.52	0.132	0.110	84.1	45.5	2.12	0.349	0.200	74.1	36.4	72	38	55	10.2	4.2	1.6	43.0	27.3
10/26/18	0.22	0.154	0.001	30.3	0.4	0.39	0.195	0.004	48.7	2.1	57	79	13	3.7	1.4	0.1	57.7	7.7
11/10/18	0.35	0.062	0.000	82.1	0.6	0.47	0.083	0.000	82.4	0.0	74	75	100	2.2	0.6	0.1	69.6	15.2
11/13/18	0.30	0.133	0.000	55.0	0.3	0.58	0.200	0.007	64.2	3.3	51	67	5	4.0	1.1	0.1	68.9	11.2
11/15/18	0.57	0.184	0.001	67.7	0.3	0.96	0.290	0.004	69.4	1.4	59	63	13	4.5	1.3	0.1	69.0	5.1
12/15/18	0.98	0.238	0.161	59.3	40.3	1.51	0.305	0.247	63.4	44.8	65	78	65	13.8	3.1	2.3	61.2	42.2
1/16/19	0.93	0.202	0.000	78.3	0.1	1.94	0.251	0.016	86.2	5.9	48	80	2	5.4	0.5	0.0	89.8	7.9
1/25/19	0.47	0.194	0.000	58.7	0.0	0.98	0.319	0.000	67.5	0.0	48	61	N/A	6.1	1.3	0.1	75.4	9.5
2/12/19	0.96	0.427	0.000	55.4	0.0	1.40	0.464	0.007	66.4	1.4	68	92	0	8.4	1.6	0.1	78.6	8.2
2/24/19	1.02	0.323	0.003	68.1	1.0	1.44	0.431	0.012	69.3	2.6	71	75	100	7.4	2.0	0.1	70.9	6.9
3/21/19	0.75	0.303	0.038	54.4	11.1	1.69	0.405	0.074	71.7	15.5	44	75	51	10.8	3.5	0.8	59.6	19.1
5/5/19	0.31	0.059	0.004	79.4	6.9	0.85	0.318	0.023	60.0	6.9	36	18	19	6.2	4.3	0.4	24.9	7.7
6/18/19	0.20	0.003	0.004	96.5	56.7	0.41	0.000	0.055	86.6	100.0	48	100	7	3.6	1.6	0.6	39.4	26.3
Total Load	**13.49**	**3.14**	**0.47**	**73.2**	**13.1**	**24.76**	**6.15**	**1.30**	**69.9**	**17.4**	**54**	**51**	**37**	**176.1**	**72.3**	**15.6**	**50.1**	**17.7**

(highlighted) indicates the inlet sample concentration was used in place of the missing bypass sample for load calculations

4.3.4 Stable Isotopes

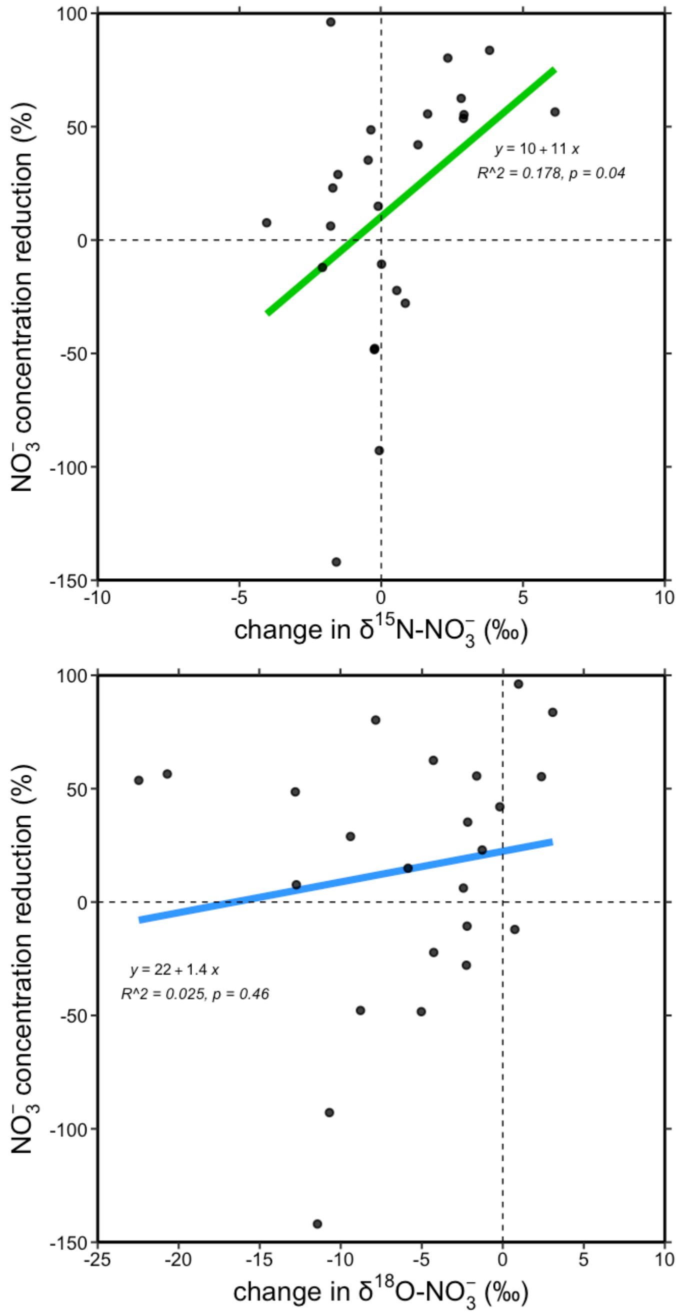

Figure C4. Relationship between bioretention nitrate concentration reduction between inlet and outlet and changes in $\delta^{15}N$-NO_3^- (top) and $\delta^{18}O$-NO_3^- (bottom) from inlet to outlet during each monitored storm. Colored lines show linear regressions with corresponding equations, R^2 and p values listed.

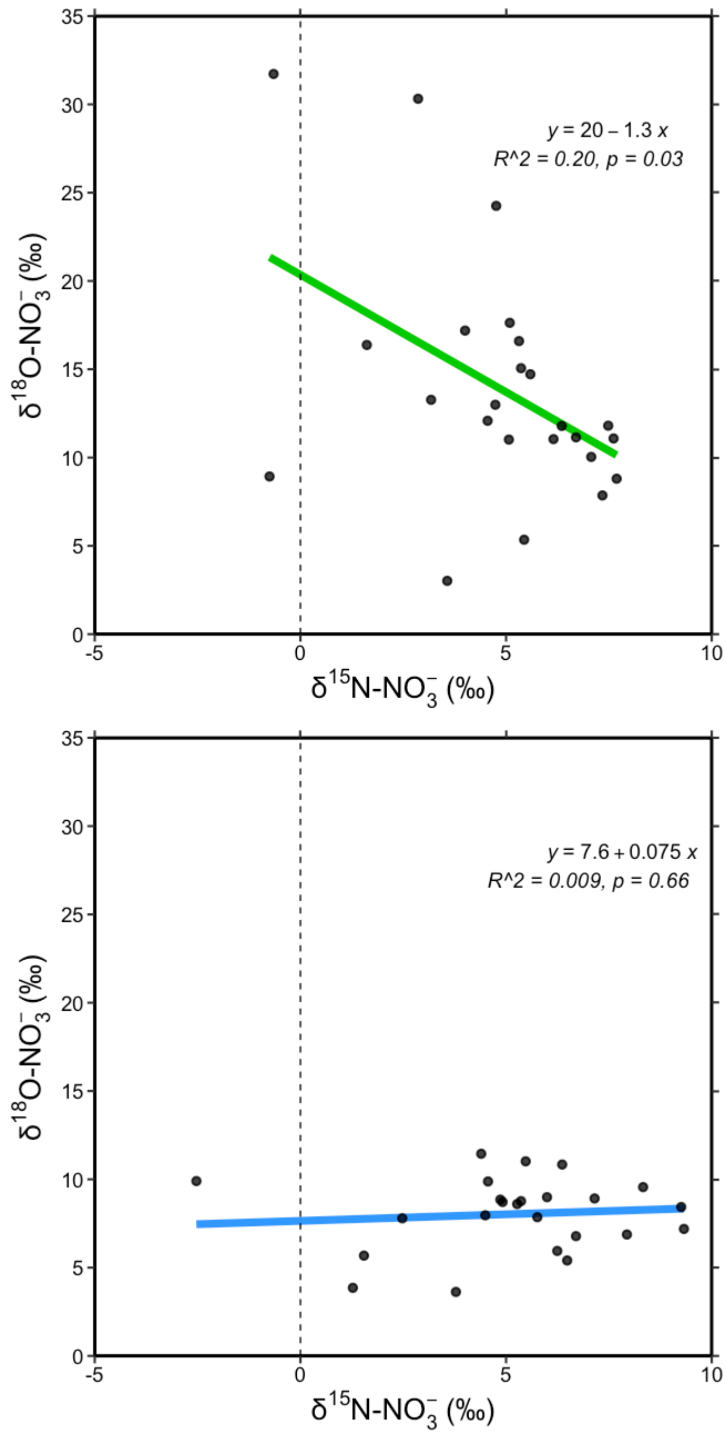

Figure C5. Relationship between sample $\delta^{15}N\text{-}NO_3^-$ and $\delta^{18}O\text{-}NO_3^-$ for the bioretention inlet (top) and outlet (bottom) during each monitored storm. Colored lines show linear regressions with corresponding equations, R^2 and p values listed.

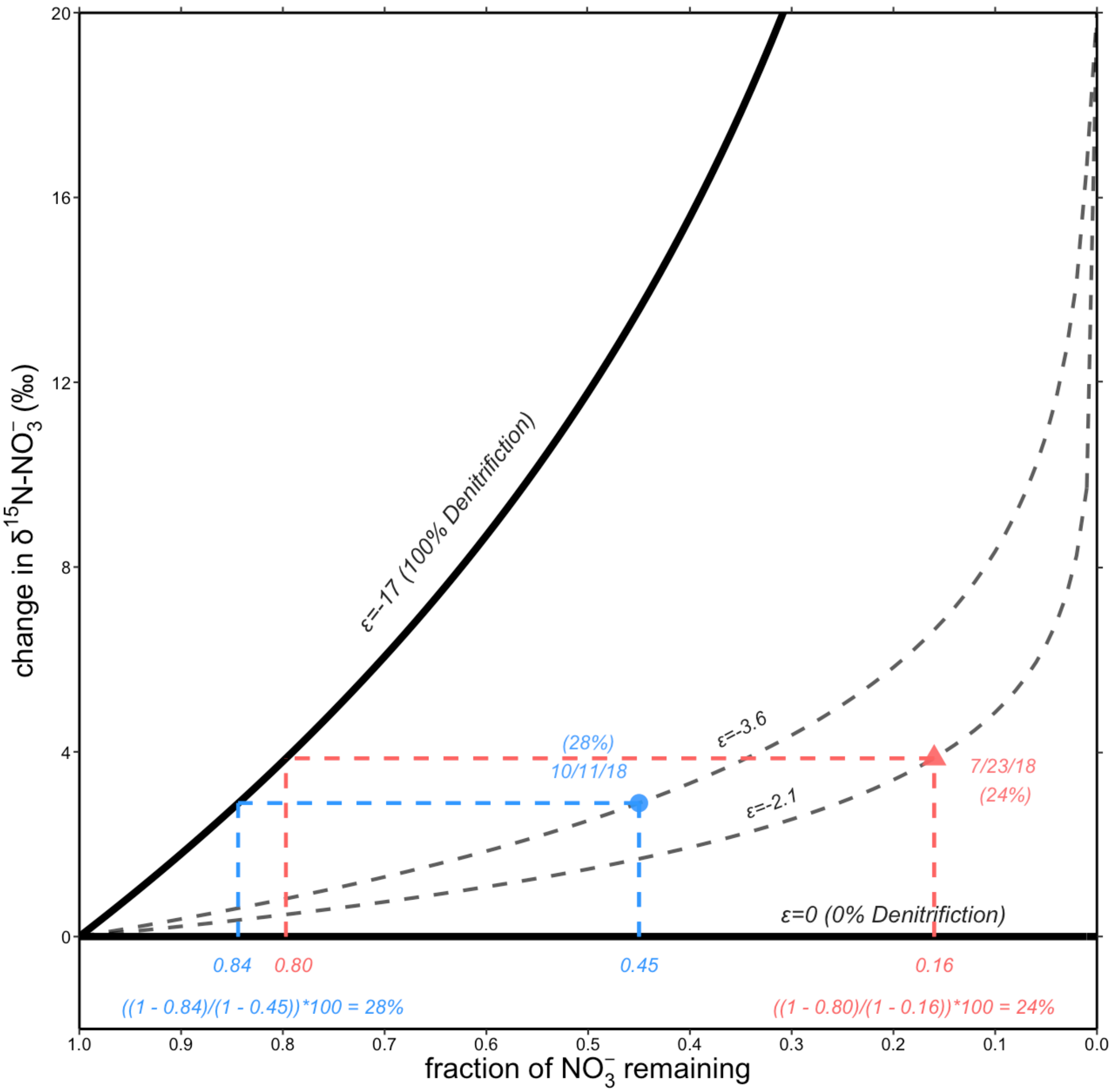

Figure C6. Relation between the fraction of nitrate concentration remaining in water and the enrichment of δ^{15}N-NO_3^- in systems with different enrichment factors (ε). These curves are used to estimate the percentage of nitrate concentration reduction that denitrification is responsible for (as shown). The blue circle and red triangle show the two events with denitrification isotope trends with their calculated denitrification percentages in parenthesis.